Reactions of Biologically Important Thiols with Nitroxyl (HNO) and Development of a HNO Marker

Biao Shen

A Thesis

in

The Department

of

Chemistry and Biochemistry

Presented in Partial Fulfillment of the Requirements
for the Degree of Master of Science at
Concordia University
Montreal, Quebec, Canada

August 2007

Your file Votre référence
ISBN: 978-0-494-34778-2
Our file Notre référence
ISBN: 978-0-494-34778-2

ABSTRACT

Reactions of Biologically Important Thiols with Nitroxyl (HNO)
and Development of a HNO Marker

Biao Shen

Biologically active nitroxyl (HNO) is one of the least understood nitrogen oxides. It may play a distinct role from NO in protecting the cardiovascular system, and thiols are suspected to be a major nitroxyl target. The major low-molecular-mass intracellular antioxidant, glutathione (GSH), is an important regulator of cellular homeostasis, and is the most likely biological target of HNO. Cysteine (Cys) and HCys (HCys) are naturally occurring thiol-containing amino acids with antioxidant properties and their levels have been linked to many diseases. Reactions of these thiols with Angeli's salt (AS), a HNO donor, were investigated here.

N-acetyl-glutathione and *N*-acetyl-homocysteine were used in this study but are unavailable commercially. An efficient and simple method was developed to prepare *N*-acetylated low-mass thiols from the corresponding disulfides (e.g., GSSG, homocystine) in aqueous buffer using sulfosuccinimidyl acetate (NHSA) followed by disulfide reduction by immobilized *tris*(2-carboxyethyl)phosphine (TCEP). The pK_a values of the low-mass thiols used here were determined by pH titration in 0.15 M KCl using the GLpKa instrument.

GSH was incubated with AS for 30 min and room temperature, and the products were analyzed by ESI-MS. The sulfinamide ($GSONH_2$) and disulfide (GSSG) were formed at pH>5 but GSSG was the dominant product at higher pHs and GSH

concentrations. Disulfides only were detected in the incubations of AS with Cys, *N*-AcCys, HCys, and penicillamine at pH>5. *N*-acetylation of penicillamine decreased its reactivity with HNO and led to sulfoxide disulfide (RSOSR) formation. Control experiments with $NaNO_2$ revealed that the products formed in the AS incubates are due to reaction with HNO at pH>5 but with HNO_2 at pH<4, which yields *S*-nitrosothiols. The results provide the first comparative study of HNO reactivity with biologically important low-mass RSHs. Furthermore, the efficient conversion of GSH to stable $GSONH_2$ and GSSG products is consistent with the reported depletion of intracellular GSH by HNO.

At present, HNO is detected mainly by monitoring its dimerization product, N_2O. Since N_2O can arise from other reactions, a specific method of HNO detection is desirable. The high reactivity of thiols with HNO to form sulfinamide was examined as a method of HNO detection. The CysGlu and CysAsp dipeptides, with two negative charges at the C-terminus, exhibited high sulfinamide yields at pH ~7.4, and are good candidates for the further development of a HNO marker.

ACKNOWLEDGMENTS

I would like to express my sincere gratitude to all those who helped me fulfill this task, especially to:

Dr. Ann M. English, my supervisor, for giving me this opportunity to study and do research in her laboratory, and for her guidance, encouragement, kindness, and patience during my time at Concordia University.

Dr. Paul Joyce and Dr. Justin Powlowski, my Research Committee Members, for their invaluable comments and scientific guidance.

All members in the Departments of Chemistry and Biochemistry, particularly Alain Tessier for always being so helpful and for showing me how to master mass spectrometry.

Dr. Angelo Filosa (AstraZeneca Canada, Montreal) and Cynthia Bazin (Merck Frosst, Montreal) for their kind help in measuring the accurate masses and pK_a values reported in this thesis.

My colleagues and friends: Ernesto Moran, Mengwei Ye, Heng Jiang, and Jean-François Roy. Their frequent discussions, suggestions, and friendship helped me to overcome all obstacles during the course of my work.

My family, for their love and endless support of every kind. I dedicate this thesis to my twin boys.

TABLE OF CONTENTS

LIST OF FIGURES ix

LIST OF TABLES xi

ABBREVIATIONS xii

1 GENERAL INTRODUCTION 1

1.1 The role of glutathione and other low-mass thiols in biological systems 1

1.2 HNO as a therapeutic target 3

1.3 Angeli's salt as an HNO donor 5

1.4 Outline of thesis 7

2 SYNTHESIS OF *N*-ACETYLATED LOW-MASS THIOLS 9

2.1 Introduction 9

2.2 Materials and methods 10

2.2.1 Materials and solutions 10

2.2.2 Reaction of NHSA with GSH, GSSG, and Hcystine 10

2.2.3 Purification of *N*-acetylated GSSG and Hcystine 12

2.2.4 Disulfide reduction on the TCEP gel 12

2.2.5 ESI-MS and HPLC-ESI-MS 13

2.3 Results 14

2.3.1 Reaction of NHSA with GSH, GSSG, and Hcystine 14

2.3.2 Purification of *N*-AcGSSG and *N*-AcHcystine 17

2.3.3 Generation of *N*-acetylated GSH and HCys 21

2.4 Discussion 23

3 THIOL pK_a MEASUREMENTS AND CORRELATION WITH STRUCTURES 26

3.1 Introduction 26

3.2 Materials and methods 26

3.2.1 Materials and solutions 26
3.2.2 Potentiometric pK_a measurements of low-mass thiols 28
3.3 Results 29
3.3.1 pK_a values 29
3.3.2 Thiol pK_a values 32
3.3.3 Amino and carboxylate pK_a values of low-mass thiols 33
3.4 Discussion 34
Appendix 3.1 Supplemental figures 35

4 REACTIONS OF GSH AND ITS DERIVATIVES WITH HNO 40
4.1 Introduction 40
4.2 Materials and methods 41
4.2.1 Materials 41
4.2.2 Reaction of GSH with AS and $NaNO_2$ 42
4.2.3 Isolation of sulfinamide formed in the GSH/AS incubation 42
4.2.4 Reactions of AS with GSH derivatives and related dipeptides 43
4.2.5 ESI-MS and HPLC-ESI-MS 43
4.2.6 HPLC-UV analysis of RSH/AS incubations 44
4.3 Results 44
4.3.1 Reaction of GSH with AS and $NaNO_2$ 44
4.3.2 Reaction of AS with the GSH derivatives 57
4.4 Discussion 59
4.4.1 Effect of HNO on the functions of GSH 59
4.4.2 Factors controlling the sulfinamide formation 62

5 REACTIONS OF CYS, HCYS, PENICILLAMINE, AND CYS-CONTAINING DIPEPTIDES WITH HNO; TOWARDS DEVELOPMENT OF A HNO MARKER 64
5.1 Introduction 64
5.2 Materials and methods 65
5.2.1 Materials and solutions 65

5.2.2 Incubations of AS with Cys, HCys, Pen, and their *N*-acetylated derivatives 66
5.2.3 Incubations of AS with the dipeptides 66
5.2.4 ESI-MS and ESI-MS/MS 66
5.3 Results 67
5.3.1 Reaction of HNO with Cys, HCys, Pen, and their *N*-acetylated derivatives 67
5.3.2 Reaction of HNO with the CX dipeptides 74
5.4 Discussion 78
5.4.1 Thiol-containing amino acids 78
5.4.2 Thiol-containing dipeptides 79
5.4.3 HNO marker developement 80

6 GENERAL CONCLUSIONS AND SUGGESTIONS FOR FUTURE WORK 82
6.1 Chapter 2 82
6.2 Chapter 3, 83
6.3 Chapters 4 and 5 83
6.4 Suggestions for future work 84

REFERENCES 86

LIST OF FIGURES

Figure 1.1	Observed rate constants (k_{obs}) of decomposition of Angeli's salt (AS) *vs* pH	6
Figure 1.2	Spectrophotometric analysis of AS decomposition at 22°C *vs* pH	6
Figure 2.1	ESI mass spectral analysis of the reaction of GSH with NHSA in water	15
Figure 2.2	ESI mass spectral analysis of the reaction of GSH with 1× and 5× NHSA	16
Figure 2.3	HPLC-UV chromatograms and mass spectra of the GSSG/NHSA incubations at different NHSA/GSSG ratios	17
Figure 2.4	Time course of GSSG *N*-acetylation by NHSA	18
Figure 2.5	HPLC-UV analysis of *N*-AcGSSG precipitation *vs* pH	18
Figure 2.6	ESI-MS monitoring of *N*-AcGSSG purification and reduction	19
Figure 2.7	HPLC-UV monitoring of *N*-AcGSSG and *N*-AcHcystine purificaiton	20
Figure 2.8	ESI-MS monitoring of *N*-AcHcystine purification and reduction	22
Figure 3.1	Bjerrum difference plot in the potentiometric titration of HCys and Pen	29
Figure 3.2	Distribution curves of species in solution as a function of pH	30
Figure 3.3	Structures of the low-mass thiols studied here	31
Figure 4.1	pH of the GSH/AS and GSH/$NaNO_2$ incubations *vs* time	45
Figure 4.2	ESI-MS analysis of 30-min equimolar GSH/AS incubations *vs* pH	46
Figure 4.3	ESI-MS analysis of GSH/AS incubations at pH 6 *vs* AS concentration	47
Figure 4.4	Product-ion spectra of the m/z 322 and m/z 339 ions	50
Figure 4.5	Expected MS/MS cleavage sites in GSH sulfinamide and in the putative cyclic GSH sulfinamide (m/z 322)	50
Figure 4.6	ESI mass spectra of *N*-AcGSH/AS incubations *vs* pH, and HPLC-UV and HPLC-MS spectra of GSH/AS and *N*-AcGSH/AS incuabates at pH ~6	51

Figure 4.7	ESI-MS analysis of $GSONH_2$ stability at pH 6	53
Figure 4.8	GSO_2H formation during isolation of $GSONH_2$	54
Figure 4.9	Protuct-ion spectrum of $GSONH_2$ (m/z 339) and GSO_2H (m/z 340)	55
Figure 4.10	ESI mass spectra of control incubations	56
Figure 4.11	Comparison of AS decomposition in the presence and absence of GSH	57
Figure 4.12	Sulfinamide *vs* disulfide formation in the EtGSH/AS, GSH/AS, and *N*-AcGSH/AS incubations *vs* pH	58
Figure 4.13	HPLC-UV analysis of the products formed in the EtGSH/AS, GSH/AS, and *N*-AcGSH/AS incubations *vs* pH	58
Figure 4.14	ESI mass spectra of 30-min γEC/AS and CG/AS incubations	60
Figure 5.1	ESI-MS analysis of 30-min AS/Cys and $NaNO_2$/Cys incubations *vs* pH	67
Figure 5.2	ESI mass spectra of 30-min AS/Cys incubations *vs* Cys/AS ratio	69
Figure 5.3	ESI-MS analysis of 30-min AS/*N*-AcCys and $NaNO_2$/*N*-AcCys incubations *vs* pH	70
Figure 5.4	ESI-MS analysis of 30-min AS/HCys and AS/*N*-AcHCys incubations *vs* pH	71
Figure 5.5	ESI mass spectra of HCys stability *vs* pH	72
Figure 5.6	ESI-MS analysis of 30-min AS/Pen and AS/*N*-AcPen incubations *vs* pH	73
Figure 5.7	Structures of the dipeptides, γEC, EC, CE, CG, CD, CW and CK	74
Figure 5.8	ESI mass spectra of 30-min AS/CE and AS/EC incubations	75
Figure 5.9	ESI mass spectra of 30-min AS/CK and AS/CD incubations	77
Figure 5.10	ESI mass spectra of 30-min AS/CW incubations	78

LIST OF TABLES

Table 2.1	Accurate masses of GSH, HCys, and their *N*-acetylated derivatives	23
Table 3.1	Published pK_a values of ionizable groups in low-mass thiols	27
Table 3.2	Observed pK_a values of ionizable groups in low-mass thiols used in this study	32
Table 4.1	Accurate mass measurements of GSH and GSH sulfinamide	48
Table 4.2	Main fragment ions of GSH, $GSONH_2$, GSSG, and the M+14 adduct observed by MS/MS	49
Table 4.3	Assignments of peaks in the ESI mass and tandem mass spectra of the AS/RSH incubations	52
Table 4.4	Sulfinamide/disulfide ratio in the reactions of AS with EtGSH, GSH, and *N*-AcGSH *vs* pH	59
Table 4.5	pK_a values of the thiol and α-amino groups in GSH and its derivatives	62
Table 5.1	Relative sulfinamide yields in the 30-min incubations of RSH with AS	81

LIST OF ABBREVIATIONS

AS	Angeli's salt
CD	CysAsp
CE	CysGlu
CG	CysGly
CK	CysLys
CW	CysTrp
Cys	*L*-cysteine
DAD	Diode-Array Detector
EC	GluCys
γEC	γ-GluCys
EDC	1-Ethyl-3-[3-dimethylaminopropyl]carbodiimide hydrochloride
ESI-MS	electrospray ionization mass spectrometry
EtGSH	*L*-glutathione reduced ethyl ester
GSH	*L*-glutathione reduced
GSSG	*L*-glutathione oxidized
HCys	*DL*-homocysteine
Hcystine	*DL*-homocystine
HPLC	high performance liquid chromatography
ITC	Isothermal titration calorimetry
N-AcCys	*N*-acetyl-*L*-cysteine
N-AcGSH	*N*-acetyl-*L*-glutathione

N-AcHCys	*N*-acetyl-HCys
N-AcPen	*N*-acetyl-*DL*-penicillamine
$NaNO_2$	sodium nitrite
NEM	*N*-ethylmaleimide
NHSA	sulfosuccinimidyl acetate
NMR	Nuclear magnetic resonance
Pen	*DL*-penicillamine
SAX	strong anion-exchange
S-MeGSH	*S*-methyl-glutathione
SPE	Solid-phase extraction
TCEP	*tris*(2-carboxyethyl)phosphine hydrochloride
R-SNO	*S*-nitrosated derivatives of R (R = Cys-containing dipeptides)
R-$SONH_2$	Sulfinamide derivatives of R (R = Cys-containing dipeptides)
dR	Disulfide derivatives of R (R = Cys-containing dipeptides)

1 GENERAL INTRODUCTION

1.1 The role of glutathione and other low-mass thiols in biological systems

Glutathione (GSH, γGlu-Cys-Gly), a tripeptide, is the predominant intracellular low-mass thiol. It is present in cells of all organisms at millimolar concentrations (0.5-10 mM) (*1*), and possesses a multitude of physiological functions (*2*). As one of the major intracellular antioxidants, GSH effectively scavenges free radicals and other reactive oxygen species (*e.g.*, hydroxyl radical, peroxynitrite and hydrogen peroxide) directly and indirectly through enzymatic reactions (*3*). Intracellular glutathione is effectively maintained in the reduced state by GSSG reductase linked to the NADPH/$NADP^+$ system. GSH/GSSG is the most important redox couple and plays crucial roles in the regulation of cellular homeostasis (maintenance of cell equilibrium). Also, GSH/GSSG deficiency contributes to oxidative stress, which accelerates aging and contributes to the pathogenesis of Parkinson's disease, liver disease, HIV, AIDS, cancer, heart attack, stroke and diabetes (*4*). Other roles of GSH include protein glutathionylation as an element of intracellular signal transduction, gene expression, apoptosis (*2, 5*), and intracellular nitric oxide (NO) storage and transport (*6*). Virtually all of these functions depend on the reactivity of the thiol group of glutathione.

Cysteine (Cys) is a naturally occurring, thiol-containing amino acid that is found in most proteins. Cys is an important source of sulfur in human metabolism and a required precursor in the production of glutathione in the body and other organisms. Thiol groups readily undergo oxidation/reduction reactions; for example, oxidation of Cys can produce a disulfide bond with another thiol, or further oxidation can produce sulfinic or sulfonic acids. Due to the ability to undergo redox reactions, Cys has

antioxidant properties. However, the intracellular ratio of Cys (Figure 3.1) to its disulfide cystine is low (1-10) compare to that of GSH/GSSG, which is in the range of 30-300 (*7*). Cys and cystine are reported to be involved in transmembrane *S*-nitrosothiol transport through a transnitrosation reaction (*8*). *N*-acetylcysteine (*N*-AcCys), the *N*-acetyl derivative of Cys, serves as a precursor of glutathione in the body and plays a role as a scavenger (antioxidant) to reduce free radicals (*9*). *N*-AcCys has been reported to be effective against oxidative damage in neurodegenerative conditions such as cerebral ischemia, Alzheimer's disease and Parkinson's disease (*10-12*).

Homocysteine (HCys) is a homologue of Cys, differing in that its side-chain contains an additional methylene (-CH_2-) before the thiol (-SH) group. Deficiencies in the vitamins, folic acid, pyridoxine (B_6), or B_{12} can lead to high HCys levels in plasma (*13*). These are linked to high concentrations of endothelial asymmetric dimethylarginine, which is a risk factor for cardiovascular disease since it interferes with the production of nitric oxide from *L*-arginine (*14-16*). Studies with animal models indicated that the effects of elevated HCys are multifactorial, affecting both the vascular wall structure and the blood coagulation system (*17-19*). Elevated HCys levels also have been linked to increased fractures in elderly persons by interfering with the cross-linking between collagen fibers and the tissues they reinforce (*20*). Elevated HCys is also found in the rare hereditary disease, homocystinuria (*21*) and in methylene-tetrahydrofolate-reductase deficiency (*22*). Direct generation of reactive oxygen species by HCys may also contribute to biological damage (*17, 23*).

1.2 HNO as a therapeutic target

Since the discoveries of nitric oxide (NO) biosynthesis in mammalian cells and the diverse biological activity associated with NO and NO-derived species, there has been extensive interest in the chemistry and biology of nitrogen oxides (NO_x). It is now established that the generation of endogenous NO_x represents important biochemical signaling pathways, critical components of the immune response, and potential pathophysiological events. NO has been shown to regulate processes such as platelet function, leukocyte recruitment, mitochondrial respiration, vascular tone and cardiac function (*24, 25*).

The one-electron reduction product of NO, nitroxyl (NO^-), or more likely its conjugate acid, HNO, with a $pK_a > 11$ (*26, 27*), remains one of the least studied and least understood among the biologically and pharmacologically relevant nitrogen oxides. HNO is known to be formed under physiological conditions. In fact, there are reports that HNO is produced by nitric oxide synthase (NOS) under certain circumstances (*28*), and *via* the metabolism of the decoupled NOS product *N*-hydroxy-*L*-arginine under oxidative stress (*29*). HNO also is formed under nitrosative stress (*30*), and by thiolysis of *S*-nitrosothiols (RSNO) following nucleophilic attack on the SNO sulfur (*31, 32*). The direct reduction of NO by mitochondrial cytochrome c (*33*), xanthine oxidase (*34*), Cu- and Mn-containing superoxide dismutases (*35*) and ubiquinol (*36*) are among further reactions reported to generate HNO.

Several reports indicate that HNO is electrophilic around neutral pH (*27, 31*), and theoretical studies predict highly favorable reactions with thiols (RSH) and amines (*27*). Electrophilic attack on RSH produces an *N*-hydroxysulfenamide addition product

(RSNHOH) that can react with a second RSH to yield the corresponding disulfide RSSR and hydroxylamine (NH_2OH) (*31, 37*), or spontaneously eliminate hydroxide ion to form a stable sulfinamide following hydration and deprotonation (Scheme 1.1) (*31*).

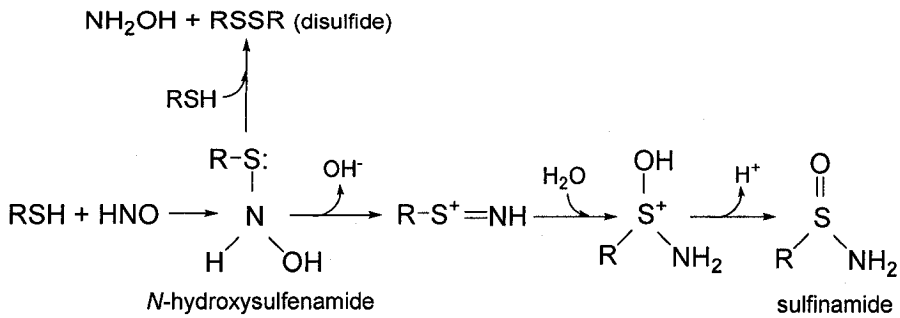

Scheme 1.1. **Proposed reactions of thiols with HNO.** This is scheme was adapted from Wong *et al.* (*31*).

HNO has recently been shown to play a significant role in biology and pharmacology, protecting the cardiovascular system, interacting with enzymes, and suggesting new drug possibilities. For example, HNO is a potent inhibitor of thiol-containing enzymes including aldehyde dehydrogenase (ALDH) and GAPDH (*38, 39*). It attenuates the activity of the NMDA receptor to provide neuroprotection, and inhibits activation of the yeast transcription factor, Ace1, *via* thiol modification (*40, 41*). These studies indicated that protein sulfhydryl groups may be major targets of HNO donors as demonstrated for NO donors (*42*). Nonetheless, NO and HNO donors elicit distinct responses under a variety of biological conditions *in vitro* and *in vivo*. For example, exposure to NO donors at the onset of cardiac reperfusion is protective whereas HNO donors increase tissue damage (*28, 43*). Under different circumstances HNO donors can promote smooth muscle relaxation (*44*) and provide thiol-sensitive myocardial protective effects that resemble early preconditioning (*45*).

1.3 Angeli's salt as an HNO donor

The widely used (*38, 39, 45-49*) Angeli's salt (AS, sodium trioxodinitrate, $Na_2N_2O_3$; Figure 1.1), which is prepared from hydroxylamine and nitrate (*50*), is currently the preferred HNO donor for studies on biomolecules and biological systems. Its monoprotonated form spontaneously releases HNO under physiological conditions (*51*):

$$HN_2O_3^- \rightarrow HNO + NO_2^- \qquad (1.1)$$

Piloty's acid (benzenesulfohydroxamic acid) also spontaneously releases HNO but only in anaerobic and basic media. This acid is subject to rapid oxidation in air, yielding NO rather than HNO (*52-54*).

Angeli's salt decomposes thermally or in aqueous solutions to give several different nitrogen oxides depending on the conditions (*55*). The products of aqueous decomposition are highly pH dependent; HNO is generated in the pH range 4-8 while NO is produced below pH 4 (eq 1.2). The rate of decomposition decreases with increasing pH

$$H_2N_2O_3 \rightarrow 2NO + H_2O \qquad (1.2)$$

and AS is quite stable at pH >10 (Figure 1.1). The rate increases dramatically below pH 4, whereas it is pH independent between pH 4 and 8 (Figure 1.1). HNO is highly reactive toward dimerization and dehydration produces nitrous oxide (N_2O) and water (eq 1.3) (*26, 27, 56*) with a second-order rate constant of 8×10^6 $M^{-1}s^{-1}$ (*26*). As reported

$$HNO + HNO \rightarrow [HO\text{-}N{=}N\text{-}OH] \rightarrow N_2O + H_2O \qquad (1.3)$$

previously, the half-life of AS is around 5 min at pH 7.4 and most of the salt decomposes within 30 min in aqueous solution (Figure 1.2) (*51, 57*).

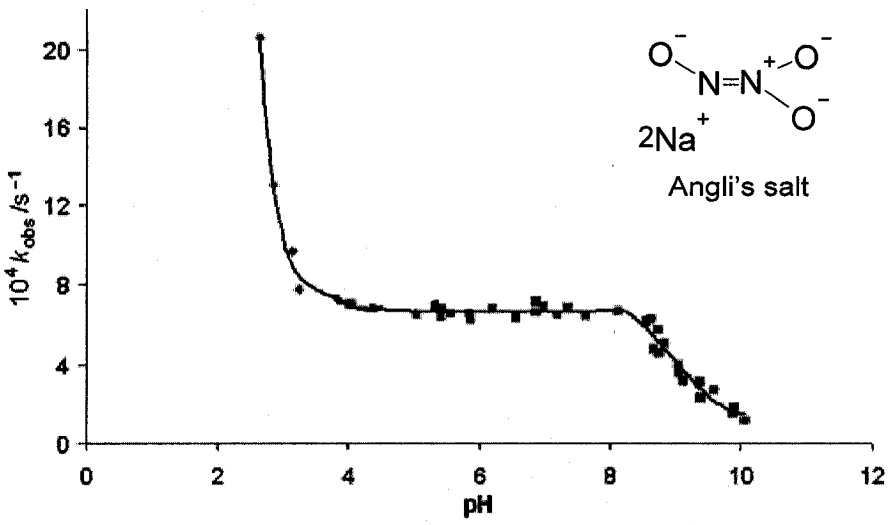

Figure 1.1. **Observed rate constants (k_{obs}) of decomposition of Angeli's salt (AS) vs pH.** The squares (■) represent the rates of the disappearance of AS to yield HNO and nitrite (NO_2^-), and the diamonds (◆) are the rates of conversion to nitric oxide (NO). Adapted from Dutton *et al.* (*55*).

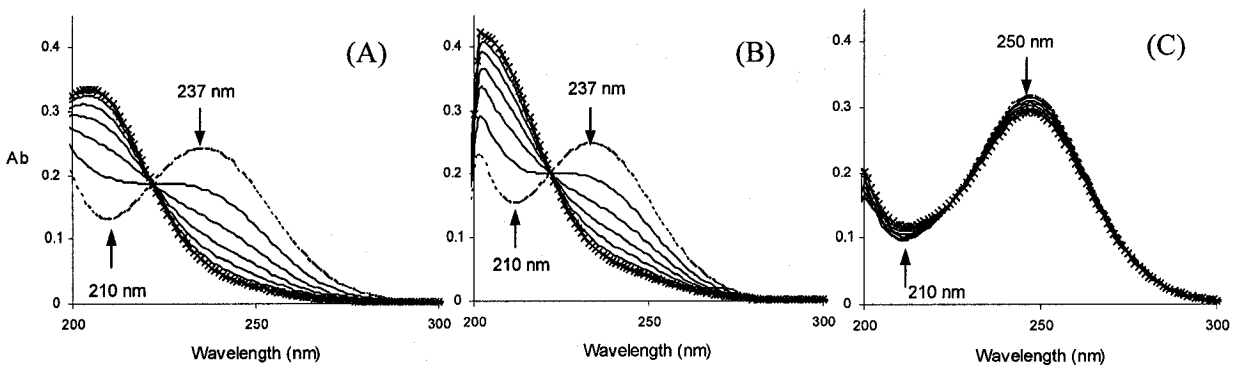

Figure 1.2. **Spectrophotometric analysis of AS decomposition at 22°C *vs* pH.** Absorption spectra of AS in: (A) water at pH 5.5, (B) 50 mM TrisHCl buffer (pH 7.4), and (C) 10 mM NaOH. The spectra recorded in 1-cm cuvettes at t = 0 (dotted line), 5, 10, 15, 20, 25, and 30 min (× symbols) are shown. The arrows indicate the decay of AS absorption at 237 nm (pH 5.5 and 7.4) and 250 nm (10 mM NaOH), as well as the growth of absorption at 210 nm due to the nitrite ion, NO_2^-. Adapted from Shen *et al.* (*57*).

The goal of the present research is to characterize and compare the products formed in the reactions of HNO with various low-mass thiols. Angeli's salt was used as a HNO donor in these studies and the products were characterized using high performance liquid chromatography (HPLC) and mass spectrometry (MS).

1.4 Outline of thesis

Biologically active nitroxyl (HNO/NO^-) is one of the least studied nitrogen oxides and it may play a distinct role from NO in protecting the cardiovascular system. Thiols are suspected to be a major nitroxyl target (*31*). Glutathione (GSH), a major low-mass intracellular antioxidant, possesses a multitude of physiological functions (*2*) and is the most likely biological target of HNO (*28, 30*). Cysteine (Cys) and homocysteine (HCys) are thiol-containing amino acids that have been linked to many diseases (*10-12, 17-19*). It is of interest to analyze the products formed in the reactions of the low-mass thiols with HNO, since their modification could affect the functions of cells.

For studies involving the use of *N*-acetyl-glutathione (*N*-AcGSH) and *N*-acetyl-homocysteine (*N*-AcHCys), the amino group of the low-mass thiols had to be acetylated since these compounds are unavailable commercially. Few methods for acetylating amino groups have been reported and these are complex and time consuming (6-24 h) (*58*). In Chapter 2, we report a simple method to produce *N*-acetylated thiols in high-yield from the corresponding disulfides (e.g., GSSG, homocystine) using *N*-hydroxysulfo-succinimidyl (NHS) acetate. Methods to purify the *N*-acetylated derivatives are described as well as their characterization by MS.

The multitude of physiological functions attributed to low-mass thiols (*1, 2*) depend in large part on the reactivity of their sulfhydryl groups. The pK_a values of ionizable species such as thiols are critically related to their structure and activity. The reported thiol pK_a values measured under a variety of experimental conditions using different methods exhibit considerable variation (Table 3.1), and were re-measured here. In Chapter 3, the pK_a values of GSH and its constitutive dipeptides (γEC, CG), Cys, HCys, and penicillamine as well as their *N*-acetylated derivatives are reported and discussed.

In Chapter 4 and 5, the products formed in incubations of low-mass thiols with AS, a HNO donor, were analyzed by mass spectrometry (MS) and LC-MS, which are powerful methods for bioanalysis. No direct method is currently available to detect HNO (*59*). A product formed only in the reaction of HNO with a specific compound would provide a marker for HNO. Thus, in Chapter 5, the products formed on AS incubation with a number of Cys-containing dipeptides were compared to investigate the effects of the Cys-flanking residues on sulfinamide formation since HNO is to date the only nitrogen oxide (NO_x) known to convert thiols to sulfinamide.

2 SYNTHESIS OF *N*-ACETYLATED LOW-MASS THIOLS

2.1 Introduction

Intracellular low-mass thiols, such as GSH, Cys, and HCys, act as antioxidants and redox buffers with a multitude of physiological functions (*1, 2*). We have been studying the roles of these low-mass thiols in protein thionylation, *trans*-*S*-nitrosation, and their direct reactions with nitrogen oxides (NO_x; e.g., NO, HNO) (*57, 60*). For studies involving the use of *N*-acetyl-glutathione (*N*-AcGSH) and *N*-acetyl-homocysteine (*N*-AcHCys), it was necessary to *N*-acetylate the amino group in-house since these compounds are unavailable commercially. The thiol group (-SH) is highly nucleophilic making it more easily oxidized or conjugated than compounds bearing hydroxyl (-OH) or amino ($-NH_2$) moieties (*7*). Thus, it is difficult to directly acetylate an amino group without blocking any thiol group in the molecule (*58, 61*). Few methods for acetylating

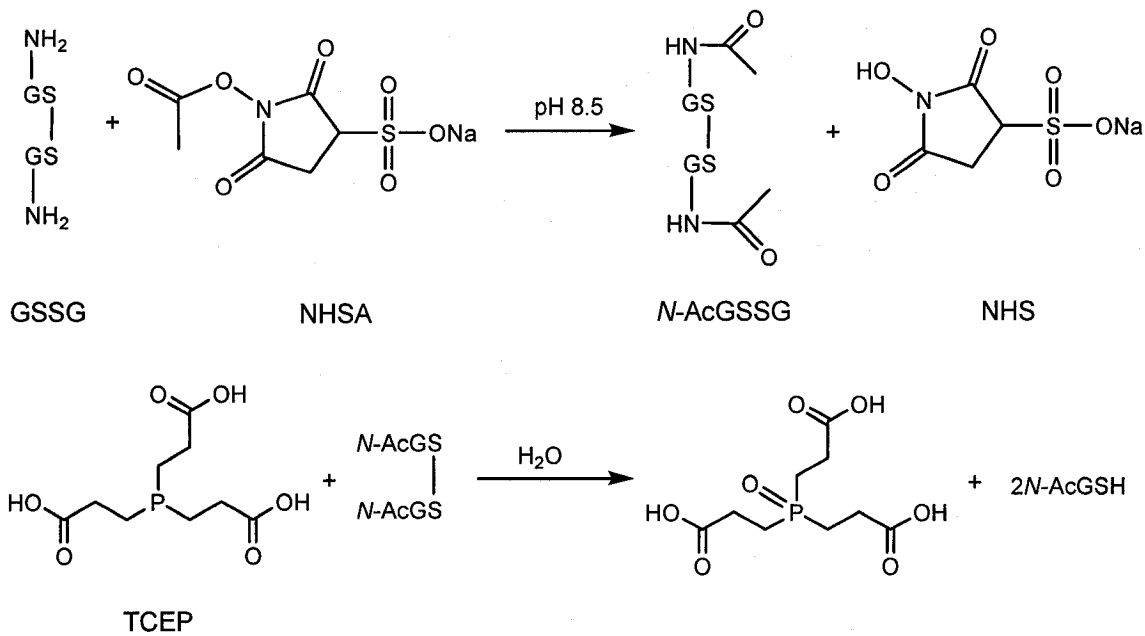

Scheme 2.1. ***N*-acetylation of GSSG by NHSA followed by reduction of the disulfide bond by TCEP**

amino groups in the presence of blocked thiols have been reported (*58*). These are slow reactions (6-24 h) (*58*), and require thiol deblocking after *N*-acetylation. Here, we report a high-yield and simple method to prepare *N*-acetylated low-mass thiols from the corresponding disulfides (e.g., GSSG, homocystine) in aqueous buffer using *N*-hydroxysulfosuccinimidyl acetate (NHSA), which is commercially available and commonly used to acetylate primary amino groups in proteins (*62-64*). The disulfide bond is reduced by immobilized *tris*(2-carboxyethyl)phosphine (TCEP, Scheme 2.1), and the *N*-acetylated derivatives are purified by simple methods optimized here.

2.2 Materials and Methods

2.2.1 Materials and solutions

DL-homocysteine (HCys), *DL*-homocystine (Hcystine), *N*-ethylmaleimide (NEM), *L*-glutathione (GSH), *L*-glutathione disulfide (GSSG) were purchased from Sigma. *N*-hydroxysulfosuccinimidyl acetate (NHSA) and *tris*(2-carboxyethyl)phosphine hydrochloride (TCEP) immobilized on agarose gel (50% water slurry) were from Pierce. For *N*-acetylation, the low-mass disulfides were dissolved in 0.1 M $NaHCO_3$ (pH 8.5) just before use and kept on ice. Strong anion-exchange (SAX) cartridges (Bond Elut-SAX , 100 MG, 3 ML) were from Varian and Sep-Pak C_{18} cartridges (1 mL) from Waters. Handee Mini-Spin columns (0.4 mL) were from Pierce. All solutions were prepared using Nanopure water (MilliQ) from a Millipore system.

2.2.2 Reaction of NHSA with GSH, GSSG, and Hcystine

To investigate thiol reactivity with NHSA, freshly prepared solutions of 2 mM

GSH were incubated with 40 mM NHSA in water at room temperature for 60 min. A 20:1 NHSA/GSH ratio was selected based on the the manufacturer's recommended ratio for modification of protein amino groups since no information on GSH modification by NHSA was available. To avoid ion suppression in the MS by buffer salts, all incubations were performed in water at pH 8.0. The 60-min GSH/NHSA incubations was mixed with NEM (NEM:GSH = 10:1), a thiol-specific reagent (eq 1.1), and incubated for another

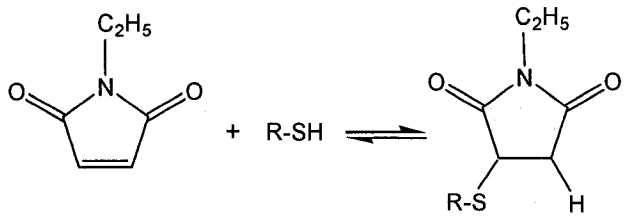

(1.1)

30 min. NEM-modified GSH prepared by 30-min incubation of GSH with NEM (NEM:GSH = 10:1) was also incubated with NHSA under the same conditions as the GSH/NHSA incubation. Since NHSA hydrolysis competes with acetylation at high pH and *N*-acetylation is extremely slow at low pH, the incubations were monitored at 10-min intervals over 60 min using an Orion Model 9810BN micro pH electrode (Thermo Electron Corporation), and NaOH or HCl was added when necessary to maintain a pH of 7-9.

To establish optimal NHSA/disulfide ratios, a freshly prepared 5 mM GSSG solution was incubated with 10 mM or 25 mM NHSA in 0.1 M $NaHCO_3$ (pH 8.5) at room temperature for 80 min. The incubations were diluted 10-fold with water and analyzed by HPLC-MS to determine the extent of *N*-acetylation *vs* NHSA/GSSG ratio and incubation time. The optimized conditions were those used above in the acetylation of GSH. Due to its low solubility (*65*), only 2 mM Hcystine dissolved in 0.1 M $NaHCO_3$ (pH 8.5) and this solution was incubated with 10 mM NHSA at room temperature for

30 min followed by HPLC-MS analysis.

2.2.3 Purification of *N*-acetylated GSSG and Hcystine

N-AcGSSG and *N*-AcHcystine were purified and desalted before reducing the disulfide bond. *N*-AcGSSG formed in 30-min GSSG/NHSA incubations was first precipitated using acetone cooled in an ice-water bath. The pH of the incubation was lowered to 4-5 with 1 N HCl, 1 mL was added to 9 mL of cold acetone, the sample was vortexed for 20 s, centrifuged at 12,000 rpm (13,000g) for 2 min, and the supernatant was discarded. A second 9-mL aliquot of cold acetone was added, the sample was vortexed and centrifuged as before, and the precipitate was air-dried in a fume hood for 1 h. The dried precipitate (~3 mg) was dissolved in 1 mL of water, and a 0.5-mL aliquot was loaded on a 3-mL Bond Elut-SAX cartridge equilibrated with 3 mL of aqueous HCl (pH 4.0). The cartridge was washed with 4 mL of the same HCl solution (pH 4.0) to remove excess salt, *N*-AcGSSG was eluted with 1 mL of 2% formic acid, and dried on a Speed Vac (Model SC110, Savant Instruments).

A 0.1-mL aliquot of 10% formic acid was added to 9.9 mL of the Hcystine/NHSA incubation, and 1 mL was loaded on a 1-mL Sep-Pak C_{18} cartridge equilibrated with 0.1% formic acid. The cartridge was washed with 4 mL of 0.1% formic acid, *N*-AcHcystine was eluted with 1 mL of 50% aqueous ACN, and the eluate was dried on the Speed Vac. Purifications were monitored by HPLC-MS.

2.2.4 Disulfide reduction on the TCEP gel

The purified *N*-acetylated disulfides were reduced with agarose-immobilized

TCEP. *N*-AcGSSG (2 mg) or *N*-AcHcystine (1 mg) were dissolved in 0.4 mL of water and mixed with a 0.2-mL bed volume of TCEP gel, which was washed twice with 0.5 mL of water. The samples were transferred to Handee Mini-Spin columns, vortexed at low speed and room temperature for 1 h, and the *N*-AcGSH or *N*-AcHCys products were collected in 2-mL microtubes by centrifugation at 3,000 rpm for 1 min. The gel was washed with 0.2 mL of water, and the washings collected by centrifugation were analyzed by ESI-MS. If residual disulfide was present, the samples were incubated with fresh TCEP gel. *N*-AcGSH and *N*-AcHCys were dried by Speed Vac at room temperature and weighed.

2.2.5 ESI-MS and HPLC-ESI-MS

Fractions collected at each step were analyzed by MS or LC-MS. Samples were diluted 10-fold into 50% aqueous ACN/0.2% formic acid or two-fold into 100% ACN/0.4% formic acid. MS analysis was carried out on a Waters Micromass Q-ToF 2 mass spectrometer operating in positive-ion mode following direct infusion of the samples into the Z-spray source. The instrument was calibrated with human [Glu^1]-fibrinopeptide B, and instrumental parameters are listed in the figure legends. Data analysis was performed using MassLynx 4.0 software (Waters Micromass).

Samples for HPLC-MS analysis were diluted 1–10-fold with water and infused into the ESI source of a SSQ 7000 mass spectrometer (ThermoFinnigan) by flow injection from a Hypersil ODS column (100×4.6 mm, 5-μm particles) attached to an Agilent 1090 HPLC. The solvents used for equilibration of the column and for the mobile phase are indicated in the figure legends. The ESI source and capillary temperature were

70°C and 250°C, respectively, and spray voltage was 4.0 kV. Mass calibration of the SSQ 7000 was carried out with L-methionyl-arginyl-phenylalanyl-alanine acetate (MRFA) and horse myoglobin (Sigma) at low and high mass, respectively. Chromatograms were also recorded with a Diode-Array Detector (DAD) at 215 nm. Data from the DAD and mass spectrometer were analyzed using ChemStation (Agilent) and XCalibur (Thermo Finnigan) software, respectively.

2.3 Results

2.3.1 Reaction of NHSA with GSH, GSSG, and Hcystine

NHSA is used to block primary amines (*62-64*). Since it was reported that NHS derivatives (e.g., NHSA) react with sulfhydryl groups (*61*), NHSA was incubated with GSH (20:1) in water to investigate its reactivity with thiols. When the thiol was blocked with NEM (m/z 433, 455; Figure 2.1B), a thiol-specific reagent (eq 1.1), the ESI mass spectrum shows peaks arising from the sodiated ions of singly acetylated GSH (m/z 497, 519; Figure 2.1C). Sodiated ions of doubly acetylated GSH (m/z 414, 436, 458; Figure 2.1D) were observed for unmodified GSH. The same spectrum was observed on addition of NEM to a 60-min GSH/NHSA incubation (Figure 2.1E), indicating that no free thiol was present after NHSA treatment. Reaction of NHSA with GSH at lower molar ratios (1:1 to 5:1) was also performed. Peaks at m/z 308, 330, 352, 374 are assigned to GSH ions, peaks at m/z 372, 394, 416 to sodiated ions of singly acetylated GSH, and peaks at m/z 414, 436, 458 to sodiated ions of doubly acetylated GSH (Figure 2.2). Sodiated ions of singly acetylated GSH dominate the spectrum of 1:1 NHSA/GSH incubation (Figure 2.2B) but doubly acetylated GSH was detected in both the 1:1 and 5:1 incubations

(Figure 2.2), indicating that the thiol group has similar reactivity with NHSA as the amino group. Thus, disulfides were used here to prevent thiol acetylation.

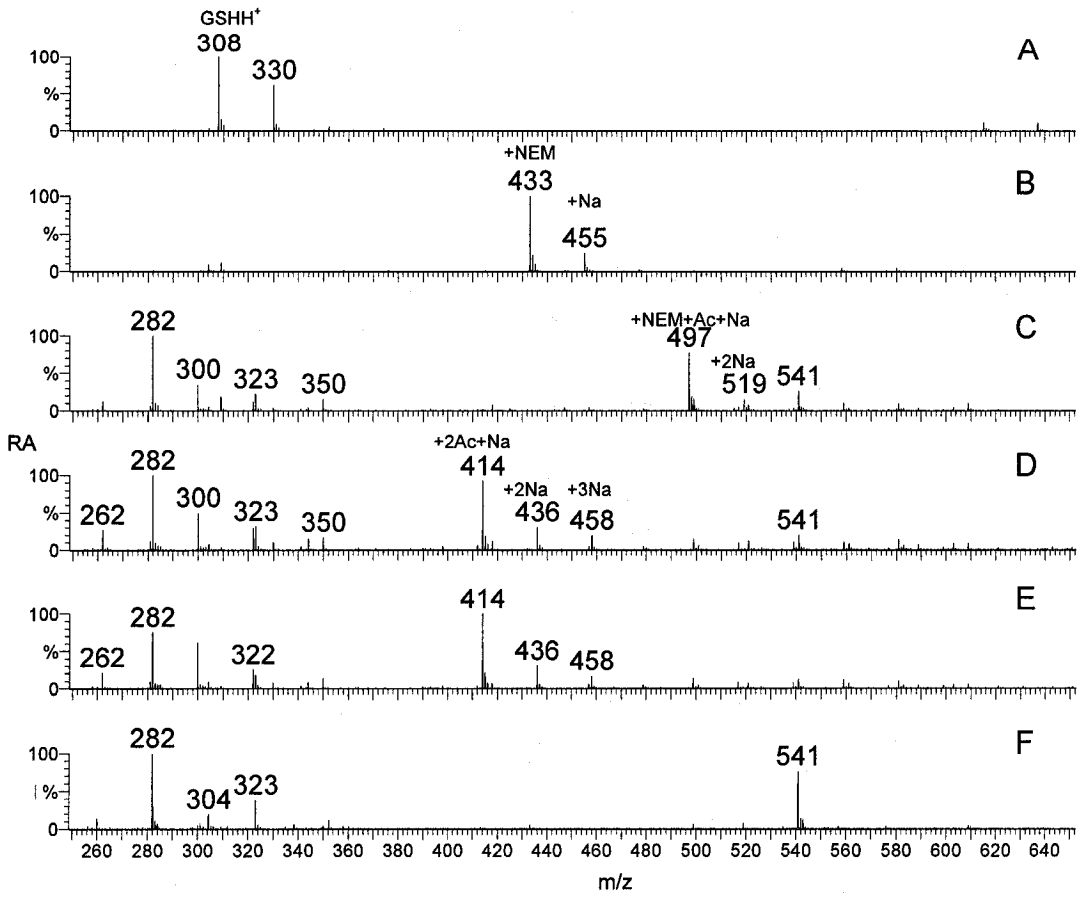

Figure 2.1. **ESI mass spectral analysis of the reaction of GSH with NHSA in water.** (A) 2 mM GSH alone, (B) 2 mM GSH with 20 mM NEM after 30 min, (C) 2 mM NEM-modified GSH with 40 mM NHSA after 60 min, (D) 2 mM GSH with 40 mM NHSA after 60 min, (E) 2 mM NHSA-treated GSH with 20 mM NEM after 30 min, and (F) NHSA alone after 60 min. Experimental conditions: Incubations were carried out in water at pH 7-9, diluted 10-fold into 50% aqueous ACN/0.2% formic acid, and directly infused into the Z-spray source of the Q-ToF 2 mass spectrometer at a flow rate of 1 μL/min. The instrument settings were: source block temperature 80°C, capillary voltage 3.2 kV, cone voltage 20 kV, collision voltage 5 V (no collision gas), MCP 2.2 kV and ToF –9.1 kV. RA is the relative abundance of the ions. Note that peaks m/z below 360 in spectra C, D, and E are present in NHSA only, spectrum F.

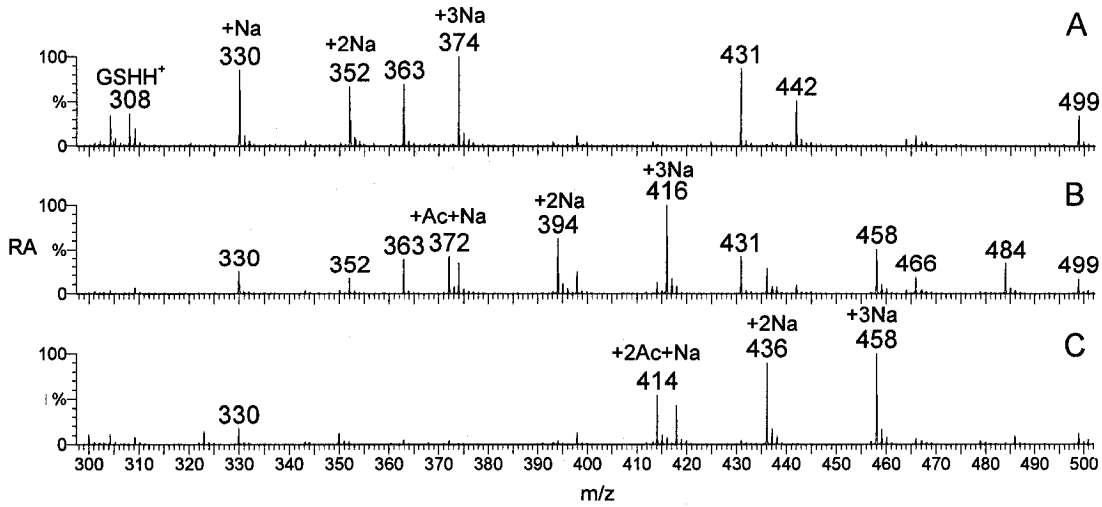

Figure 2.2. **ESI mass spectral analysis of the reaction of GSH with 1× and 5× NHSA.** (A) 5 mM GSH alone, (B) 5 mM GSH with 5 mM NHSA after 50 min incubation, and (C) 5 mM GSH with 25 mM NHSA after 30 min incubation in 0.1 M $NaHCO_3$ (pH 8.5) ar room temperature. Experimental conditions and MS parameter settings are given in the legend to Figure 2.1.

The minimum NHSA/GSSG ratio required for efficient acetylation was investigated since no data have been reported for the modification of small peptides with NHSA. After 80-min incubation in 0.1 mM $NaHCO_3$ at NHSA/GSSG molar ratios of 2:1 and 5:1 (1.0 and 2.5 NHSA per amino group), HPLC-UV and HPLC-MS analysis showed that 5-fold molar excess of NHSA is sufficient for complete acetylation of GSSG. At a molar ratio of 2:1, peaks corresponding to singly acetylated GSSG were observed in the HPLC-UV chromatograms and the mass spectra (m/z 655, Figure 2.3A, C), whereas only doubly acetylated GSSG was detected in the HPLC-UV chromatograms and mass spectra following incubation with 5-fold excess NHSA (Figure 2.3A, D). Also, 30 min is sufficient for complete GSSG acetylation with 5-fold molar excess NHSA (Figure 2.4). Hence, 30 min incubation of the disulfides with 5-fold molar excess NHSA in 0.1 mM $NaHCO_3$ (pH 8.5) were the conditions used to synthesize *N*-AcGSH. These

conditions were also found to be suitable for the synthesis of *N*-AcHCys (data not shown).

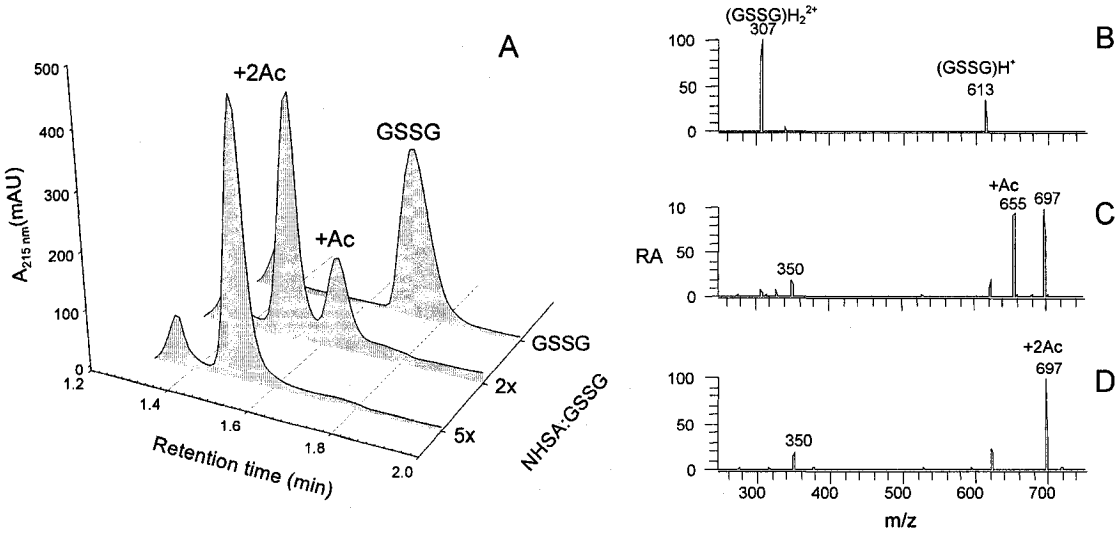

Figure 2.3. **HPLC-UV chromatograms and mass spectra of the GSSG/NHSA incubations at different NHSA/GSSG ratios.** (A) Chromatogram of free GSSG and of incubations with a 2-fold (2×) and 5-fold (5×) molar excess of NHSA. ESI mass spectra of (B) GSSG alone, (C) GSSG with 2× NHSA, and (D) GSSG with 5× NHSA. Experimental conditions: 5 mM GSSG was incubated with 10 or 25 mM NHSA in 0.1 M $NaHCO_3$ (pH 8.5) at room temperature for 80 min. The samples were diluted 10-fold with water before injection into a SSQ 7000 mass spectrometer at 1.5 mL/min from a Hypersil ODS column (100×4.6 mm, 5-μm particles) attached to an Agilent 1090 HPLC and the mobile phase was 10% aqueous ACN/0.1% formic acid. The HPLC and MS settings are given in Section 2.2.5.

2.3.2 Purification of *N*-AcGSSG and *N*-AcHcystine

The pH of the 30-min GSSG/NHSA incubations was lowered from ~8 to 4-5 with 1 N HCl. Addition of 90% cold acetone resulted in precipitation of *N*-AcGSSG, while most of the side products remained in solution. Note that *N*-AcGSSG did not precipitate from 90% aqueous acetone until the pH was >3.0 since it was present in the supernatants at pH 2.0 and 3.0 (Figure 2.5B, C). The mass spectrum of precipitated *N*-AcGSSG shows a dominant MNa^+ ion at m/z 719 (Figure 2.6B), but no *N*-AcGSSG was detected in the

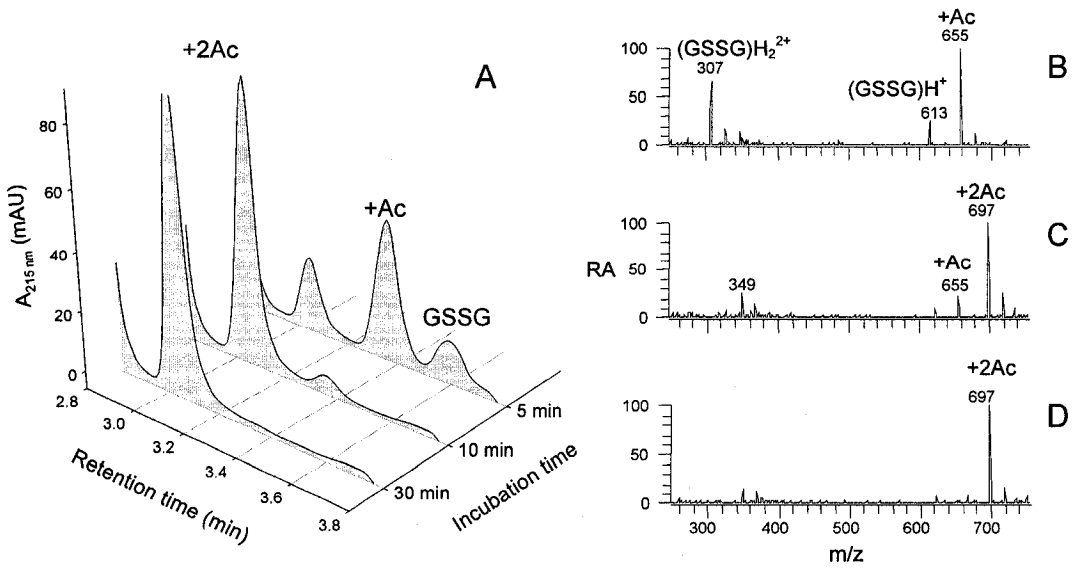

Figure 2.4. **Time course of GSSG *N*-acetylation by NHSA.** (A) HPLC-UV chromatograms and ESI mass spectra recorded after (B) 5 min, (C) 10 min, and (D) 30 min incubation of 5 mM GSSG with 25 mM NHSA in 0.1 M $NaHCO_3$ (pH 8.5) at room temperature. The conditions for the HPLC-UV and HPLC-MS analysis are given in the legend to Figure 2.3, except that the flow rate of the mobile phase was 1 mL/min.

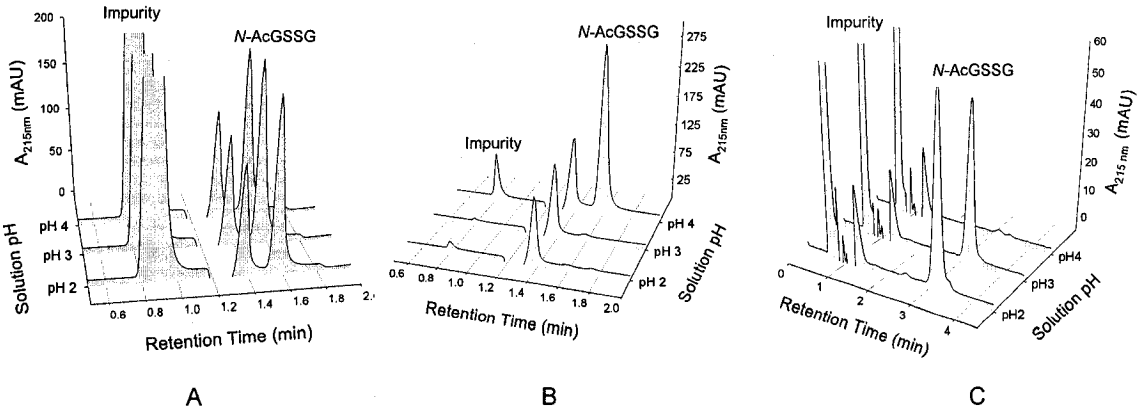

Figure 2.5. **HPLC-UV analysis of *N*-AcGSSG precipitation *vs* pH.** 30-min GSSG/NHSA incubations (A) before and (B) after precipitation in cold actone at pH 2.0, 3.0, and 4.0; (C) supernatants of *N*-AcGSSG precipitation after centrifugation. Experimental procedues: 5 mM GSSG was incubated with 25 mM NHSA in 0.1 M $NaHCO_3$ (pH 8.5) at room temperature for 30 min, the pH of 0.5-mL aliquots was adjusted to 2.0, 3.0, or 4.0 with dilute HCl, cold acetone was added (90%, v/v), and supernatants were removed after centrifugation. Samples from each step were diluted 10-fold with water before injection into HPLC column at 1.5 mL/min for A and B, and 1 mL/min for C. Other experimental conditions and are given in the legend to Figure 2.3.

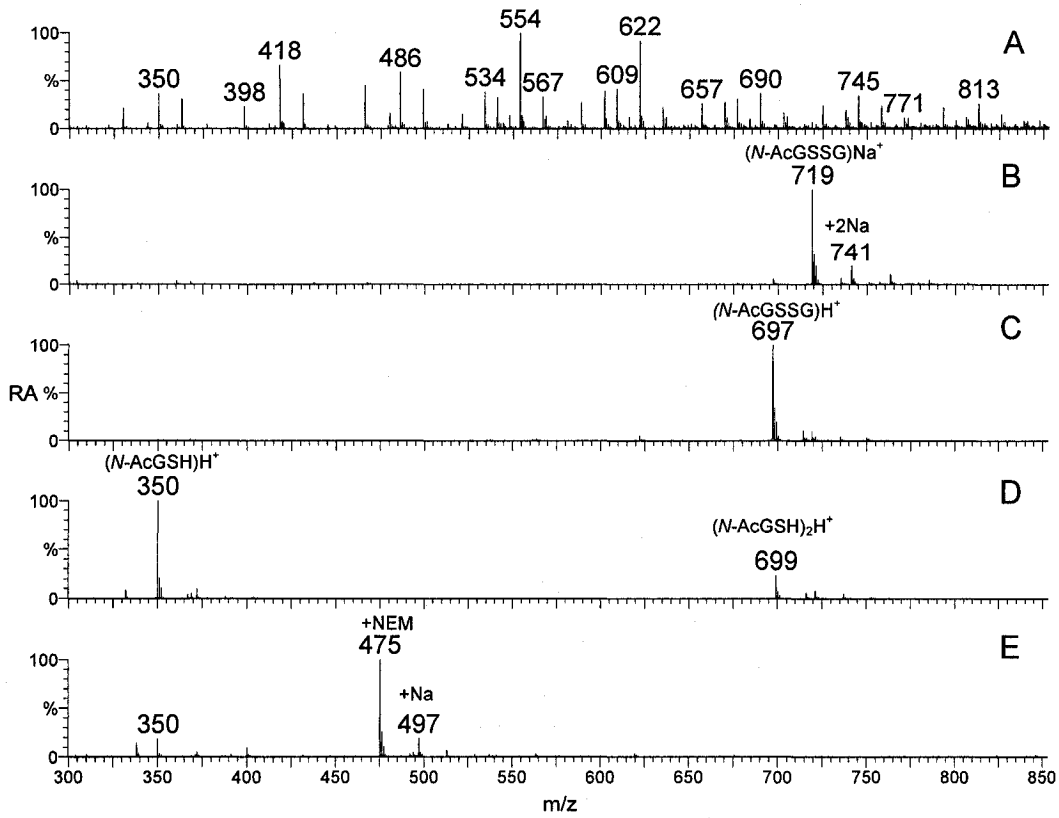

Figure 2.6. **ESI-MS monitoring of *N*-AcGSSG purification and reduction.** Mass spectrum of (A) 5 mM GSSG with 25 mM NHSA after 30 min incubation, (B) *N*-AcGSSG following precipitating with cold acetone, (C) *N*-AcGSSG following further purification on the SAX cartridge, (D) *N*-AcGSH following reduction on the TCEP gel, (E) 5 mM *N*-AcGSH from the TCEP gel after 30 min incubation with 10 mM NEM. Experimental conditions: GSSG/NHSA and *N*-AcGSH/NEM incubations were carried out in 0.1 M $NaHCO_3$ (pH 8.5) and in water (pH 2.23), respectively, at room temperature for 30 min. The *N*-AcGSSG product was purified as described in Section 2.2.3. Samples were diluted 20-fold for ESI-MS analysis which was performed as described in the legend to Figure 2.1.

spectrum of the untreated sample (Figure 2.6A) due to ion suppression from the salts and side products.

To remove sodium, the precipitated *N*-AcGSSG (~1.5 mg) was dissolved in 0.5 mL of water, loaded on the SAX cartridge equilibrated with dilute HCl (pH 4) and washed with the same solution. *N*-AcGSSG was not detected in the HPLC-UV

chromatograms of the loading and wash fractions (Figure 2.7A), indicating that it remained bound to the SAX cartridge. However, a peak at the same retention time as acetone-isolated *N*-AcGSSG (Figure 2.7A) was observed in the HPLC-UV chromatogram of the first 1-mL fraction (Figure 2.7A) eluted with 2% formic acid. The eluate containing *N*-AcGSSG was dried on the Speed Vac, redissolved in water, and examined by ESI-MS. The MH^+ ion of *N*-AcGSSG dominated the mass spectrum but no sodiated ions were detected (Figure 2.6C vs B), indicating that *N*-AcGSSG was eluated

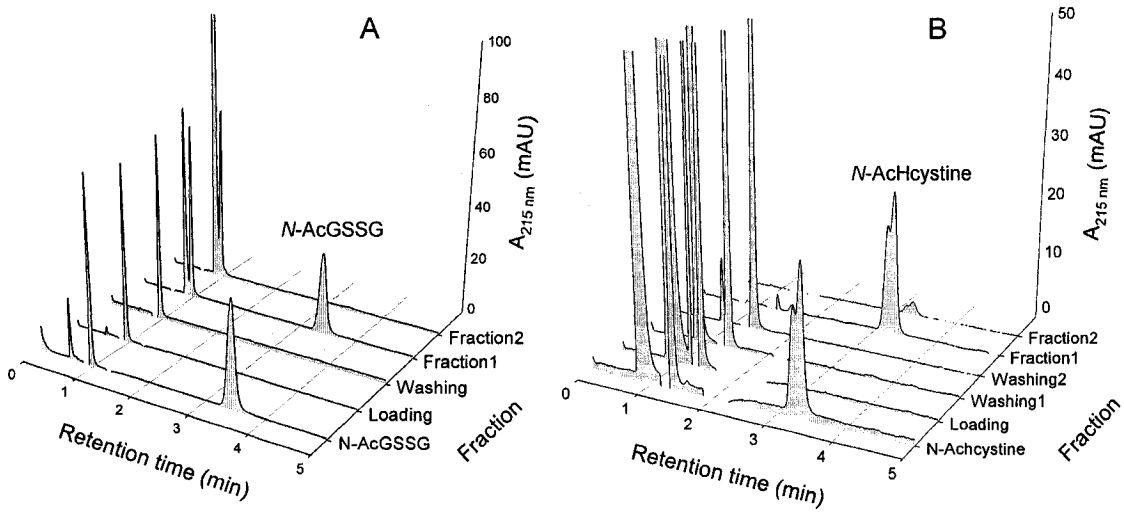

Figure 2.7. **HPLC-UV monitoring of *N*-AcGSSG and *N*-AcHcystine purification.** (A) Acetone precipitated *N*-AcGSSG (~1.5 mg) was dissolved in 0.5 mL of water and the pH was adjusted to 4.0 for loading on a SAX cartridge equilibrated at pH 4.0. Fractions (1 mL) were collected following loading, washing and elution, and analyzed by HPLC-MS. (B) A 2 mM *N*-AcHcystine and 10 mM NHSA incubation was adjusted to 0.1% formic acid (pH 2.7) for loading on a C18 cartridge equilibrated at pH 2.7, 0.5-mL fractions were collected following loading, washing and elution, and analyzed by HPLC-MS. Experimental conditions: The HPLC mobile phase, which was also used to equilibrate the HPLC column described in the legend of Figure 2.3, was 10% aqueous ACN /0.1%FA and 15% aqueous ACN /0.1%FA for *N*-AcGSSG and *N*-AcHcystine, respectively. The settings for the Agilent 1090 HPLC and SSQ 7000 mass spectrometer are given in Section 2.2.5.

from the SAX column as the free acid. *N*-AcGSSG is stable in the range of pH 2-9 (Figure 2.5A for pH 2-4 data; data at pH 4-9 not shown).

N-AcHcystine was purified on a C_{18} cartridge equilibrated with 0.1% formic acid. No *N*-AcHcystine peak was observed in the HPLC-UV chromatograms of the loading and wash fractions (Figure 2.7B), but the disulfide was eluted with 50% aqueous ACN at the same retention time as the unpurified product from the Hcystine/NHSA incubation (fraction 1, Figure 2.7B). *N*-AcHcystine was dried by Speed Vac, and ESI-MS analysis revealed that the MH^+ ion was dominant (Figure 2.8B vs A), indicating that purified *N*-AcHcystine was present as the free acid.

2.3.3 Generation of *N*-acetylated GSH and HCys

N-AcGSH and *N*-AcHCys were produced by reducing the disulfide bonds of *N*-AcGSSG and *N*-AcHcystine, respectively, using TCEP bound to agarose. The free thiols were collected by centrifugation and characterized by ESI-MS. A major peak corresponding to the MH^+ (m/z 350) and a minor peak of the protonated dimer (M_2H^+, m/z 699) were present in the mass spectrum of *N*-AcGSH (Figure 2.6D). Following 30-min incubation of *N*-AcGSH with the thiol-specific regent NEM (eq 1.1), a dominant $(M+125)H^+$ peak at m/z 475 and a minor $(M+125)Na^+$ peak at m/z 497 (Figure 2.6E) confirmed the presence of a free sulfhydryl with the expected mass increase per NEM label (125 u). Thus, *N*-AcGSH was efficiently produced in a pure form (Figures 2.6D, 2.7) by reduction of *N*-AcGSSG using the TCEP gel. Similarly, on *N*-AcHcystine reduction and alkylation, MH^+ (m/z 178), M_2H^+ (m/z 355) and $(M+125)H^+$ peaks were observed in the ESI mass spectra (Figure 2.8C, D). The peak at m/z 160 in Figure 2.8C is

assigned to the $(M-18)H^+$ ion due to loss of H_2O from *N*-AcHCys (m/z 178) in the ESI source.

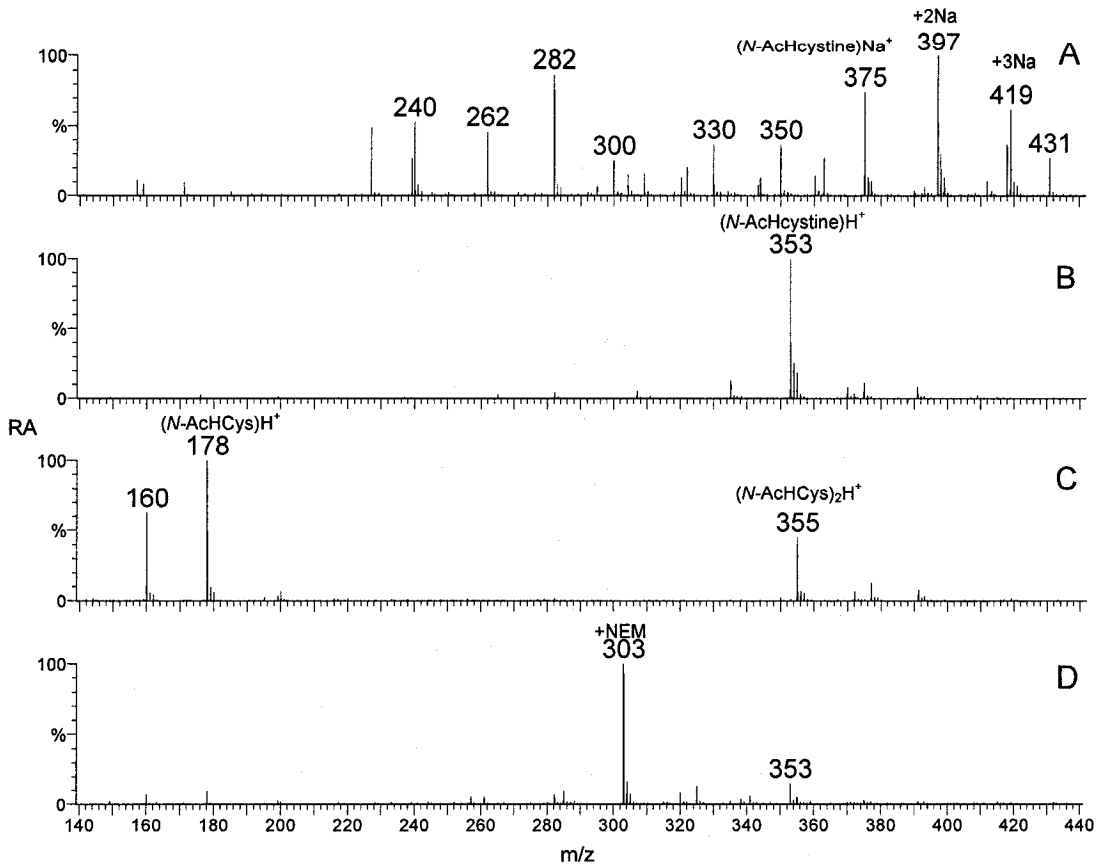

Figure 2.8. **ESI-MS monitoring of *N*-AcHcystine purification and reduction.** Mass spectrum of (A) 2 mM Hcystine with 10 mM NHSA after 30 min incubation, (B) *N*-AcHcystine following purification on the C_{18} cartridge, (C) *N*-AcHCys following reduction on the TCEP gel, (D) 2 mM *N*-AcHCys from the TCEP gel after 30 min incubation with 4 mM NEM. Experimental conditions: Hcystine/NHSA and *N*-AcHCys/NEM incubations were carried out in 0.1 M $NaHCO_3$ (pH 8.5) and in water (pH 2.77), respectively, at room temperature for 30 min. The *N*-AcHcystine product was purified as described in Section 2.2.3. Samples were diluted 10-fold for ESI-MS analysis, which was performed as described in the legend to Figure 2.1.

The identities of *N*-AcGSH and *N*-AcHCys were confirmed by accurate mass measurements on the purified products using a LC/MSD TOF MS (Agilent). The measurements were performed by Dr. Angelo Filosa at AstraZeneca Canada (Montreal). The errors in the observed masses of *N*-AcGSH and *N*-AcHCys are less than 1 ppm (Table 2.1). Yields of *N*-AcGSH and *N*-AcHCys synthesized and purified by the methods described here are >85% based on the initial disulfides.

Table 2.1. **Accurate masses of GSH, HCys, and their *N*-acetylated derivatives**[a]

Compound	Formula	M_r (u)	m/z of MH^+		Error (ppm)
			Calculated	Measured[a]	
GSH	$C_{10}H_{17}N_3O_6S$	307.08381	308.09108	308.09062	-1.49
N-AcGSH	$C_{12}H_{19}N_3O_7S$	349.09437	350.10165	350.10167	0.07
HCys	$C_4H_9NO_2S$	135.03540	136.04268	136.04256	-0.83
N-AcHCys	$C_6H_{11}NO_3S$	177.04596	178.05324	178.05329	0.29

[a] Accurate masses were measured on an Agilent LC/MSD TOF MS. Samples diluted to ~ 100 μM in water (pH 5.5) were injected into the ESI source at 3.5 mL/min from a Zorbax SB 4.6x30 mm (1.8-μm particles) column (equilibrated with solvent A at 70°C) attached to an Agilent 1100 HPLC. A 4.5-min of gradient 5-95% B (A: 0.05%TFA in water; B: ACN) was used for elution, and the MS settings were: fragmentor 125 V, ESI capillary 3000 V, gas temperature 350°C, drying gas flow 12 L/min. Internal reference masses at m/z 121.050873 and 922.009798 was used for mass calibration of the instrument.

2.4 Discussion

The procedure described here for the synthesis of *N*-acetylated GSH and HCys involves the *N*-acetylation, purification, and reduction of the corresponding disulfides. All procedures were performed at room temperature in aqueous media. The single reagent used for *N*-acetylation was NHSA which is very effective at acetyl transfer in a

short time (≤30 min) in $NaHCO_3$ (pH 8.5) (Figure 2.4). Previous methods required catalysts such as dimethylaminopyridine in addition to the acylating agent (acyl chloride) and long (6-24 h) reaction times due to the low reactivity of the GSH amino group (*58*). Also, dimethylaminopyridine and acyl chloride had to be added more than once during acetylation to increase the yield of the *N*-acetylated derivatives. The reaction was carried out in dioxane ($C_4H_8O_2$) (*58*), which was used as an aprotic solvent for *N*-acetylation, and the pH of the solution was adjusted for extraction by diethyl ether followed by ethyl acetate and then washed with water.

NHSA may be formed *in situ* by reacting NHS with acetic acid in the presence of a carbodiimide such as EDC (Scheme 2.2) (*61*). NHSA then reacts with primary amines present in solution (Scheme 2.1). The acyl group added to the primary amine can be altered by selecting a carboxylic acid containing the desired alkyl group.

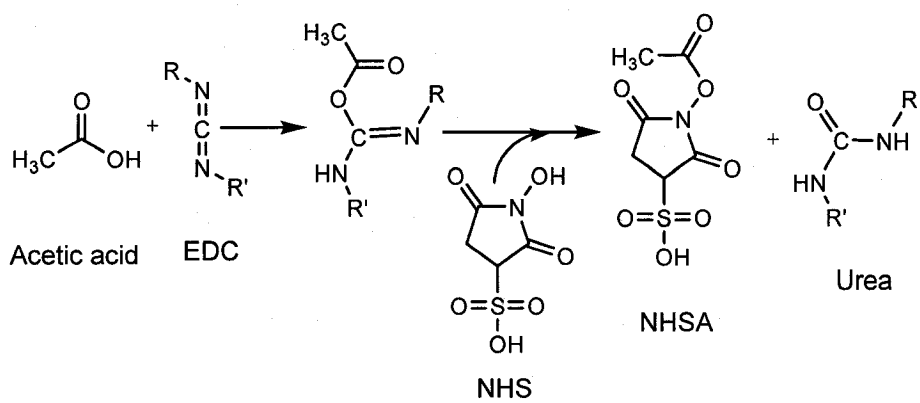

Scheme 2.2. **NHSA formation through the reaction of acetic acid with NHS** (*66*)

The *N*-acetylated disulfides formed in the RSSR/NHSA incubations are stable (Figure 2.5A) and easy to purify using solid-phase extraction (SPE). Since *N*-acetylation using NHSA is carried out in one step, the side products are NHS (Scheme 2.1) and

acetic acid formed on hydrolysis of NHSA (eq 2.1) (*67*). The *N*-acetylated thiols, produced using gel-bound TCEP suspended in water are collected from spin columns and do not need any further purification since both TCEP and its oxidized form (Scheme 2.1) are immobilized on the agarose gel. Additionally, immobilized TCEP is odorless,

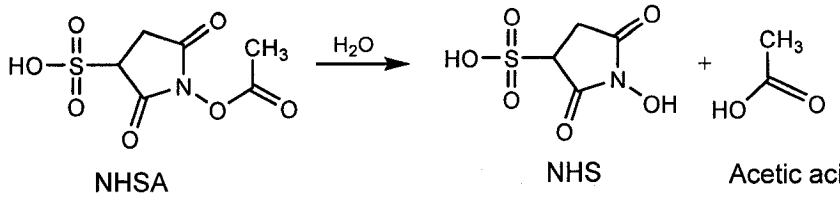

NHSA NHS Acetic acid (2.1)

effective, and stable in aqueous solution. The literature methods required removal of side products and multiple extraction steps (*58*), which can reduce product purity and yield, although *N*-AcGSH yields were not reported (*58*).

Thiol blocking and unblocking during *N*-acetylation increases reagent and solvent use, which requires more purification and lowers the yield. Acetamidomethyl and trityl groups are often used to protect the thiol of Cys residues and are removed by iodine oxidation in acetic acid/water (*68*). Benzyl groups are also used in the protection of thiols (*69*). Removal of protecting groups requires conditions that may reverse the *N*-acetylation of RSH; for example, the trityl group is removed in strongly acidic media (*68, 69*). Protection and deprotection of the GSH thiol has not been reported (*58*).

The procedure described here is a simple, fast and effective method for *N*-acetylation of free-thiol-containing molecules in high yield (>85%). A drawback of the method described here is the cost for large scale production of *N*-acetylated thiols due to the high cost of NHSA ($139 Cdn per 100 mg NHSA which will *N*-acetylate ~100 mg of GSH or ~40 mg of HCys) and of immobilized TCEP ($146 Cdn per 10 mL of a 50% water slurry, which will reduce ~ 40 mg of *N*-AcGSSG or 20 mg of *N*-AcHcystine).

3 THIOL pK_a MEASUREMENTS AND CORRELATION WITH STRUCTURE

3.1 Introduction

Intracellular low-mass thiols act as intracellular antioxidants and redox buffers. They also possess a multitude of physiological functions (*1, 2*) that depend on the reactivity of their thiol groups, which are potent nucleophilic agents. The pK_a values of ionizable groups such as thiols are critically related to their structure and activity. Many Cys residues in proteins have a thiol pK_a in the range of 8 to 9 (*70*) such that Cys residues are found predominantly in the unionized state under physiological conditions although the protein structure can dramatically affect thiol pK_as [reviewed in (*71*)]. Despite their importance in understanding reactivity, the pK_a values of only a few low-mass thiols have reported (Table 3.1). Also, the reported pK_a values were measured at different ionic strength by a variety of methods such as pH-titration, NMR, and ITC. Here, we report the pK_a values of the low-mass thiols used in this study: GSH, Cys, HCys, penicillamine and their *N*-acetylated derivatives. Also, the dipeptides derived from GSH, γEC and CG, were studied. All pK_a values were determined by pH titration in 0.15 M KCl using the GLpKa instrument and software.

3.2 Materials and Methods

3.2.1 Materials and solutions

L-cysteine (Cys; $C_3H_7NO_2S$, free base), *N*-acetyl-*L*-cysteine (*N*-AcCys), *DL*-HCys (HCys), *DL*-penicillamine (Pen), *L*-glutathione (GSH), *S*-methyl-glutathione (*S*-MeGSH), *L*-glutathione ethyl ester (γ-*L*-glutamyl-*L*-cysteinyl-glycine ethyl ester, EtGSH) were purchased from Sigma, and *N*-acetyl-*DL*-penicillamine (*N*-AcPen) from Aldrich. The

dipeptides, γ-GluCys (Des-Gly-glutathione), GluCys and CysGly were obtained from CanPeptide (Montreal). *N*-acetyl-*L*-glutathione (*N*-AcGSH) and *N*-acetyl-*DL*-HCys (*N*-AcHCys) were synthesized as described in Chapter 2. All solutions were prepared using Nanopure water (MilliQ) from a Millipore system.

Table 3.1. **Published pK_a values of ionizable groups in low-mass thiols**

Compound[a]	pK_a				I[b]	**Method**	**Ref.**
	-SH	$-NH_3^+$	α-COOH	γ-COOH			
GSH	8.74	9.66	3.51	2.13	0.10	pH-metric	(*72*)
	8.27	8.93	3.47	2.18	0.20	pH-metric	(*72*)
	9.09	9.65				NMR	(*72*)
	9.42					ITC	(*73*)
	8.68	9.55			0.10	pH-metric	(*74*)
	8.75	9.65			0.15	?	(*75*)
	8.56	9.57			0.30	pH-metric	(*76*)
EtGSH	8.46	9.50	2.33		0.10	pH-metric	(*72*)
	8.17	8.97	2.47		0.20	pH-metric	(*72*)
Cys	8.38	10.09			0.30	calculated	(*77*)
	8.22					ITC	(*73*)
	8.48	10.55			0.15	?	(*75*)
	8.53	10.36			0.16	pH-metric	(*78*)
	8.15	10.37			0.30	pH-metric	(*76*)
***N*-AcCys**	9.52				0.30	pH-metric	(*76*)
HCys	8.70	10.46			0.30	pH-metric	(*76*)
Pen	10.29	8.03			0.30	calculated	(*77*)
***N*-AcPen**	10.28		3.48		0.30	pH-metric	(*77*)
	9.90				0.30	pH-metric	(*76*)

[a] Abbreviations and structures are given in Figure 3.3.

[b] Ionic strength

3.2.2 Potentiometric determination of pK_a values of low-mass thiols

The pK_a values reported here were measured by Cynthia Bazin at Merck Frosst (Montreal, Canada) by pH-metric titrations using a GLpKa instrument (Sirius Analytical Instruments) running RefinementPro V1.104 software. Titrations were performed in aqueous media (0.15 M KCl) at 25°C using 0.5 M HCl or 0.5 M KOH as titrants with 60 mL/min argon flow to remove CO_2 in solution. The KOH titrant was standardized with potassium hydrogen phthalate (KHP) (Aldrich). Sample solutions were pre-acidified to pH 1.8-2.0 with 0.5 M HCl, and titrated with standardized 0.5 M KOH solution to pH values between 3.0 and 11.0. The pH change per titrant addition was about 0.2 pH units and 25-30 pH readings were collected for each titration. For each compound, three separate tirations were performed, and average pK_a values along with their standard deviations were calculated with the RefinementPro software.

The four-parameter Four-Plus™ technique was used to standardize the pH electrode in aqueous medium as previously described (*79, 80*). The operational pH scale was established by calibrating the pH measuring circuit with a single aqueous phosphate buffer (pH 7.0) and assuming the Nernst slope. The operational pH reading is related to the concentration pH ($p_cH = -\log[H^+]$) by:

$$pH = \alpha + Sp_cH + j_H[H^+] + j_{OH}[OH^-] \qquad (3.1)$$

The Four-Plus parameters used here were: $\alpha = 0.100$, $S = 1.000$, $j_H = 0.0$, $j_{OH} = -1.0$. The intercept parameter α in aqueous solution mainly corresponds to the negative logarithm of the activity coefficient of H^+ at the working temperature and ionic strength. The S factor denotes the ratio between the actual slope and the Nernst slope. The j_H term corrects the pH readings for the nonlinear pH response due to liquid-junction and

asymmetry potentials in moderately acidic solutions, while the j_{OH} term corrects for the high-pH nonlinear effect. These parameters are determined by a weighted non-linear least-squares procedure (*81*).

3.3 Results

3.3.1 pK_a values

Difference curves were generated from the sample titrations *vs* a blank aqueous titration. These curves, which are called Bjerrum difference plots ($\bar{n}_H$ *vs* pH, where $\bar{n}_H$ is the average number of bound protons), provide the initial estimates of the pK_a values, called the "seed" pK_a. Bjerrum plots of diprotic HCys and Pen are presented in Figure 3.1 and pK_a values were obtained at $\bar{n}_H$ = 0.5 and 1.5, corresponding to groups that are 50% ionized. Distribution curves of the XH_n species directly show the pK_a values measured, and curves for HCys and Pen are presented in Figure 3.2.

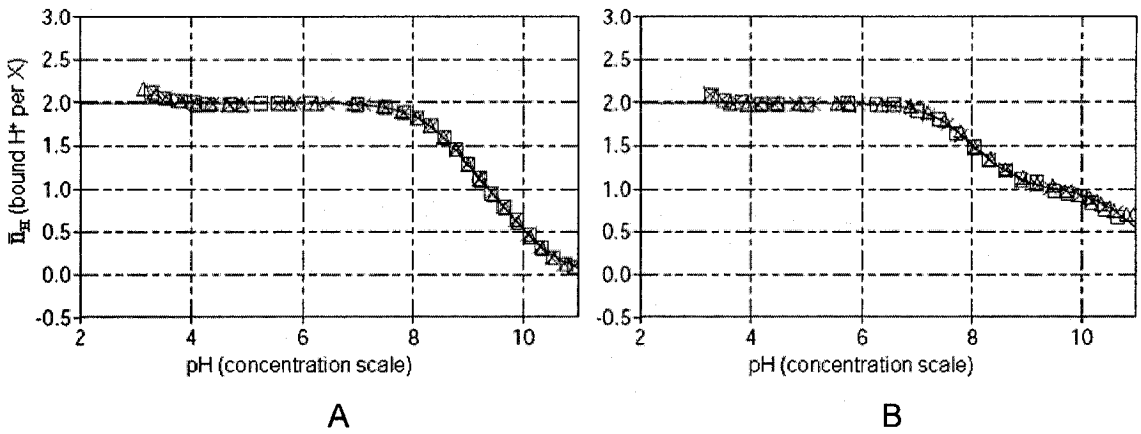

Figure 3.1. **Bjerrum difference plots in the potentiometric titration of HCys and Pen.** The titration of (A) HCys and (B) Pen was performed in 0.15 M KCl at 25°C. The symbols ×, □, and Δ represent three replicative titrations. Experimental conditions are given in Section 3.2.2.

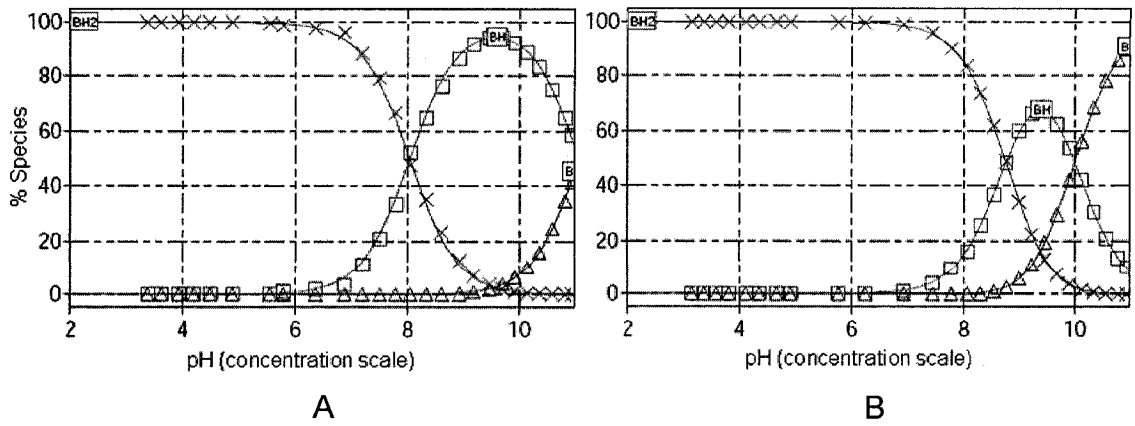

Figure 3.2. **Distribution curves of species in solution as a function of pH.** Species of (A) HCys and (B) Pen in 0.15 M KCl solution at 25°C. The symbols ×, □, and Δ represent different species formed during the titration and the solid lines were calculated by the Refinement Pro V1.104 software from the input data (Section 3.3.1).

A theoretical Bjerrum plot (solid lines in Figure 3.1) was constructed by calculating the pH at each titrant volume used in the experiment. The calculation requires fixed data including MW, titration concentration, variable data including acidity, sample concentration, and the seed pK_as from the experimental data. Input of the molecular formula (X, XH, XH_2...XH_n) and the expected number of pK_as allows the instrument to create a model for ionization which is helpful for pK_a assignment. Commercial programs (e.g., ACD Labs, Pallas) for pK_a prediction were used in some cases. These work by a fragment approach, applying corrections to a parent compound of known pK_a (substituent method), or by using mathematical models (*82*). The experimental pH values (pH_{obs}) are compared to the calculated pH values (pH_{calc}), and the variable data and pK_as are adjusted systematically to minimize differences between pH_{obs} and $pH_{calc.}$ A goodness-of-fit (GOF) is calculated after each iteration, and the pK_a values that yield the lowest GOF are taken to be the measured pK_as. Low GOF values indicate better quality solutions and an ideal GOF value is 1.00. The GOFs for HCys and Pen are 2.38 and 1.48, respectively,

and the Bjerrum plots and GOFs of the other RSHs are given in Appendix 3.1.

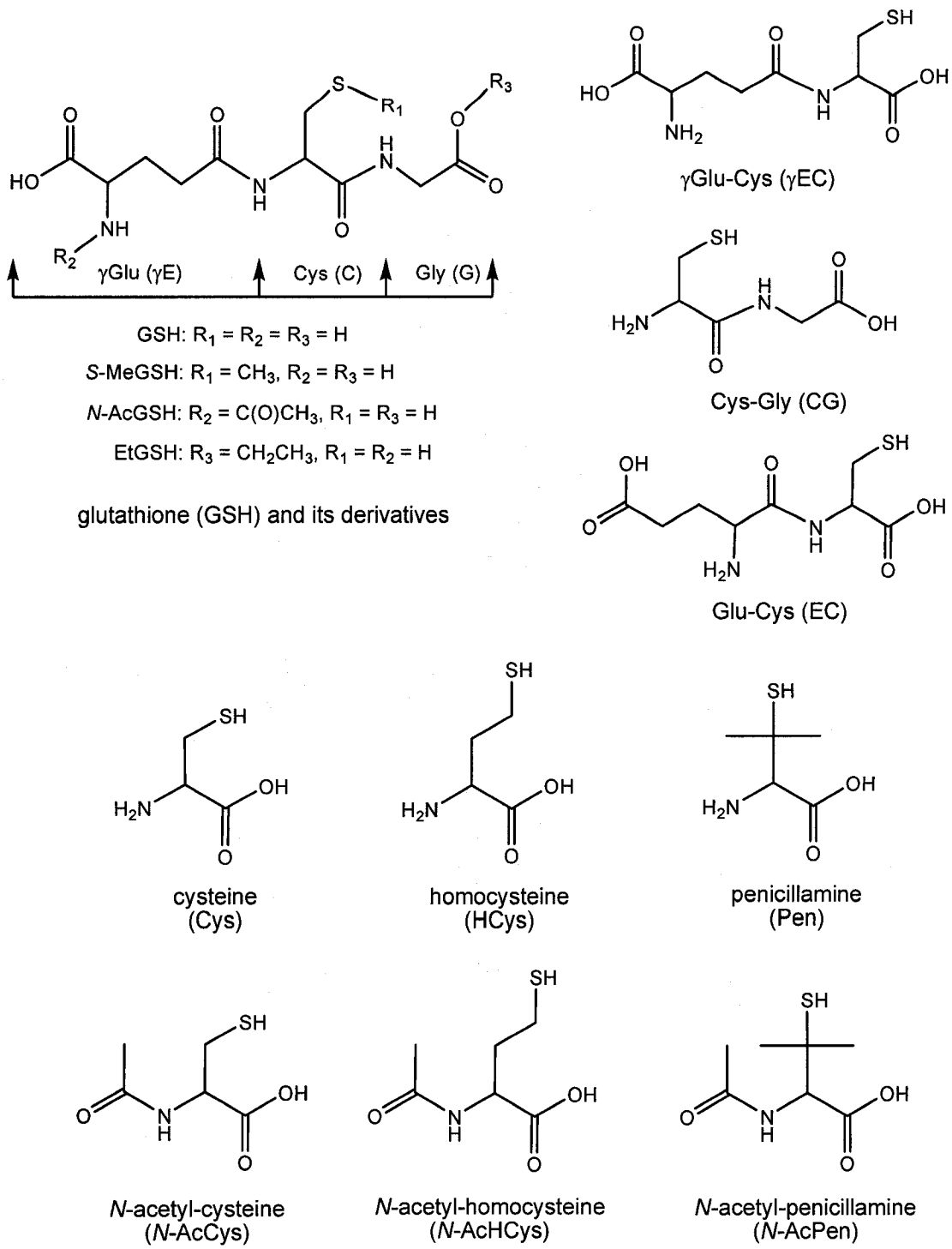

Figure 3.3. **Structures of the low-mass thiols studied here**

3.3.2 Thiol pK_a values

Ionization of neighbouring groups affect thiol reactivity. Negative charges near the thiol tend to destabilize the thiolate and decrease reaction rates, while positive charges are expected to increase the reactivity (*83*). For example, the C-terminal residue in GSH reportedly affects the reactivity of its thiol (*72*). Upon *N*-acetylation, the thiol pK_as of Cys and HCys increase whereas those of GSH and Pen decrease (Table 3.2), indicating that *N*-acetylation alters the amino group's influence on thiol activity. However, the decrease in thiol pK_a (−0.17) on GSH *N*-acetylation is significantly less than that (−0.66) on

Table 3.2. **Observed pK_a values of the ionizable groups in the low-mass thiols used in this study**

Groups	pK_a[a]						
	GSH[b]	***N*-AcGSH**	**EtGSH**	***S*-MeGSH**	**γEC**	**CG**	**EC**
-SH	9.16 ± 0.02	8.99 ± 0.05	8.55 ± 0.02	---	11.23 ± 0.03	9.24 ± 0.02	10.32 ± 0.04
α-NH_3^+	9.06 ± 0.02	---	9.33 ± 0.02	9.00 ± 0.04	9.28 ± 0.01	6.84 ± 0.02	8.04 ± 0.04
α-COOH	3.72 ± 0.02	3.68 ± 0.07	3.63 ± 0.03	3.32 ± 0.05	2.90 ± 0.03	3.4 ± 0.03	3.83 ± 0.05
γ-COOH	< 3.0	3.39 ± 0.10	---	3.10 ± 0.08	2.60 ± 0.06	---	2.96 ± 0.08
	Cys	***N*-AcCys**	**HCys**	***N*-AcHCys**	**Pen**	***N*-AcPen**	
-SH	8.33 ± 0.01	9.53 ± 0.01	8.76 ± 0.01	9.66 ± 0.05	11.08 ± 0.03	10.21 ± 0.02	
α-NH_3^+	10.84 ± 0.02	---	10.00 ± 0.02	---	8.03 ± 0.01	---	
α-COOH	< 3.0	< 3.0	< 3.0	3.44 ± 0.05	< 3.0	3.43 ± 0.02	

[a] Titrations were performed in aqueous media (0.15 M KCl) under argon (60 mL/min) at 25°C

[b] Structures are given in Figure 3.3.

esterification (Table 3.2). Also, the thiol pK_a increased dramatically (+2.07) when the Gly residue was removed from GSH (γEC), but increased only slightly (+0.08) when the γGlu was removed (CG) (Table 3.2, Figure 3.3). Thus, the N-terminal residue has much

less effect on the thiol pK_a than the C-terminal of GSH. However, since the thiol pK_a of EC (10.32) is lower than that of γEC (11.23) but higher than that of CG (9.24), the proximity of amino group (Figure 3.3) obviously modulates the thiol pK_a.

3.3.3 Amino and carboxylate pK_a values of low-mass thiols

The pK_as of the amino and carboxylate groups determine the ionized or charged state of low-mass thiol around neutral pH. The α-carboxylate of GSH and its derivatives and related dipeptides exhibit pK_a values between 3 and 4 except that of γEC is <3. The γ-carboxylate pK_a values of GSH, γEC and EC are <3 but those of *N*-AcGSH and EtGSH are between 3 and 4 (Table 3.2). The α-carboxylate pK_a values of the other thiols are <3 except those of *N*-AcHCys and *N*-AcPen, which lie between 3-4. Thus, the carboxylate is always ionized and carries a negative charge at pH >4.

The α-amino pK_a of CG (6.84) is much lower than that of free Cys (10.84), indicating the stabilizing effect of the carboxylate on the α-NH_3^+ group. The α-amino pK_a of EC (8.04) is between that of CG and Cys due to the presence of its γ-carboxylate (Figure 3.3). The α-amino pK_a value of HCys (10.00) is slightly lower than that of Cys (10.84), but both are higher than that of Pen (8.03). Cys and Pen differ by substitution at the β-carbon (Figure 3.3), which results in reversing the α-amino and thiol pK_a values. Modification of the thiol (*S*-MeGSH, 9.00) or the C-terminal carboxylate (EtGSH, 9.33) of GSH (9.06) does not change the α-amino pK_a value significantly (Table 3.2) since in all cases the α-carbon bears a carboxylate group (Figure 3.3).

3.4 Discussion

The pK_a values of 13 low-mass thiols and their derivatives were reported here at an ionic strength of 0.15 M. Only five of the compounds were examined previously (Table 3.1), and there is good agreement in the pK_a values (Table 3.2 *vs* 3.1). The difference between our results and the literature data might be due to differences in the measurement methods (e.g., NMR, ITC) and the experimental conditions used such as ionic strength. Acid pK_as are lowered with increasing ionic strength (*84*); for example, the pK_a of benzoic acid is 4.20 at 0.0 M I and 3.99 at 0.15 M I. Base pK_as increase with increasing ionic strength but the effect is not as large as with acids; for example, the pK_a of pyridine is 5.23 at 0.0 M I and 5.31 at 0.5 M I.

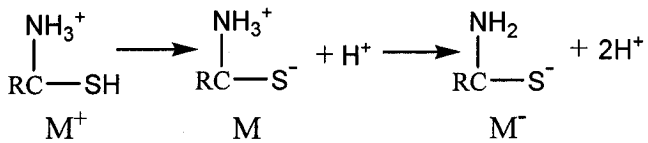

(3.1)

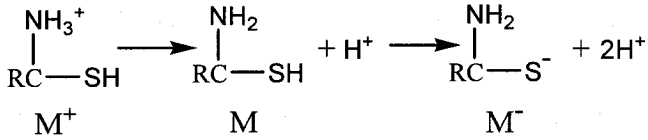

(3.2)

The effects of *N*-acetylation on thiol ionization depends on the relative values of the thiol and α-amino pK_as. If $pK_a(NH_3^+) > pK_a(SH)$ (e.g., Cys, Hcys; Table 3.2), the molecule is neutral on ionization of the thiol (eq 3.1), but negatively charged in the *N*-acetylated form, so the thiol pK_a increases. However, if $pK_a(NH_3^+) < pK_a(SH)$ (e.g., Pen; Table 3.2), the molecule is negatively charged on thiol ionization (eq 3.2) and *N*-acetylation decrease the thiol pK_a. Since the α-amino and thiol pK_a values of GSH are very close, the thiol pK_a changed only slightly (Table 3.2) on *N*-acetylation, but decreases

by -0.61 units when the C-terminal carboxylate group was blocked by esterification (Table 3.2, Figure 3.3). Furthermore, the thiol pK_a of γEC (11.23) and EC (10.32) are 2 and 1 pH units, respectively, higher than those of GSH and CG. This suggests that the C-terminal residue (G) exerts more control than the N-terminal residue (γE) over thiol ionization in GSH, consistent with the report (*72*) that the C-terminal carboxylate stabilizes the protonated form of the thiol or that thiol ionization is suppressed by neighbouring acidic groups (*85*). Also, neutralization of the charge on the α-amino group by the γ-carboxylate increases the thiol pK_a [CG (9.24) < EC (10.32) < γEC (11.23)] (Table 3.2) whereas esterification of the C-terminus decreases this pK_a [EtGSH (8.55) < GSH (9.16)]. Clearly, in the CX dipeptides the carboxylate group interacts more with the thiol to suppress its ionization than in free Cys or the XC dipeptide [e.g., pK_a Cys (8.33) < pK_a CG (9.24)] (Table 3.2).

Appendix 3.1

The Bjerrum difference plots for the potentiometric titrations of the RSHs and the GOFs are presented below. The experimental conditions are given in the legend to Figure 3.1.

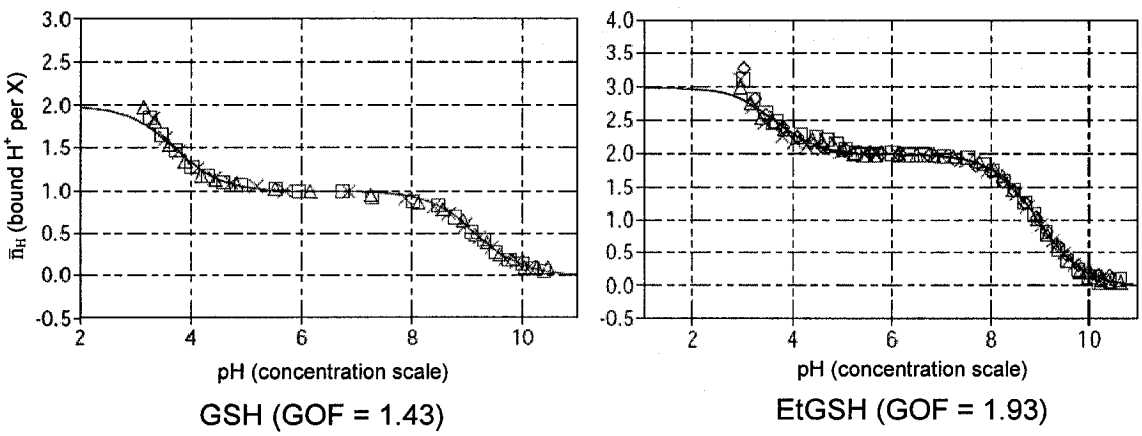

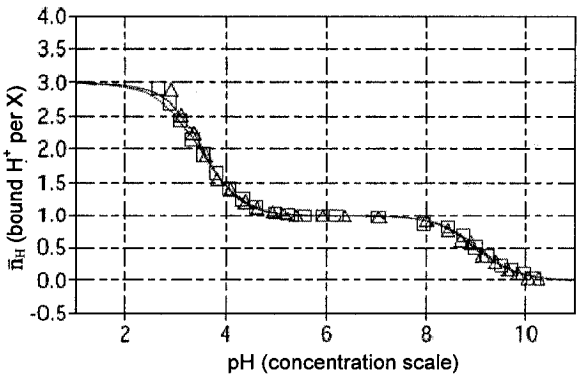

N-AcGSH (GOF = 0.50)

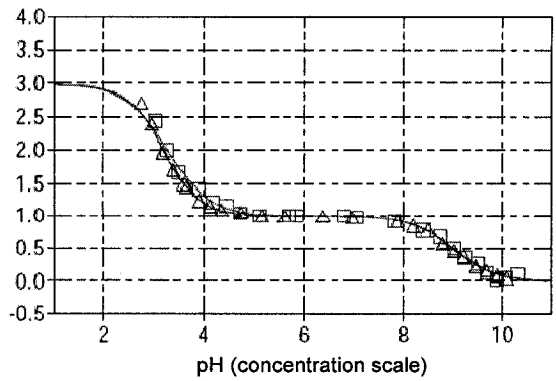

S-MeGSH (GOF = 0.70)

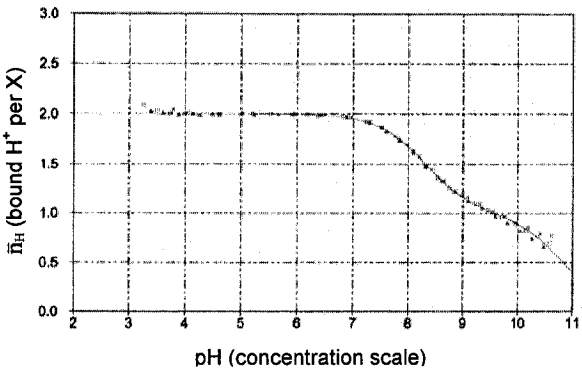

Cys (GOF = 1.50)

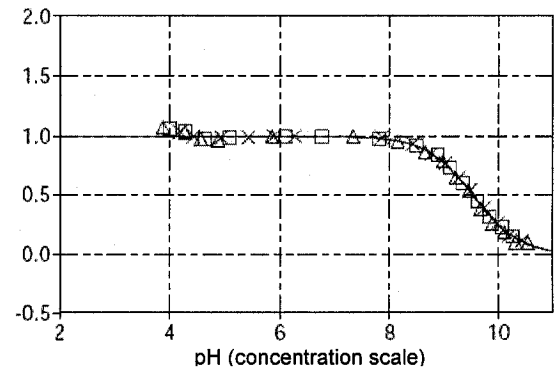

N-AcCys (GOF = 1.62)

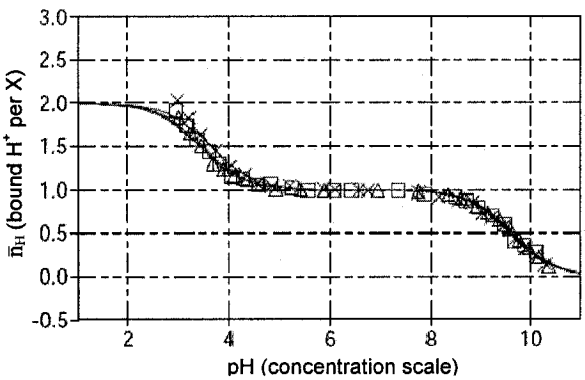

N-AcHCys (GOF = 0.80)

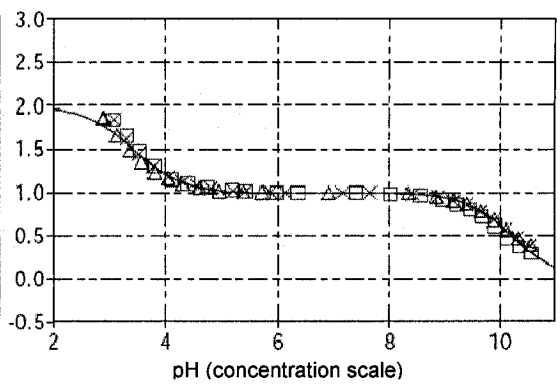

N-AcPen (GOF = 1.91)

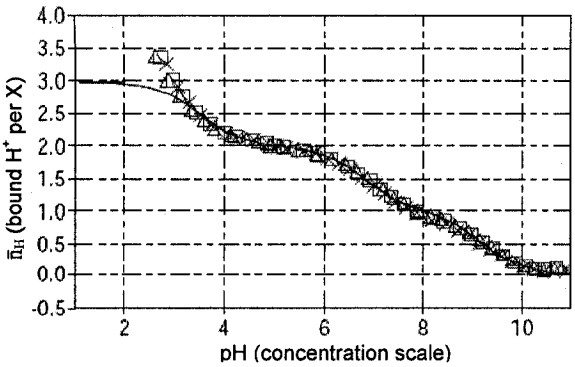

CG (GOF = 3.00)

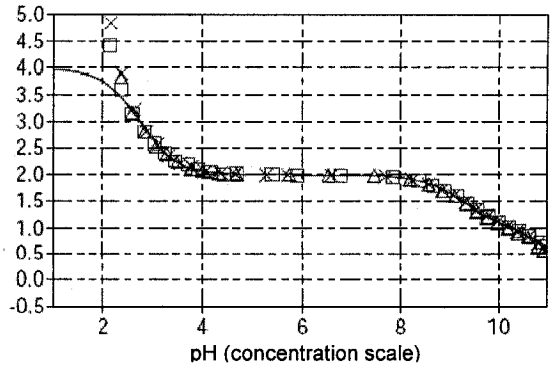

γEC (GOF = 1.10)

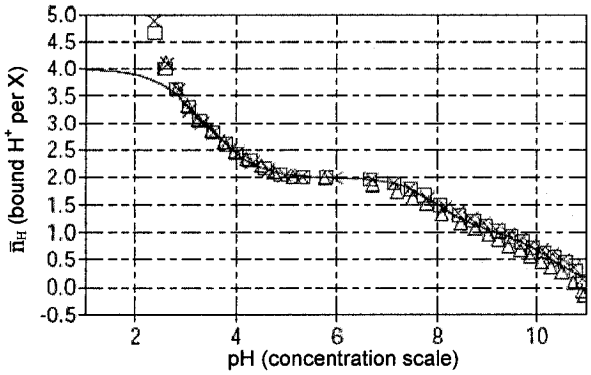

EC (GOF = 2.57)

The Distribution curves of XH_n species in solution as a function of pH for the RSHs are presented below. The experimental conditions are given in the legend to Figure 3.2.

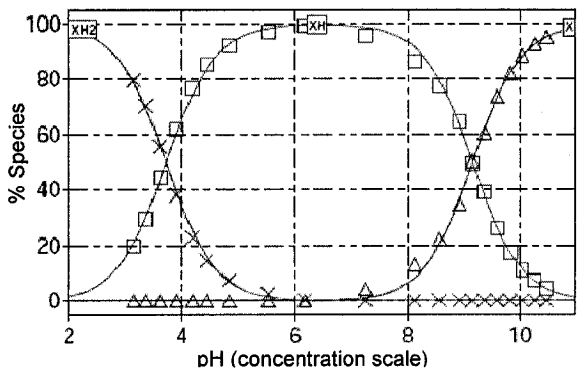

GSH

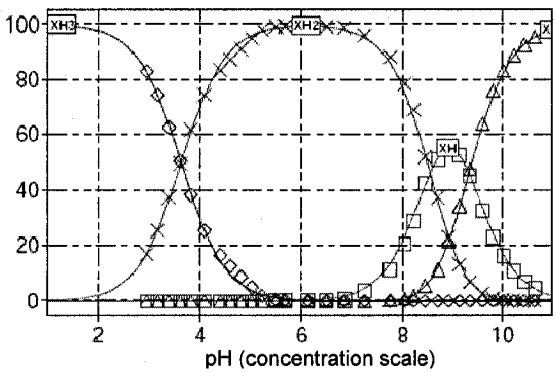

EtGSH

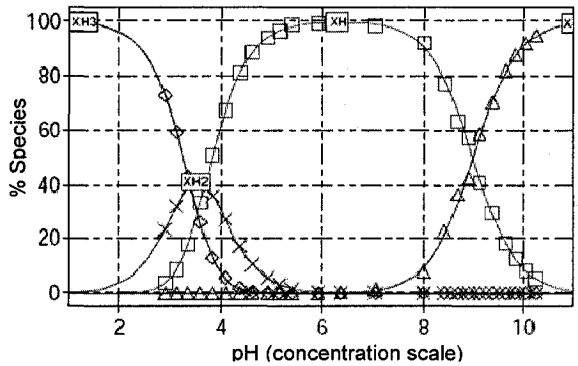

N-AcGSH

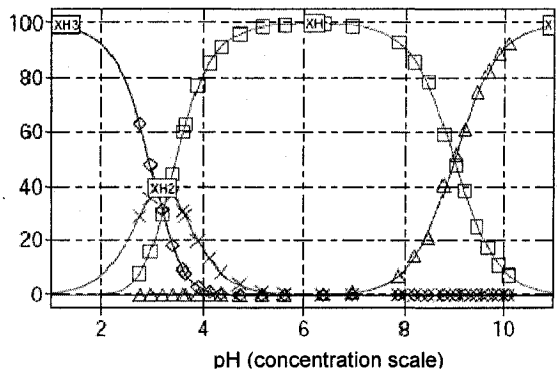

S-MeGSH

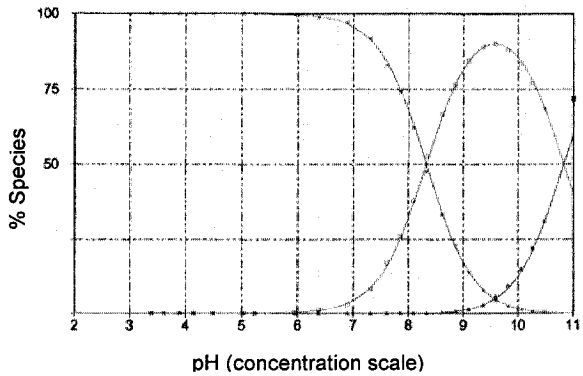

Cys

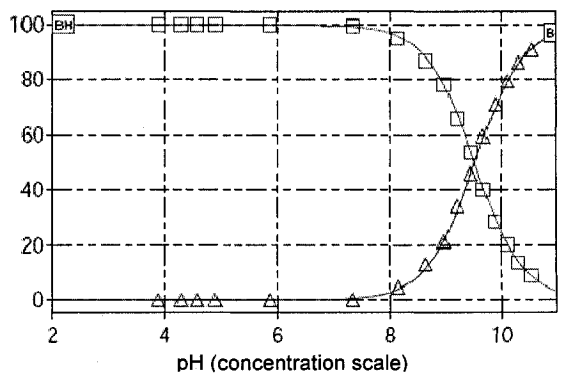

N-AcCys

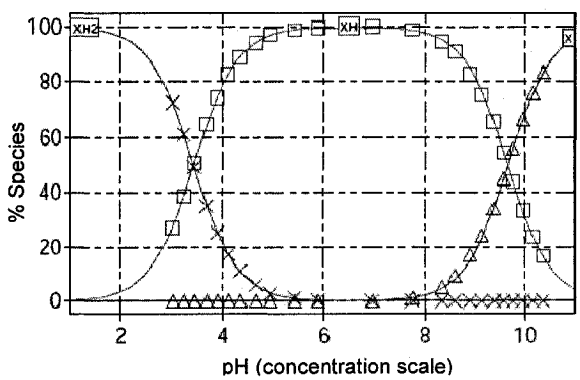

N-AcHCys

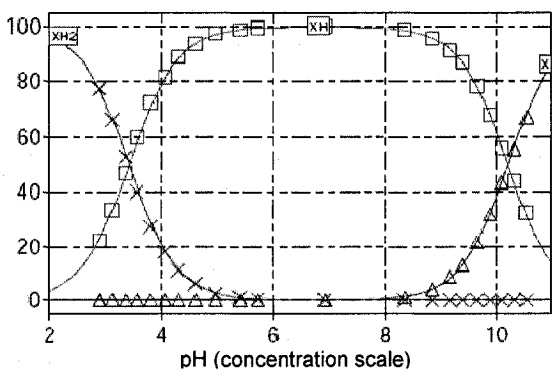

N-AcPen

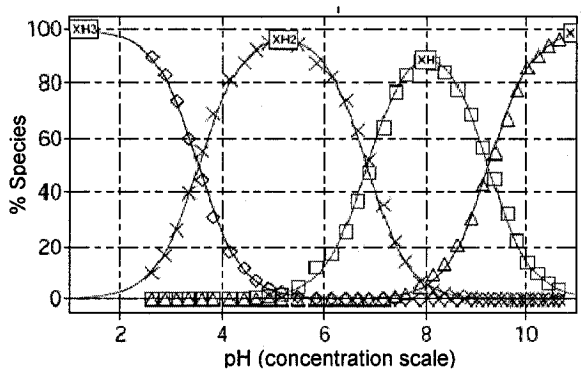
% Species
pH (concentration scale)
XH3
XH2
XH

CG

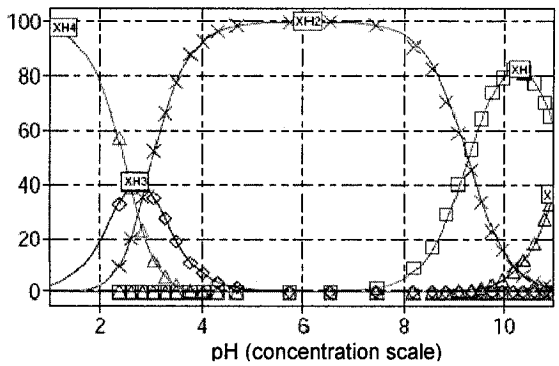
pH (concentration scale)
XH4
XH2
XH3
XH

γEC

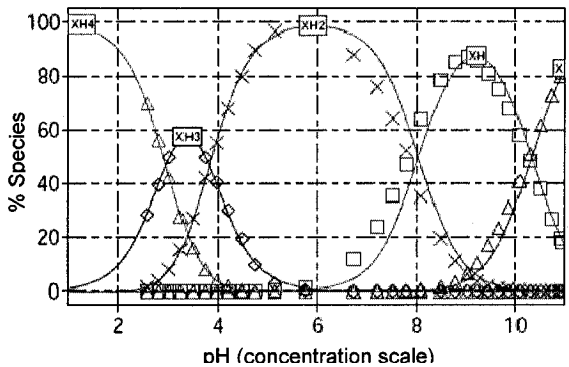
% Species
pH (concentration scale)
XH4
XH2
XH3
XH

EC

4 REACTIONS OF GSH AND ITS DERIVATIVES WITH HNO

4.1 Introduction

GSH is the predominant intracellular low-mass thiol. It is present in the cells of all organisms at millimolar concentrations (0.5-10 mM) (*1*), and possesses a multitude of physiological functions (*2*). Virtually all functions of GSH depend on the reactivity of its thiol group. Biologically active nitroxyl (HNO/NO^-, pK_a11.4) is highly thiophilic (*27*) and we have reported the formation of sulfinamides and disulfides on incubation of protein-based thiols with HNO (*57*). GSH has been proposed the most likely biological target of HNO (*28*) and it is almost completely depleted upon the exposure of fibroblasts to HNO (*30*). The ability of HNO to affect intracellular GSH levels should allow it to alter cell function or to be involved in cell signaling.

It has been proposed that HNO generated at physiological pH reacts readily as an electrophile with thiols to yield a *N*-hydroxysulfenamide addition product (*27, 31*). This intermediate can generate a disulfide or sulfinamide depending on the reaction conditions (*31, 57*). In this study, we have characterized by electrospray ionization mass spectrometry (ESI-MS) the products of the reaction of GSH with AS-derived HNO (Scheme 4.1). Formation of GSSG and sulfinamide ($GSONH_2$) were reported to follow path ***a*** and ***b***, respectively, in Scheme 4.1 (*31, 86*). Also, (M+14) adducts corresponding to the mass increase expected on intramolecular sulfinamide formation via path ***c*** (*57*) were reported in our previous studies on the reactions of protein-based thiols with HNO (*57*). The present ESI-MS results confirm the generation of the sulfinamide and disulfide during the incubation of GSH with HNO at pH 5-9, with competitive generation of the disulfide at higher pH and GSH concentration, consistent with Scheme 4.1. However, the

(M+14) adduct observed in the mass spectrum is due to fragmentation of the sulfinamide formed in ESI source and not to intramolecular sulfinamide formation. Interestingly, GSH, GSH monoethyl ester, *N*-acetyl-GSH, γ-EC and CG (Figure 3.3), all yield different sulfinamide/disulfide ratios on reaction with HNO as reported here.

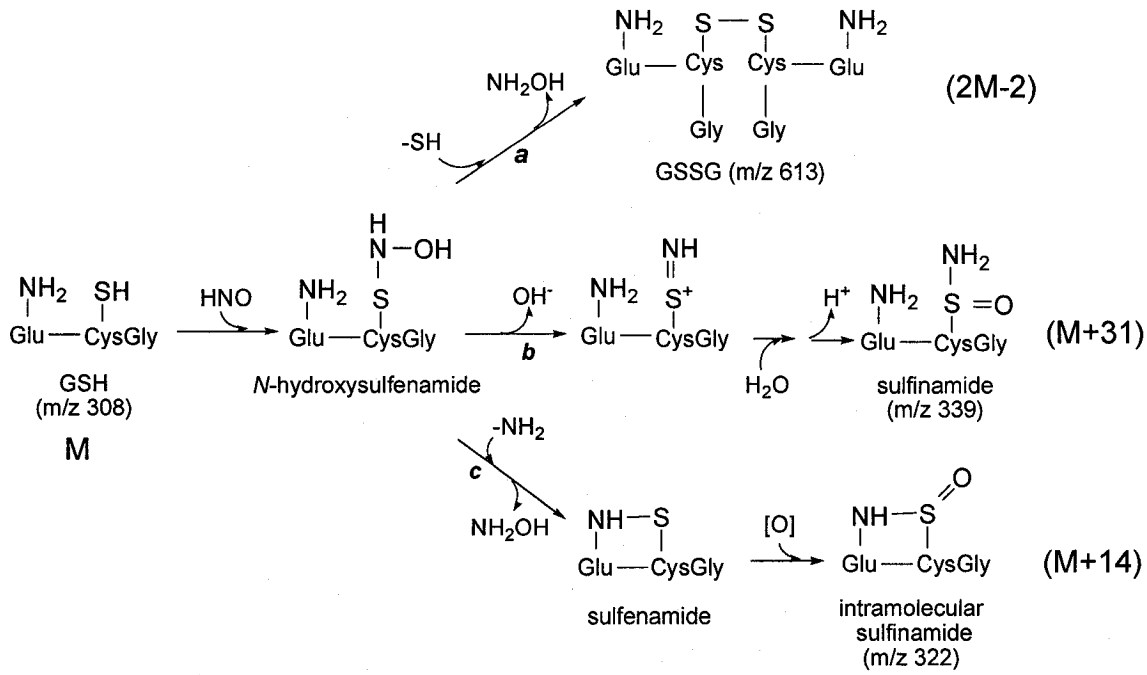

Scheme 4.1. **Proposed reactions of GSH with HNO.** M is mass of GSH; adapted from (*31*) and (*57*)

4.2 Materials and Methods

4.2.1 Materials

Stock ~300-450 mM solutions of Angeli's salt (AS; Cayman) were prepared in 10 mM NaOH, stored at -20°C and used once thawed to avoid decomposition (*51*). Sodium nitrite ($NaNO_2$), *L*-glutathione reduced (GSH), *L*-glutathione oxidized (GSSG), *S*-methyl-glutathione (*S*-MeGSH), *L*-glutathione reduced ethyl ester (γ-*L*-Glutamyl-*L*-cysteinyl-glycine ethyl ester, EtGSH) and the dipeptides γ-EC (des-Gly-glutathione reduced form,

88%) and CG (85%) were purchased from Sigma. *N*-AcGSH was synthesized and purified as described in Chapter 2. Strong anion-exchange (SAX) cartridges (Bond Elut-SAX , 100 MG, 3 ML) were from Varian. All thiols were dissolved in Nanopure water (MilliQ) from a Millipore system just before use and kept on ice.

4.2.2 Reaction of GSH with AS and $NaNO_2$

Freshly prepared stock solutions of GSH in water (pH 3.11) and AS in 10 mM NaOH were mixed to give 5 mM of each reagent, and incubated at different pHs within the range of 3-9 at room temperature for 30 min. The pH of the incubations was monitored at 10-min intervals over 30 min using an Orion Model 9810BN micro pH electrode (Thermo Electron Corporation) and adjusted with HCl or NaOH. Since AS releases both HNO and nitrite (NO_2^-) (*51*), GSH/$NaNO_2$ incubations were examined as controls. The expected *in vivo* concentrations of HNO are much lower than those of GSH, so incubations containing 2:1 and 5:1 GSH/AS molar ratios at a constant GSH concentration were examined. Direct reaction of GSH with AS ($H_2N_2O_3$) was probed by comparing the UV-Vis spectra of 0.1 mM AS alone and GSH/AS (1:1) in 20 mM ammonium acetate (pH 5.85) and TrisHCl (pH 7.4) buffers over 30 min at room temperature in a 1-cm cuvette on a Beckman DU800 spectrophotometer. Additionally, the GSH/AS (1:1) incubations at pH ~6 were analyzed by ESI-MS at 0.5, 1, 2, and 23 h to investigate the stability of the sulfinamide product.

4.2.3 Isolation of the sulfinamide formed in the GSH/AS incubation

GSH sulfinamide was purified using a SAX cartridge equilibrated with 3 mL of

aqueous HCl (pH 5.0). A 0.5-mL aliquot of GSH/AS incubation was loaded on the cartridge, washed with 2 mL of aqueous HCl (pH 5.0) and 1 mL of 0.01% formic acid (pH 3.1), and eluted with 1 mL of 0.1% formic acid (pH 2.7). The eluate was dried on a Speed Vac SC110 (Savant Instruments, Inc.) at room temperature, and resuspended in 0.5 mL of water. The purification was monitored by ESI-MS and HPLC-MS.

4.2.4 Reactions of AS with GSH derivatives and related dipeptides

To confirm that the free thiol is the target of HNO, 5 mM AS was incubated with equimolar *S*-MeGSH or GSSG, the thiols of which are blocked by methylation and oxidation, respectively. Additionally, 5 mM *N*-AcGSH, EtGSH, γEC, and CG in water were incubated with equimolar AS to probe the structural determinants of HNO reactivity. All incubations were carried out at room temperature for 30 min. The pH was adjusted with NaOH or HCl as needed and monitored at 10-min intervals using a micro pH electrode (Orion Model 9810BN). The products were analyzed by ESI-MS and HPLC-MS.

4.2.5 ESI-MS and HPLC-ESI-MS

Incubations were diluted 10–20-fold into 50% aqueous ACN/0.2% formic acid for MS analysis. ESI-MS and MS/MS were carried out on a Waters Micromass Q-ToF 2 mass spectrometer as described in Section 2.2.5. Instrumental parameters are listed in the figure legends. Samples for HPLC-MS analysis were diluted 10-fold with water and analyzed as described in Section 2.2.5. The solutions used for column equilibration and the mobile phases are indicated in the figure legends.

4.2.6 HPLC-UV analysis of the RSH/AS incubations

The formation of sulfinamide *vs* disulfide in incubations of AS with GSH, EtGSH and *N*-AcGSH as a function of pH was monitored by HPLC-UV. The HPLC column, mobile phases and parameter settings (wavelength, flow rate) are given in Section 2.2.5 and the figure legends. The HPLC-UV chromatograms were recorded on an Agilent 1100 with a variable wavelength detector (VWD) and analyzed using ChemStation (Agilent).

4.3 Results

4.3.1 Reaction of GSH with AS and $NaNO_2$

The pH of the GSH/AS and GSH/$NaNO_2$ incubations in water was monitored using the micro pH electrode at 10-min intervals (Figure 4.1). Hydroxylamine (NH_2OH), formed on conversion of the *N*-hydroxysulfenamide to the disulfide (Scheme 4.1 ***a***), will consume protons at pH <6.0 ($NH_3OH^+ \rightarrow NH_2OH + H^+$, pK_a = 5.96), but negligible solution pH changes are predicted on disulfide formation above the pK_a of NH_2OH or on sulfinamide formation since both OH^- and H^+ are released (Scheme 4.1 ***b***). The relatively small pH increases in the GSH/AS incubations at pH >7 (Figure 4.1A) are consistent with disulfide and NH_2OH formation above the pK_a of the latter (Figure 4.2C, D), and predominantly sulfinamide formation at pH 4-7 (Figure 4.2B). The ΔpH of +0.82 units at pH 6.0 was caused by disulfide and NH_2OH formation close to the pK_a of NH_2OH (5.96) which consumes protons. In contrast, only disulfide and NH_2OH were formed in the Cys/AS incubations at pH ~4.5 and a ΔpH of 2.5 units was reported (*57*).

No reaction is expected in the pH >4.5 GSH/$NaNO_2$ incubations because NO_2^- is a weak nitrosating agent at higher pH (*87*). However, a ΔpH increase of +0.65 was

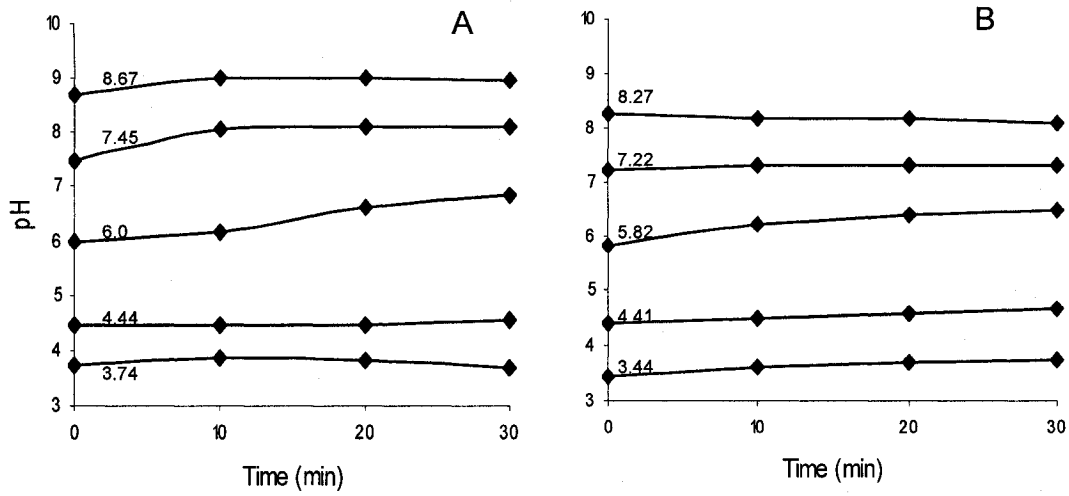

Figure 4.1. **pH of the GSH/AS and GSH/$NaNO_2$ incubations *vs* time.** GSH (5 mM) was incubated with (A) 5 mM AS and (B) 5 mM $NaNO_2$ in water at room temperature. Experimental procedures: The initial pHs were adjusted to the values indicated on the plots with HCl or NaOH. The diamonds indicate the pH values measured at 10-min intervals using a micro pH electrode and the connecting lines were added to clarify the variation in pH in each incubation.

detected in the pH 5.82 incubation (Figures 4.1B), which may be due to loss of HNO_2 (pK_a 3.15) from this weakly acidic solution. The NO released from AS (eq 1.2) at pH <4 (*55*) will react with O_2 to yield a number of *S*-nitrosating agents including HNO_2 (*7*). The GSH/AS incubation with an initial pH of 3.74 undergoes a small pH change (ΔpH = 0.13) over 30 min similar to the pH 3.44 GSH/$NaNO_2$ incubation (Figure 4.1A, B). *S*-nitrosation of GSH was expected to occur in both incubations at pH <4 (eq 4.1) and this was confirmed by ESI-MS. The *S*-nitrosating species in acidic solutions of HNO_2 include NO^+ (*87*).

$$GSH + HNO_2 \rightarrow GSNO + H_2O \qquad (4.1)$$

The GSH/AS incubations were examined by ESI-MS after 30 min since the decomposition of the salt (half-life ~5 min) is complete within this time period at pH 4-8 (*51, 57*). At pH >7, the abundant peaks at m/z 613, 635, 657, 679, 701, and 723 present in

the mass spectra (Figure 4.2C, D) are assigned to the MH^+ and $[M-(n-1)H+nNa]^+$ (n=1-5) ions of the disulfide, GSSG. At pH ~6, major peaks at m/z 339, 361, 383, and 405, corresponding to the protonated and sodiated ions of the sulfinamide ($GSONH_2$), were observed with very weak GSSG peaks above m/z 600 (Figure 4.2B). The m/z 322 peak in the spectrum of the incubations at pH >6 (Figure 4.2B, C) has a mass of (M+14) u, and could arise from intramolecular sulfinamide formation (Scheme 4.1*c*) or from a fragment ion as discussed below.

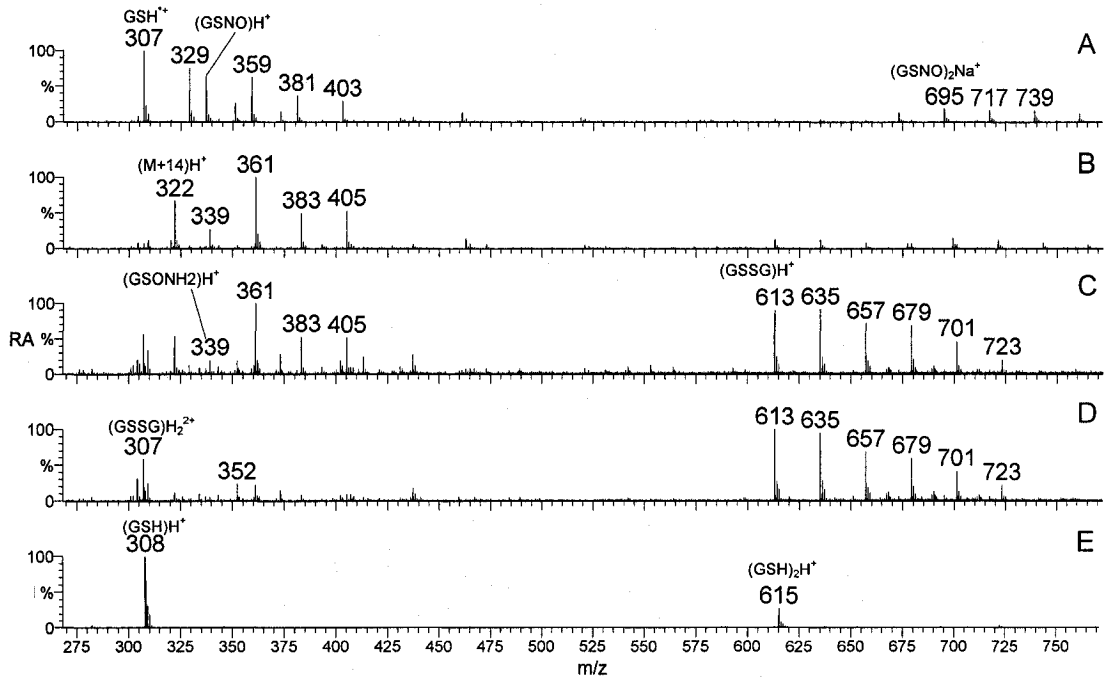

Figure 4.2. **ESI-MS analysis of 30-min equimolar GSH/AS incubations *vs* pH.** The initial and final pH values of the GSH/AS incubations were (A) 3.74 and 3.69, (B) 6.00 and 6.82, (C) 7.45 and 8.11, and (D) 8.67 and 8.98, (E) GSH only at an initial pH of 3.11 and a final pH of 3.05. Experimental conditions: 5 mM GSH in water was incubated with 5 mM AS at room temperature for 30 min. The pH was adjusted to the initial value with HCl or NaOH and the final pHs are those measured after 30 min. For MS analysis, the incubations were diluted 20-fold into 50% aqueous ACN/0.2% formic acid, and directly infused into the ESI source of the Q-ToF 2 mass spectrometer at a flow rate of 1 μL/min. The instrument parameters were: source block temperature 80°C, capillary voltage 3.2 kV, cone voltage 20 kV, collision voltage 5 V (no collision gas), MCP 2.2 kV and ToF –9.1 kV. RA is the relative abundance of the ions.

Low-mass protonated and sodiated ions of GSNO (m/z 337, 359, 381, 403) and $GS^{\bullet}$ (m/z 307, 329, 351, 373), which arise from GSNO homolysis (GSNO $\rightarrow$ $GS^{\bullet}$ + $NO^{\bullet}$) in the ESI source, dominate the spectrum of GSH/AS incubations at pH <4 (Figure 4.2A). AS liberates NO but no HNO at pH <4.0 (*55*) and the NO released will react with O_2 to yield a number of *S*-nitrosating agents including HNO_2 (eq 1.1) (*7*). The peak at m/z 307 in the spectra of the GSH/AS incubations at pH >7 (Figure 4.2C, D) is assigned to the doubly charged MH_2^{2+} ions of GSSG since the $(GS^{\bullet})H^+$ ion at m/z 307 is singly charged. A prominent peak at m/z 308 assigned to $(GSH)H^+$ and a minor peak at m/z 615 assigned to $(GSH)_2H^+$, the non-covalent dimer, appear in the GSH-only spectrum (Figure 4.2E). No sodiated ions appear in spectrum E since the GSH solid ($C_{10}H_{17}N_3O_6S$ >98%) was in the free acid form and no sodium salts such as AS ($Na_2N_2O_3$) were added. At pH 6.0 and 5 mM AS, the sulfinamide was the dominant product whereas the disulfide was dominant

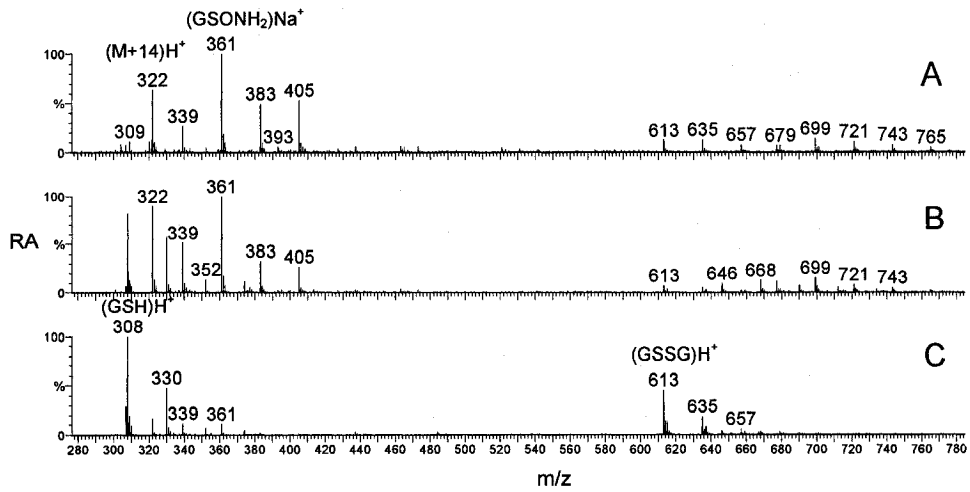

Figure 4.3. **ESI-MS analysis of GSH/AS incubations at pH 6 *vs* AS concentration.** (A) 5 mM GSH with 5 mM AS, (B) 5 mM GSH with 2.5 mM AS, and (C) 5 mM GSH with 1 mM AS in water at an initial pH of ~6.0 and final pH of (A) 6.82, (B) 6.91, and (C) 5.86. The experimental conditions are given in the legend to Figure 4.2.

at 1 mM AS (Figure 4.3). Formation of the sulfinamide in the GSH/AS incubations was confirmed by accurate mass measurements (<2 ppm) on a LC/MSD TOF (Agilent) mass spectrometer (Table 4.1). The stability of GSH in water over the pH range of 3-9 was also investigated and all the ESI mass spectra are similar (Figure 4.10C), confirming that GSH is stable in the pH range investigated over 30 min.

Table 4.1. **Accurate mass measurements of GSH and GSH sulfinamide**[a]

Compound	Formula	M_r (u)	MH^+ (m/z)		Error (ppm)
			Calculated	Measured[a]	
GSH	$C_{10}H_{17}N_3O_6S$	307.08381	308.09108	308.09062	-1.49
GSH sulfinamide[b]	$C_{10}H_{18}N_4O_7S$	338.08962	339.09690	339.09698	0.25

[a] Accurate masses were measured on an Agilent LC/MSD TOF MS. The instrumental settings are given the footnote to Table 2.1.

[b] GSH sulfinamide was formed in the reaction of 5 mM GSH with 5 mM AS in water (pH 6.0) at room temperature for 30 min.

The $GSONH_2$ and GSSG products, and the M+14 adducts were further characterized by MS/MS. Fragmentation of their MH^+ ions at m/z 339, 613, and 322, respectively, on the Q-ToF 2 yielded the product ions listed in Table 4.2. The product-ion spectra of $(GSH)H^+$ and GSSG were also recorded and the GSSG fragments are consistent with those previously reported (Table 4.2) (*88*), confirming its formation in the GSH/AS incubations. At low collision voltage (5 V), the (M+14) adduct at m/z 322 did not fragment, but the sulfinamide ion at m/z 339 yielded a fragment ion at m/z 322 (Figure 4.4A, D), which was not observed without collision gas (Figure 4.4E). The m/z 322 and m/z 339 product-ion spectra are identical (Figure 4.4B *vs* C) at higher collision voltage (15 V), which strongly suggests that m/z 322 is a fragment of m/z 339 since

cyclic and acyclic sulfinamides are not expected to yield identical fragment ions (Figure 4.5). Therefore, the (M+14) adduct observed at m/z 322 in the ESI-MS spectrum of the GSH/AS incubations is assigned to $(GSONH_2\text{-}NH_3)H^+$.

Table 4.2. **Main fragment ions of GSH, $GSONH_2$, GSSG, and the M+14 adduct observed by MS/MS[a]**

Compound	MH^+ (m/z)	Fragment ion (m/z) assignment[b]							
GSH	308	291 NH_3	290 H_2O	233 290–G	215 233–H_2O	179 γE	162 146	144 162–H_2O	130 E^+
GSSG	613	595 H_2O	538 G	484 γE	466 484–H_2O	409 484–G	355 484–γE		
$GSONH_2$	339	322 NH_3	304 322–H_2O	256 322–H_2O –SO	247 322–G	239 256–NH_3	193 322–γE	181 256–G	155
M+14	322		304	256	247	239	193	181	155

[a] Product-ion spectra (Figures 4.4, 4.5) were recorded on the Q-ToF 2 with the instrument settings given in Section 4.2.5.

[b] Neutral fragments lost from the molecular (MH^+) ions or from fragment ions at the m/z values indicated.

To confirm (M+14) assignment, *N*-AcGSH was incubated with AS and the products were analyzed by MS. With the α-amino group blocked by acetylation, intramolecular sulfinamide formation should not occur in the *N*-AcGSH/AS incubations, but NH_3 loss from the sulfinamide group (Figure 4.5A) in the ion source would yield a m/z 364 ion. Only sodiated ions were observed in the spectrum of the 30-min *N*-AcGSH/AS incubation (Figure 4.6), and the peak assignments suggest products similar to those formed in the GSH/AS incubations (Table 4.3). Specifically, no $(M+14)H^+$ or

$(M+14)Na^+$ ions were detected at any pH (Figure 4.6) since (N-AcGSONH$_2$)Na^+ ions likely fragment by loss of neutural N-AcGSONH$_2$ and Na^+ (m/z 23) cannot be detected within the m/z range (50-4000) of the Q-ToF 2.

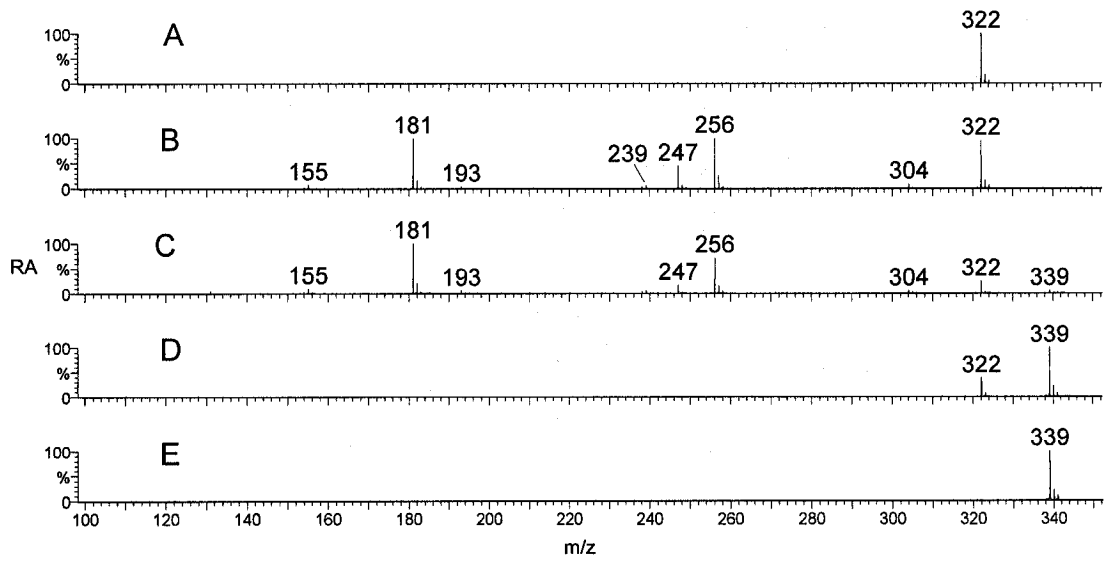

Figure 4.4. **Product-ion spectra of the m/z 322 and m/z 339 ions.** Spectrum of the m/z 322 ion at a collision voltage of (A) 5 V, (B) 15 V; spectrum of the m/z 339 ion at (C) 5 V, (D) 15 V, and (E) 5 V but without collision gas. The other experimental conditions are given in the legend of Figure 4.2.

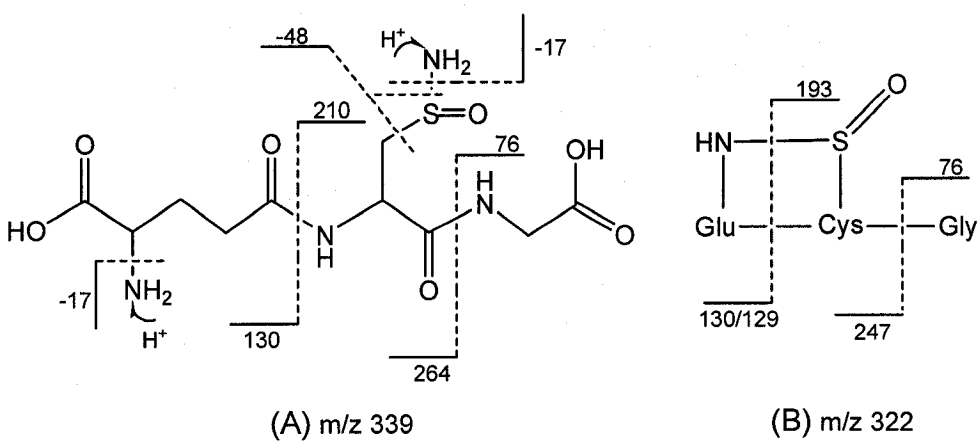

Figure 4.5. **Expected MS/MS cleavage sites in (A) GSH sulfinamide and in (B) the putative cyclic GSH sulfinamide (m/z 322)**

Protonated ions of $GSONH_2$ were observed following desalting on the HPLC column and both $(M+31)H^+$ (m/z 339) and $(M+14)H^+$ (m/z 322) ions (Figure 4.6E inset) arose from the same peak in the HPLC chromatogram (Figure 4.6E). Using various mobile phases (5% aqueous ACN/0.1% formic acid, 3% aqueous MeOH/0.05 TFA, or a 1-10% aqueous MeOH/0.05 TFA gradient in 30 min), the m/z 322 and 339 peaks coeluted, suggesting that they arise from the same molecule. Since the $(M+14)H^+$ ion dominates the mass spectrum (Figure 4.6F), *N*-AcGSONH$_2$ must readily lose NH_3 (-17 amu) in the ion source. Thus, a cyclic sulfinamide is not formed in the reaction of

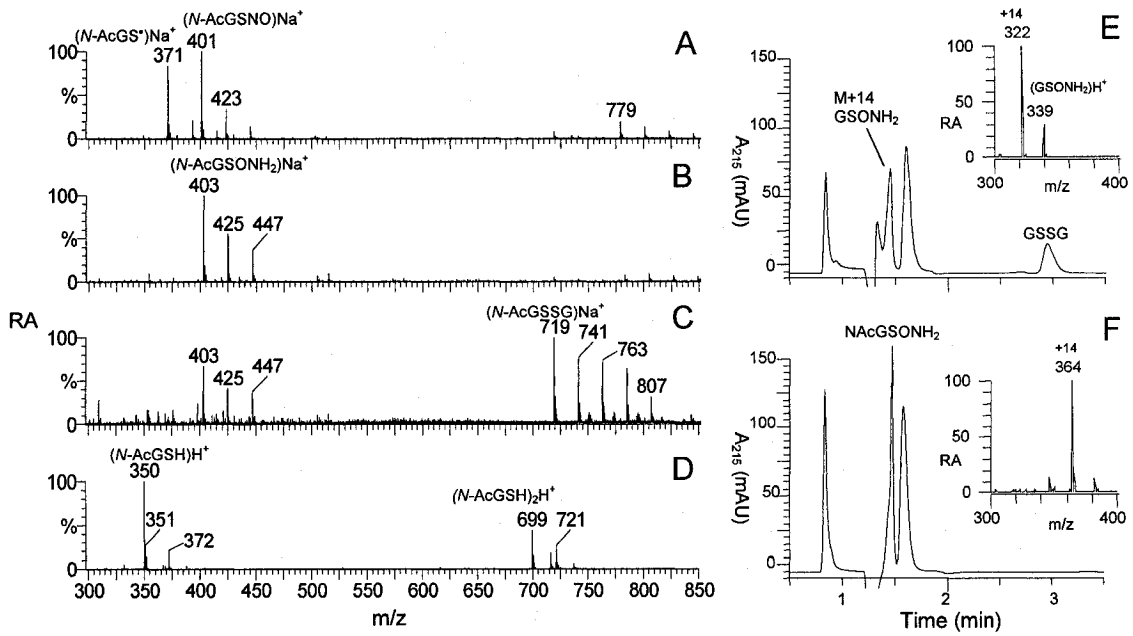

Figure 4.6. **ESI mass spectra of *N*-AcGSH/AS incubations *vs* pH, and HPLC-UV and HPLC-MS spectra of GSH/AS and *N*-AcGSH/AS incubations at pH ~6.** Mass spectra of 5 mM *N*-AcGSH and 5 mM AS after 30 min incubation at pH (A) 3.59, (B) 5.82, and (C) 8.28. (D) *N*-AcGSH only at pH 2.75. HPLC-UV chromatograms of (E) GSH/AS and (F) *N*-AcGSH/AS incubations and the mass spectra (insets) of the peaks labeled in chromatograms. The HPLC column was equilibrated with 5% aqueous ACN/0.1% formic acid, which was also used as the mobile phase. The other experimental conditions are given in Section 4.2 and the legend of Figure 4.2.

N-AcGSH or GSH with HNO, and the $(M+14)H^+$ adducts serve as a marker of acyclic sulfinamide formation.

Table 4.3. **Assignment of peaks in the ESI mass and tandem mass spectra of the AS/RSH incubations**[a]

Observed peaks (m/z)[b]					Assignment	
GSH	***N*-AcGSH**	**EtGSH**	**γEC**	**CG**	**Ion**[c]	**Compound**
pH >5						
308	350	336	251	179	M+H	**RSH**
615	699	671	501	357	2M+H	
307		335	250		2M-2+2H	**RSSR (disulfide)**
613		669	499	355	2M-2+H	
635	719	691	521	377	2M-2+Na	
657	741	713	543	399	2M-2+2Na-H	
679	763	735	565		2M-2+3Na-2H	
701	785		587		2M-2+4Na-3H	
723	807		609		2M-2+5Na-4H	
322		350		193	M+14+H	**$RSONH_2$ (sulfinamide)**
339		367		210	M+31+H	
361	403	389		232	M+31+Na	
383	425			254	M+31+2Na-H	
405	447				M+31+3Na-2H	
677		733		419	2(M+31)+H	
699	783	755		441	2(M+31)+Na	
pH <4						
337		365	280	208	M+29+H	**RSNO**
359	401	387	302	230	M+29+Na	
381	423		324	252	M+29+2Na-H	
403	445		346		M+29+3Na-2H	
673				415	2(M+29)+H	
695	779			437	2(M+29)+Na	
307		335	250	178	M-1+H	**RS•**
329	371		272	200	M-1+Na	
351	393		294		M-1+2Na-H	
373	415				M-1+3Na-2H	

[a] Samples were incubated under the conditions described in Section 4.2 and in the legend of Figure 4.2

[b] Peaks from the spectra in Figures 4.2, 4.3, 4.4, 4.6, 4.12, 4.14

[c] M corresponds to RSH

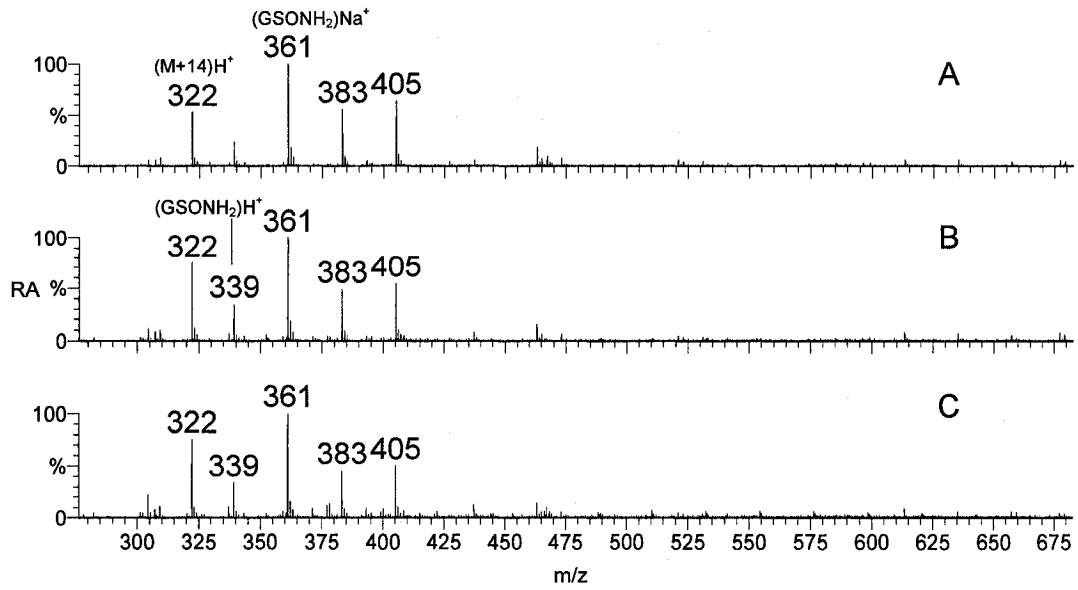

Figuer 4.7. **ESI-MS analysis of $GSONH_2$ stability at pH 6.** 5 mM GSH was incubated with 5 mM AS at pH 6 and room temperature and analyzed by ESI-MS after (A) 0.5 h, (B) 2 h, and (C) 23 h. The other experimental conditions are given in the legend to Figure 4.2.

Since $GSONH_2$ is stable in solution at pH 6-7 (Figure 4.7), its purification was attempted using a SAX cartridge. $(GSONH_2)H^+$ ions (m/z 339) were detected (Figure 4.8A) 10 min after elution by 0.1% formic acid (pH 2.7), but the sulfinic (GSO_2H, m/z 340) and sulfonic acids (GSO_3H, m/z 356) were also detected in the spectrum of samples that were left standing at pH 2.7 for 4 h at room temperature (Figure 4.8B). If the SAX eluate was dried under vacuum on the Speed Vac, the dominant peak was that of the sulfinic acid (m/z 340) (Figure 4.8C), which was confirmed by MS/MS (Figure 4.9). The m/z 340 ion is more stable than the $(GSONH_2)H^+$ ion at m/z 339 at a collision voltage of 10 V (Figure 4.9B *vs* A). Also, two fragment ions, m/z 265 and 211, are present in the product-ion spectrum of m/z 340 at 15 V but not that of m/z 339, confirming that the m/z 340 and m/z 339 ions arise from different GSH derivatives. The m/z 265 peak is a b_2 ion formed on loss of Gly (-75 u) from $(GSO_2H)H^+$, and the m/z 211 peak is a y_2 ion formed

on loss of γE (-129) from $(GSO_2H)H^+$, while the m/z 322 ions are due to the loss of H_2O from $(GSO_2H)H^+$ and NH_3 from $(GSONH_2)H^+$. These results confirm the formation of sulfinic acid, and the HPLC-UV chromatogram also showed that the acid (peak #1) increased at the expense of the sulfinamide (peak #2) on exposure to vacuum (Figure 4.8D). However, no sulfinic acid peak was present in the chromatograms of the GSH/AS incubations maintained at pH 6.0 (Figure 4.8D), indicating that the sulfinamide is stable around neutral pH.

Since Angeli's salt releases both HNO and NO_2^- (eq 1.1, 1.2), GSH was incubated with $NaNO_2$ as a control. The spectrum of the 30-min GSH/$NaNO_2$ incubation at pH 7.22 shows only GSH ions that are also present in the spectrum of GSH alone (Figure 4.10B *vs* C) as expected since NO_2^- is not an effective *S*-nitrosating agent at neutral pH (*87*).

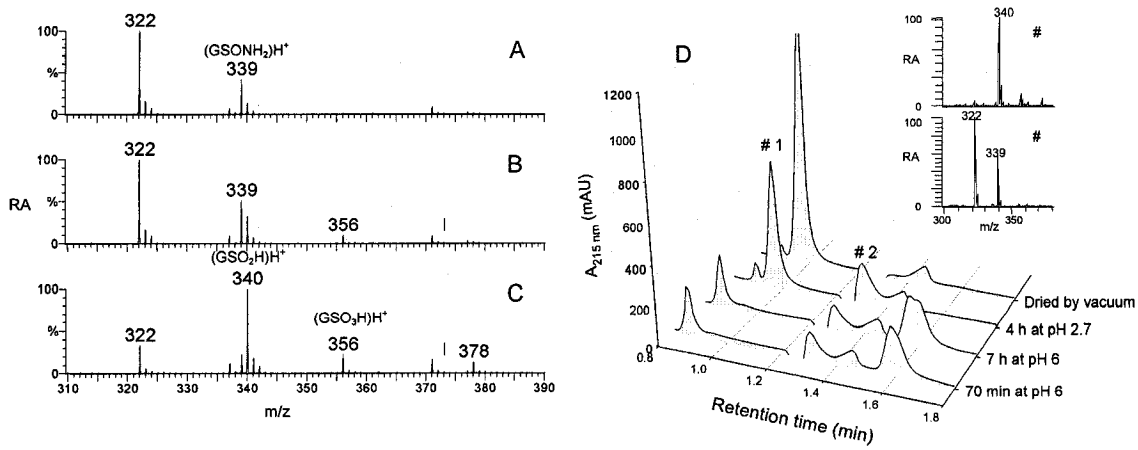

Figure 4.8. **GSO_2H formation during isolation of $GSONH_2$.** A 0.5-mL aliquot of a 30-min GSH/AS incubation was loaded on a SAX cartridge equilibrated with HCl (pH 5.0) and eluted with 0.1% formic acid (pH 2.7). The eluate was left standing on the bench for (A) 10 min, (B) 4 h, and (C) dried on a Speed Vac, and analyzed by ESI-MS on a Q-ToF 2. (D) The SAX eluate (pH 2.7) and the untreated GSH/AS incubations (pH 6.0) were analyzed by HPLC-UV and HPLC-MS (inset). The mobile phase used for HPLC was 5% aqueous ACN/0.1%formic acid and the other experimental conditions are given in the legend to Figure 4.2.

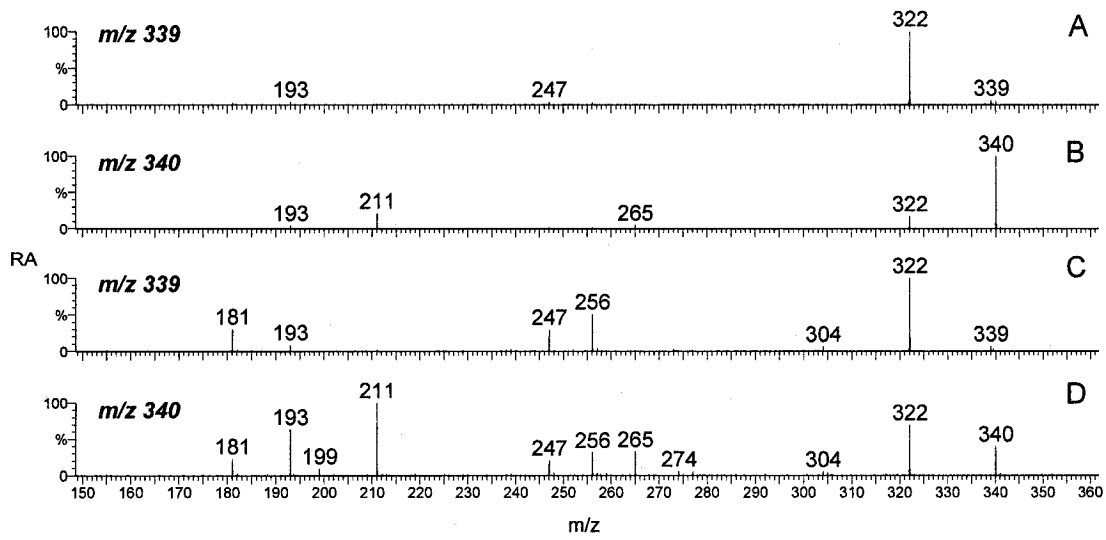

Figure 4.9. **Product-ion spectrum of $GSONH_2$ (m/z 339) and GSO_2H (m/z 340).** The parent ions selected were (A, C) m/z 339 and (B, D) m/z 340 and MS/MS were performed with collision voltage (A, B) 10 V and (C, D) 15 V. Other instrument settings are given in the legend of Figure 4.2.

The sodiated ions are more intense in spectrum B *vs* C because of the addition of $NaNO_2$ to this sample. The spectra of the GSH/$NaNO_2$ and GSH/AS incubations at pH <4 are similar (Figures 4.10A and 4.2A), with $(GSNO)H^+$ (m/z 337) and $(GSH^{\bullet+}$ (m/z 307) ions present, confirming that GSNO is produced in both incubations at low pH. $GS^\bullet$ is formed on GSNO homolysis in the ESI ion source as reported (*60*). In summary, GSSG and $GSONH_2$ are products of the GSH reaction with HNO (Scheme 4.1) at pH >5, and GSNO is the product of the reaction of GSH with HNO_2-derived nitrosating agents at pH <4.0.

Since sulfinamide is detected in the GSH/AS incubations but not in the Cys/AS incubations (*57*), AS decomposition was compared in the presence and absence of GSH. GSH retarded slightly the initial rate of AS decomposition at pH 5.85 but did not alter the rate at pH 7.4 (Figure 4.11), so $GSONH_2$ formation is unlikely due to the direct reaction of GSH with AS but to its reaction with the HNO released on AS decomposition. The

slight acceleration by GSH at longer times (Figure 4.11) suggests that AS decomposition (eq 1.1) may be reversible.

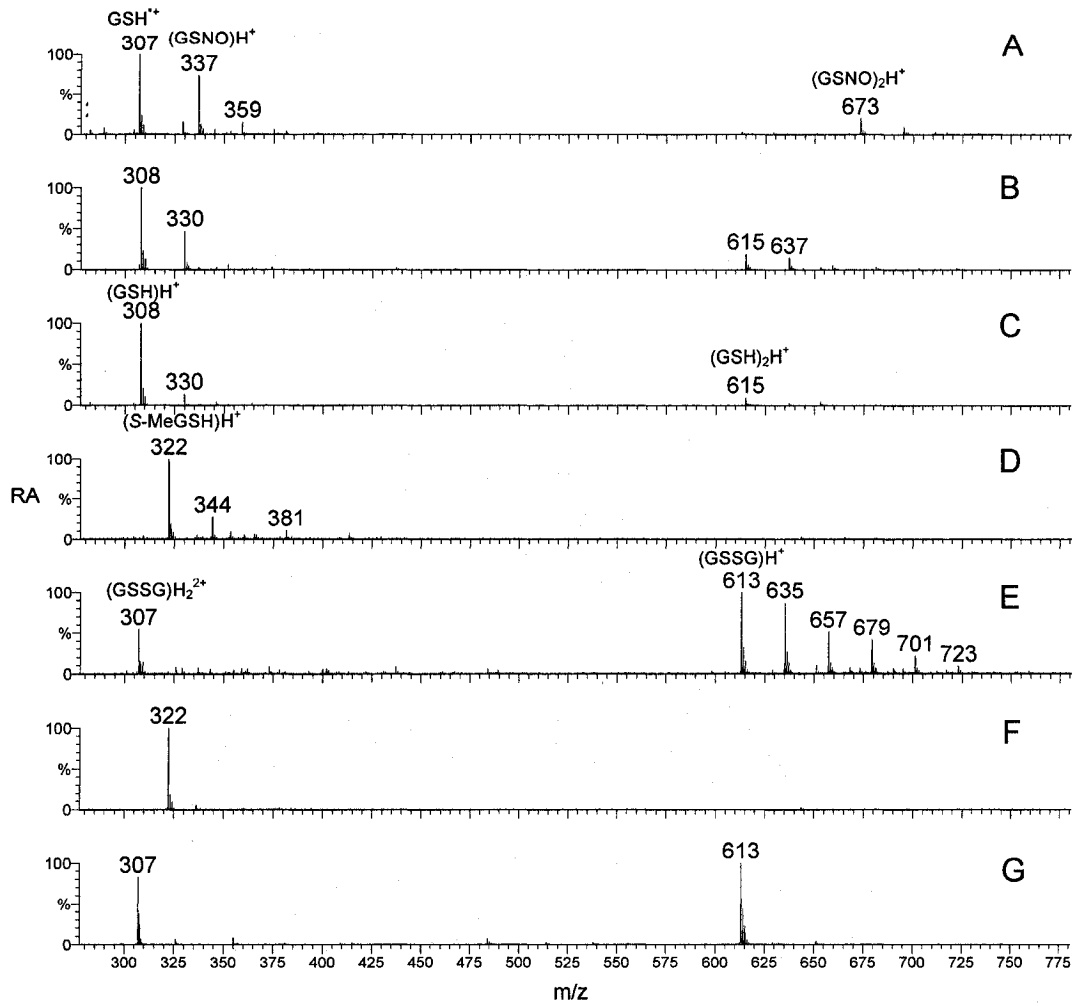

Figure 4.10. **ESI mass spectra of control incubations.** 5 mM GSH and 5 mM $NaNO_2$ after 30-min incubation at (A) pH 2.46 and (B) pH 7.22. (C) GSH alone at pH 7.53. (D) 5 mM *S*-MeGSH and 5 mM AS after 30-min incubation at pH 6.41. (E) 5 mM GSSG and 5 mM AS after 30-min incubation at pH 5.53. (F) *S*-MeGSH alone at pH 3.11 and (G) GSSG alone at pH 3.24. The GSH, *S*-MeGSH and GSSG were prepared freshly in water. The experimental conditions are given in the legend of Figure 4.2.

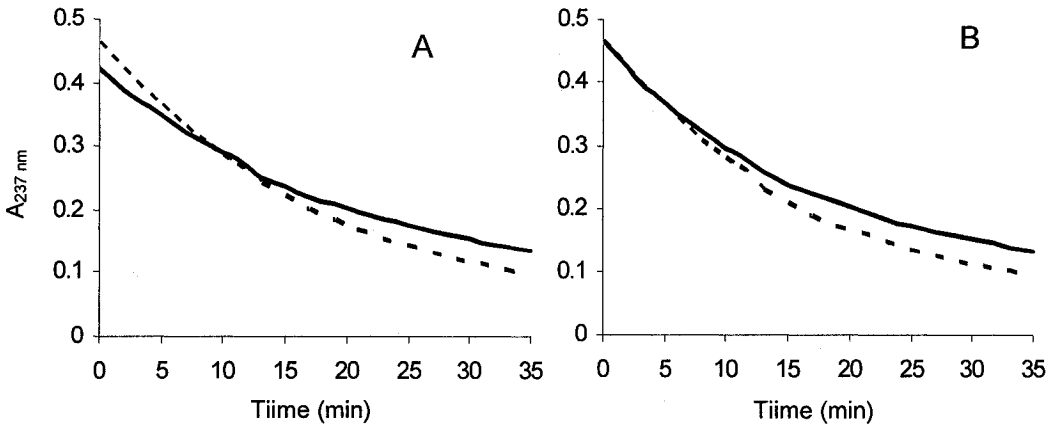

Figure 4.11. **Comparison of AS decomposition in the presence and absence of GSH.** AS decomposition at pH (A) 5.85 and (B) 7.4. Experimental conditions: An AS stock in 10 mM NaOH was diluted 4×10^3-fold to 0.1 mM with 20 mM ammonium acetate (pH 5.85) or 20 mM TrisHCl (pH 7.4) buffers with (dashed line) and without (solid line) 0.1 mM GSH. Spectra were recorded at 1-min intervals at 22°C in 1-cm cuvettes, and the curves show the decay of AS absorption at 237 nm (*51*).

4.3.2 Reaction of AS with the GSH derivatives

The reactions of AS with *S*-MeGSH and GSSG were also investigated by ESI-MS to confirm that the thiol is the target of HNO. The ESI mass spectra of the *S*-MeGSH/AS and GSSG/AS incubations are are the same as those of *S*-MeGSH or GSSG alone (Figure 4.10D *vs* F, E *vs* G), indicating that HNO does not react with the thiol-blocked GSH derivatives. Thus, the formation of $GSONH_2$ and GSSG are due exclusively to the reaction of the GSH thiol with HNO at pH >5.

Esterification of its C-terminus and *N*-acetylation of GSH altered the products formed in the AS reaction at pH >5. Relative to GSH, more sulfinamide was produced in the *N*-AcGSH reaction and more disulfide in the EtGSH reaction at the same pH (Figure 4.12). Consistent with the MS results (Figure 4.2, 4.10), the HPLC-UV chromatograms of the *N*-AcGSH/AS, GSH/AS, and EtGSH/AS incubations show that the disulfide increased at the expense of the sulfinamide with increasing pH (Figure 4.13). At a given

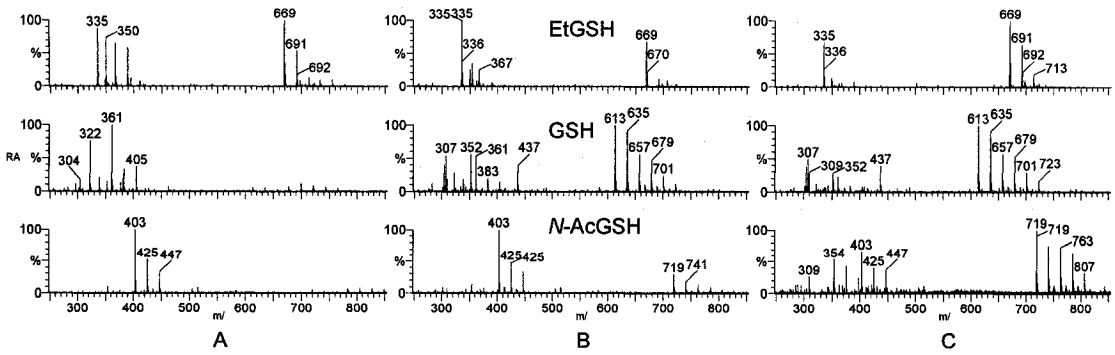

Figure 4.12. **Sulfinamide *vs* disulfide formation in the EtGSH/AS, GSH/AS, and *N*-AcGSH/AS incubations *vs* pH.** Incubations at pH (A) ~6, (B) ~7 and (C) 8.7. The top row: ESI mass spectra of the 5 mM EtGSH and 5 mM AS after 30-min incubation; middle row: 5 mM GSH and 5 mM AS after 30-min incubation; bottom row: 5 mM *N*-AcGSH and 5 mM AS after 30-min incubation at different pH levels. The other experimental conditions are given in the legend of Figure 4.2.

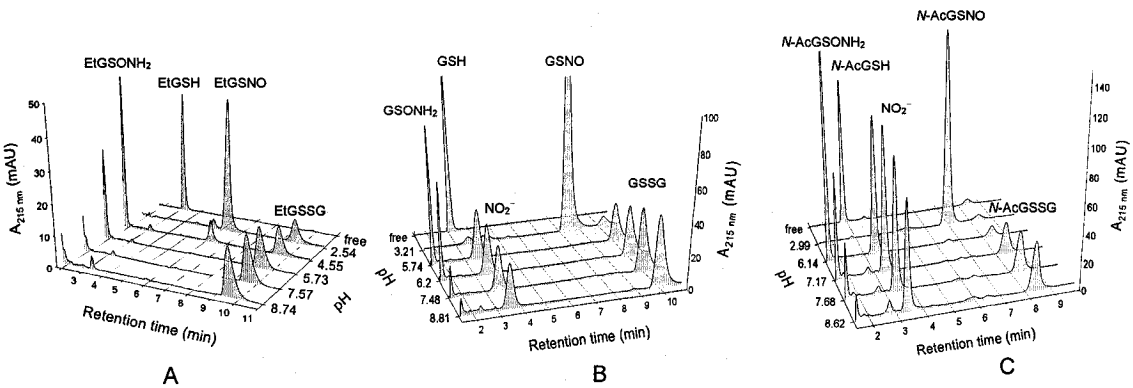

Figure 4.13. **HPLC-UV analysis of the products formed in the EtGSH/AS, GSH/AS, and *N*-AcGSH/AS incubations *vs* pH.** Chromatograms of 5 mM AS with 5 mM (A) EtGSH, (B) GSH, and (C) *N*-AcGSH after 30-min incubation in water at room temperature and the pH values indicated. The mobile phases used for HPLC were (A) 15% aqueous ACN/0.1% FA, (B) 3% aqueous MeOH/0.05% TFA, and (C) 10% aqueous MeOH/0.05% TFA. Other experimental conditions and parameter settings for HPLC are given in the legend of Figure 4.2 and in Section 4.2. Note that NO_2^- eluted close to the solvent front and before $EtGSONH_2$ peak in (A).

pH, the sulfinamide level is highest in *N*-AcGSH/AS chromatogram and lowest in EtGSH/AS chromatogram (Table 4.4), in agreement with the MS data (Figure 4.12, Table 4.5).

Table 4.4. **Sulfinamide/disulfide ratio[a] in the reaction of AS with EtGSH, GSH, and *N*-AcGSH *vs* pH**

Compound	EtGSH				GSH				*N*-AcGSH			
pH	8.74	7.57	5.73	4.55	8.81	7.48	6.20	5.74	8.62	7.68	7.17	6.14
sulfinamide / disulfide	0.03	0.06	0.63	1.54	0.03	0.08	0.35	0.70	0.09	0.29	0.82	6.55

[a] Estimated from peak areas of HPLC-UV chromatograms in Figure 4.13

More sulfinamide (CG-$SONH_2$, m/z 210) was formed at pH <7 (Figure 4.14F) but more disulfide (dCG, m/z 355) was formed at pH >7 (Figure 4.14G) in the CG/AS compared to the GSH/AS incubations (Figure 4.2). As observed for free Cys (*57*), disulfide (dγEC, m/z 499) but negligible sulfinamide (m/z 282) was detected in the γEC/AS incubations (Figure 4.14B, C). Analysis of the incubations of AS with GSH and its derivatives (Table 4.3) reveal that the product distribution is controlled by the C-terminus.

4.4 Discussion

4.4.1 Effect of HNO on the functions of GSH

The data obtained by ESI-MS are consistent with previous reports that HNO is highly thiolphilic (*27*). The conversion of GSH to GSSG and $GSONH_2$ is also consistent with a previous study showing GSH depletion upon exposure of fibroblasts to HNO (*30*). Sulfinamide is formed via path ***b*** from the *N*-hydroxysulfenamide intermediate on OH^- release (Scheme 4.1). In the acidic incubations (pH 4-6), H^+ ions consume the released OH^- and drive the reaction toward sulfinamide formation. In contrast, in the neutral and slightly basic incubations (pH 7-9), OH^- release would not be promoted whereas

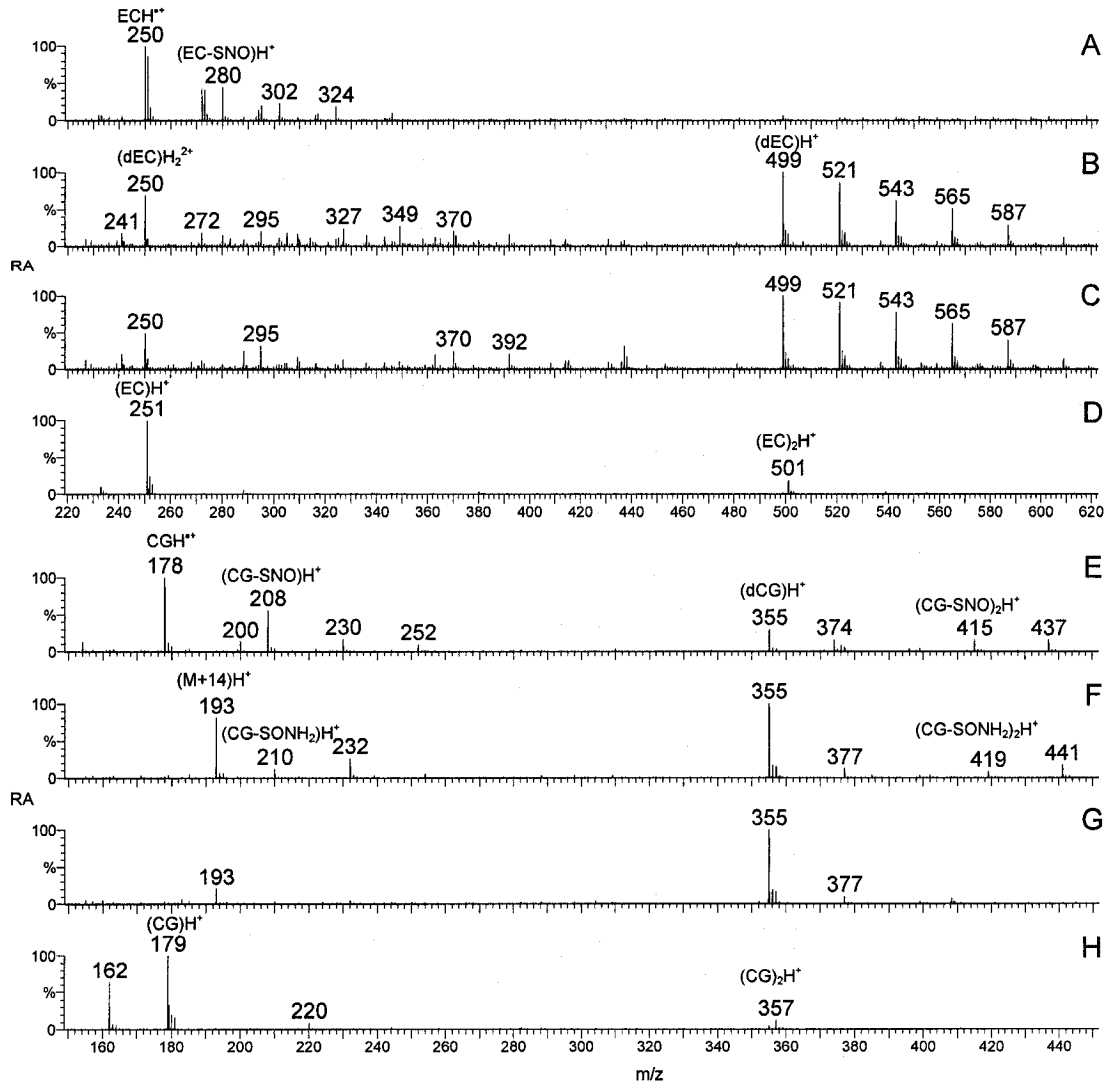

Figure 4.14. **ESI mass spectra of 30-min γEC/AS and CG/AS incubations.** The initial pH values of the γEC/AS incubations were (A) 3.58, (B) 5.41, and (C) 6.70; and of the CG/AS incubations were (E) 2.10, (F) 5.74, and (G) 6.93. (D) γEC alone in water at pH 2.51; (H) CG alone in water at pH 4.76. The experimental conditions are given in the legend of Figure 4.2. Note: dEC and dCG represent the disulfide of EC and CG, respectively.

deprotonation of the thiol will accelerate disulfide formation via path ***a***. Higher GSH concentrations also increase disulfide formation even at low pH (Figure 4.3), and since the GSH concentration is high *in vivo* (0.5-10 mM) (*1*), HNO will most likely convert GSH to disulfide GSSG at physiological pH (7.4). This would alter the GSH/GSSG

balance in cells at the site of HNO production and result in physiological change (*4*). Local HNO concentrations could be controlled *in vivo* by metabolism and the immune response, or altered by disease.

The local pH *in vivo* can be lower than 7.0 (*89-91*), suggesting that under certain conditions, HNO might irreversibly convert GSH to the sulfinamide (*31, 39*). However, hydrolysis of the sulfinamide to the sulfinic acid was proposed (eq 4.2) (*31*), and

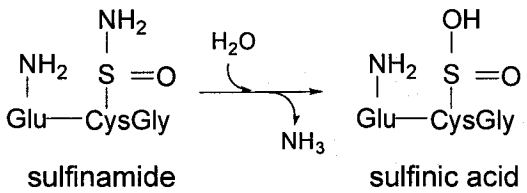

(4.2)

confirmed here by ESI-MS during isolation of the sulfinamide at pH 2.7 (Figure 4.8). Removal of the NH_3 released under vacuum accelerated formation of the sulfinic acid (Figure 4.8), which was partially oxidized to the sulfonic acid as reported previously (*92*). Hydrolysis of the sulfinamide and reduction of the sulfinic acid by excess thiol could result in regeneration of GSH *in vivo* (Scheme 4.2). Although the pH in most cells

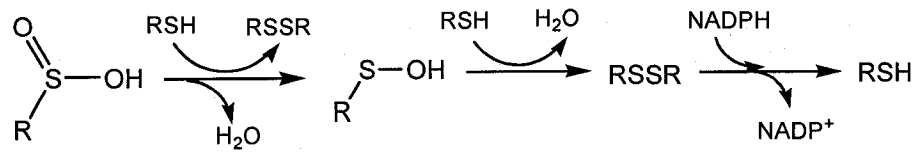

Scheme 4.2. **Sulfinic acid (RSO_2H) convertion to free thiol (RSH) in present of excess thiol**

is >> 3, $GSONH_2$ hydrolysis could be enzymatically catalyzed. Reduction of Cys-based sulfinic acid *in vivo* has been recently demonstrated (*93-95*). Whether cells possess the ability to metabolize $GSONH_2$, which is stable at neutral pH (Figure 4.7), remains to be seen.

4.4.2 Factors controlling sulfinamide formation

To determine what controls sulfinamide *vs* disulfide formation on the reaction of GSH with HNO, incubations of AS with the GSH derivatives, EtGSH, *N*-AcGSH, γEC, and CG, were also analyzed. Compared to GSH, more sulfinamide was formed in the *N*-AcGSH reaction and less in the EtGSH reaction at pH 7 (Table 4.4). The thiol pK_a (Table 4.5) does not control sulfinamide yields since more is formed at lower pH (Table 4.4). Also, free Cys, which exhibits the lowest thiol pK_a (8.33), forms no sulfinamide on exposure to AS.

Table 4.5. **pK_a values of the thiol and α-amino groups in GSH and its derivatives**

Group	**pK_a values[a] (charge at pH 7.0; *sulfinamide yield* at pH 7.4)[b]**						
	GSH (-1; *0.43*)	***S*-MeGSH** (-1; ---)	***N*-AcGSH** (-2; *1.19*)	**EtGSH** (0; *0.13*)	**γEC** (-1; *0*)	**CG** (0/-1; *0.10*)	**Cys** (0; *0*)
-SH	9.16 ± 0.02	---	8.99 ± 0.05	8.55 ± 0.02	11.23 ± 0.03	9.24 ± 0.02	8.33 ± 0.01
$-NH_3^+$	9.06 ± 0.02	9.00 ± 0.04	---	9.33 ± 0.02	9.28 ± 0.01	6.84 ± 0.02	10.84 ± 0.02

[a] pH titrations were performed in aqueous 0.15 M KCl under argon (60 mL/min) at 25°C (Section 3.2.2)

[b] Yields (in italics) estimated by summing the relative abundances of all peaks derived from the sulfinamide or the disulfide in the ESI mass spectra.

The overall charge of the molecule (Table 4.5) will indirectly affect sulfinamide yields by modulating disulfide formation. Electrostatic repulsion will inhibit the latter bimolecular process (Scheme 4.1) in the *N*-AcGSH/AS incubations but not in the EtGSH/AS incubations as observed (Figure 4.12). However, more sulfinamide was

detected in the CG/AS incubations than in the γEC/AS incubations (Figure 4.14) although γEC carries a greater negative charge than CG (Table 4.5). Also, Cys and EtGSH are both neutral but do not exhibit the same product profile with HNO (Figure 4.14 *vs* 4.10). The molecular conformation of the thiol is likely another factor that controls the stability of the *N*-hydroxysulfenamide intermediate (Scheme 4.1) and hence the products formed with HNO. In Chapter 5, sulfinamide yields in the reaction of HNO with thiols are further investigated towards developing a HNO marker that forms exclusively the sulfinamide.

5 REACTIONS OF CYS, HCYS, PENICILLAMINE, AND CYS-CONTAINING DIPEPTIDES WITH HNO; TOWARDS DEVELOPMENT OF A HNO MARKER

5.1 Introduction

Cysteine (Cys) and HCys (HCys) are naturally occurring thiol-containing amino acids with antioxidant properties due to the ability of thiols to undergo redox reactions. Cys, HCys, and *N*-AcCys levels have been linked to many diseases such as cerebral ischemia, Alzheimer's disease, Parkinson's disease (*10-12*) and cardiovascular disease (*17-19*). Cys and cystine are also involved in transmembrane *S*-nitrosothiol transport through a *trans*-*S*-nitrosation reaction (*8*). Penicillamine (Pen), β,β-dimethyl cysteine, is an antirheumatic drug (*96*) and is also used as a metal chelating agent in the treatment of Wilson's disease which results in excessive copper deposits in tissues (*96*). The structures of Cys, HCys and Pen are shown in Figure 3.3 and the pK_a values of their thiol and amino groups are given in Table 3.2.

At present, all common methods to detect HNO are indirect (*59*). For example, detection of N_2O, which forms on HNO dimerization and dehydration, has been used extensively (eq 1.3) (*39, 59, 97, 98*). However, this approach is nonspecific in bioassays because N_2O can be formed from species other than HNO, and it is also difficult to collect N_2O *in vivo*. Therefore, studies on HNO, particularly *in vivo* studies, are severely hampered by the lack of an efficient and highly specific indirect or direct method of HNO detection. Thus, so far there is no unequivocal evidence for the endogenous generation of HNO in mammalian systems (*59*). However, its high reactivity with thiols (Scheme 1.1) (*31, 38*) may provide an additional probe of HNO. Since it is the only NO_x known to

produce sulfinamides, the goal is to find a thiol that forms exclusively the sulfinamide with AS. Such a thiol would likely be suitable as a HNO trap and marker.

To further probe sulfinamide yields, the reactions of Cys, HCys, and Pen with Angeli's salt (AS) were investigated. Since a residue on the C-terminus of Cys appears to increase sulfinamide formation (Tables 4.4 and 4.5), four CX dipeptides, CE, CD, CK, CW, with differently charged C-terminal residues were reacted with the HNO released from AS. The influence of X on the sulfinamide/disulfide ratio relative to that obtained for CG sheds lights on HNO/thiol reactions, which will aid in the development of a HNO marker.

5.2 Materials and Methods

5.2.1 Materials and solutions

Stock solutions of Angeli's salt (AS, Cayman) were prepared as described in Section 4.2.1. *L*-cysteine (Cys; $C_3H_7NO_2S$, free base), *N*-acetyl-*L*-cysteine (*N*-AcCys), *DL*-homocysteine (HCys), *DL*-penicillamine (Pen) were purchased from Sigma and *N*-acetyl-*DL*-penicillamine (*N*-AcPen) from Aldrich. *N*-acetyl-HCys (*N*-AcHCys) were synthesized and purified as above described in Chapter 2. The dipeptides GluCys (EC), CysAsp (CD), CysGlu (CE), CysLys (CK), CysTrp (CW) were obtained from CanPeptide (Montreal). Other materials used here were obtained from the suppliers listed in previous Chapters. All solutions were prepared using Nanopure water (MilliQ) from a Millipore system.

5.2.2 Incubations of AS with Cys, HCys, Pen, and their *N*-acetylated derivatives

Freshly prepared 10 mM solutions of Cys, *N*-AcCys, HCys, *N*-AcHCys, Pen, *N*-AcPen in water were incubated with equimolar AS from a ~400 mM stock solution at room temperature for 30 min. The pH of the solutions was adjusted with HCl or NaOH, and monitored at 10-min intervals using an Orion Model 9810BN micro pH electrode (Thermo Electron Corporation). Control incubations containing 10 mM RSH and 10 mM $NaNO_2$ also were examined. The products were analyzed by ESI-MS.

5.2.3 Incubations of AS with the dipeptides

Freshly prepared 5 mM solutions of the dipeptides EC, CD, CE, CK, and CW in water were incubated with equimolar AS under the same conditions as in Section 5.2.2, and the products were analyzed by ESI-MS. Control incubations containing the dipeptides and $NaNO_2$ were also performed, and the experimental details are given in the figure legends.

5.2.4 ESI-MS and ESI-MS/MS

Incubations were diluted 10-20-fold into 50% aqueous ACN/0.2% formic acid. ESI-MS and ESI-MS/MS were carried out on a Waters Micromass Q-ToF 2 mass spectrometer operating in positive-ion mode following direct infusion of the samples into the Z-spray source. The instrument was calibrated as described in Section 4.2.5, and the instrumental parameters are listed in the figure legends. Data analysis was performed using MassLynx 4.0 software (Waters Micromass).

5.3 Results

5.3.1 Reaction of HNO with Cys, HCys, Pen, and their *N*-acetylated derivatives

The products formed in AS/Cys incubations were examined by ESI-MS after 30 min since the decomposition of the salt is complete within this time period at pH 4-8 (Figure 1.2). Peaks at m/z 241, 263, and 285 in the spectrum of the pH 5-9 incubations (pH 5.85 spectrum in Figure 5.1A) are assigned to the protonated (MH^+) and sodiated [$[M-(n-1)H+nNa]^+$, n=1-3] ions of the disulfide, cystine. Formation of cystine was confirmed by fragmentation of the MH^+ ion at m/z 241, which yielded a MS/MS spectrum with fragment ions at m/z 224, 195, 158, 152, 122, and 120 as reported

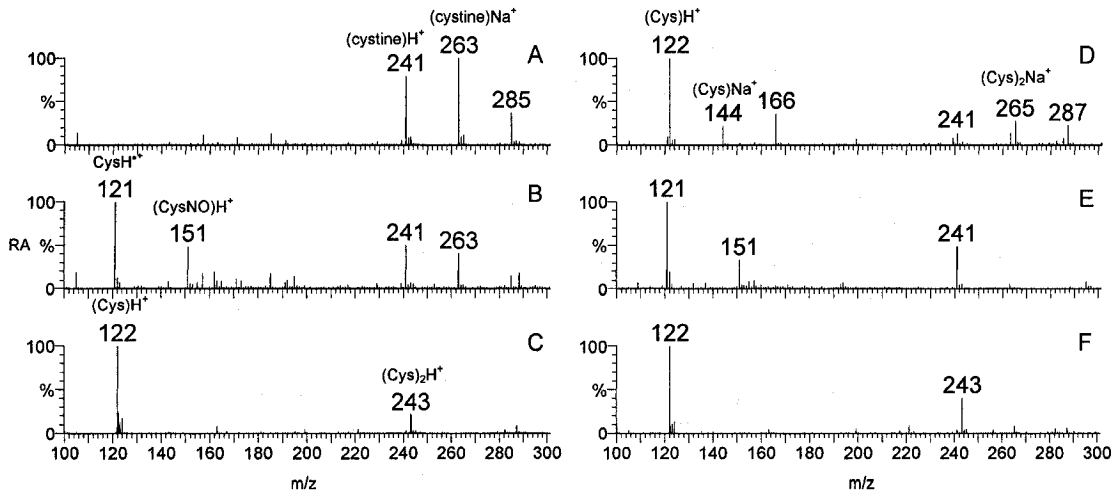

Figure 5.1. **ESI-MS analysis of 30-min AS/Cys and $NaNO_2$/Cys incubations *vs* pH.** 10 mM Cys was incubated with 10 mM AS at pH (A) 5.85, (B) 3.22, or 10 mM $NaNO_2$ at pH (D) 7.21, (E) 3.06 at room temperature for 30 min; the controls contained Cys only (C) in water (pH 5.43) and (F) at pH 6.92 for 30 min. Experimental conditions: The pH was adjusted to the values indicated with HCl or NaOH and measured at 10-min intervals. For MS analysis, the incubations were diluted 10- or 20-fold into 50% aqueous ACN/0.2% formic acid, and directly infused at a flow rate of 1 μL/min into the Z-spray ion source of the Q-ToF 2 mass spectrometer. The instrumental parameters were: source block temperature 80°C, capillary voltage 3.2 kV, cone voltage 20 kV, collision voltage 5 V (no collision gas), ToF -9.1 kV and MCP 2.0 kV. RA is the relative abundance of the ions.

previously (*88*). In contrast, prominent peaks at m/z 122 and 243, assigned to the MH^+ ions of Cys and the noncovalent Cys dimer $(Cys)_2$ respectively, appear in the Cys-only spectrum (Figure 5.1C). Their sodiated ions are of low abundance since the free-base form of Cys ($C_3H_7NO_2S$) was used and the Cys-only solution contained no added sodium salts such as AS ($Na_2N_2O_3$).

At pH < 4, AS releases NO but no HNO (*55*). Similar to GSH, *S*-nitrosation of Cys likely occurs below pH 4:

$$Cys + HNO_2 \rightarrow CysNO + H_2O \qquad (5.1)$$

$CysNOH^+$ (m/z 151) and $CysH^{\bullet+}$ (m/z 121) ions, which are indicative of CysNO formation (*60*), are clearly visible in the spectrum of the pH 3.22 AS/Cys incubation (Figure 5.1B), and all incubations at pH <4 (data not shown). The odd-electron $CysH^{\bullet+}$ ion arises from protonation of the cysteinyl thiyl radicals ($Cys^{\bullet}$) formed on CysNO homolysis in the ESI source (*60*):

$$CysNO \rightarrow Cys^{\bullet} + NO^{\bullet} \qquad (5.2)$$

The $(cystine)H^+$ peak (m/z 241) in Figure 5.1B is assumed to arise from $Cys^{\bullet}$ dimerization ($Cys^{\bullet} + Cys^{\bullet} \rightarrow$ cystine) in the ESI source since AS does not liberate HNO at pH <4.0 (*55*) to generate the disulfide *via* Scheme 4.1***a***.

The ESI mass spectra of the $NaNO_2$/Cys incubations at pH 3-9 (spectra at pH 7.21 and 3.06 in Figure 5.1D, E) support this conclusion. The pH 5-9 incubations yield spectra that are dominated by the $(Cys)H^+$ ion (m/z 122) seen in the spectrum of Cys alone (Figure 5.1D *vs* C), which was expected since NO_2^- is not an effective *S*-nitrosating agent at neutral pH (*87*). The spectra of the pH 3.06 $NaNO_2$/Cys and pH 3.22 AS/Cys incubations are essentially identical (Figure 5.1E and B) and contain the $CysH^{\bullet+}$ ion (m/z

121), confirming that CysNO is formed in both incubations at low pH. Significantly, unlike the GSH/AS incubations, no Cys sulfinamide ions (m/z 153; M+31) were detected in the spectra of the AS/Cys incubations at any pH, revealing that the *N*-hydroxysulfenamide intermediate reacts with a second Cys molecule faster than it releases OH^- (Scheme 4.1). Also, the mass spectrum of Cys only was found to be pH-independent within the range of 3-9 over 30 min (spectrum at pH 6.92 in Figure 5.1F), confirming that the thiol group is stable in the absence of AS. In summary, incubation of

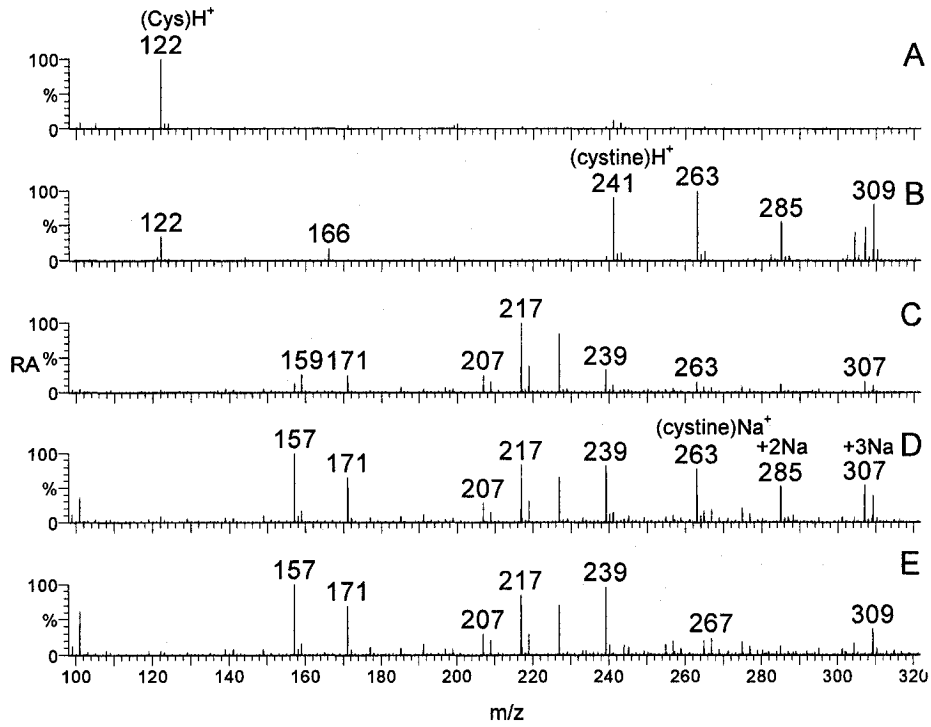

Figure 5.2. **ESI mass spectra of 30-min AS/Cys incubations *vs* Cys/AS ratio.** (A) 10 mM Cys alone in water at pH 5.43; (B) 10 mM Cys with 10 mM AS at pH 6.40, (C) 1 mM Cys with 10 mM AS at pH 6.82, and (D) 5 mM Cys with 50 mM AS at pH 6.80; (E) 10 mM AS alone in water at pH 5.16. All incubations were carried out at room temperature and the other experimental conditions are given in the legend of Figure 5.1. Peaks at m/z 157, 171, 207, 217, 227, 239, 267, and 309 in spectra C, D are due to the present of excess AS and correspond to those seen in spectrum E of AS alone.

free Cys with AS produces the disulfide, cystine, due to reaction with HNO (Scheme 4.1) at pH 5-9, and CysNO due to reaction with HNO_2-derived nitrosating agents at pH <4.0. Variation in the AS and Cys concentrations (1–10 mM) or the AS/Cys ratios (1:1–10:1) at pH >5 gave rise to cystine exclusively (Figure 5.2), underscoring the efficiency of path ***a*** in Scheme 4.1 when RSH is Cys.

The reactions of HNO with *N*-AcCys were performed under the same conditions as those with Cys. The ESI mass spectra showed that only the *N*-acetylated disulfide was formed between pH 5-9 while *N*-AcCysNO was observed at pH <4, but no sulfinamide was detected at any pH. However, the sodiated ions of the disulfide (m/z 347, 369, 391) and of *N*-AcCysNO (m/z 215, 237) and not their protonated forms (m/z 325 and m/z 193, respectively) appear in the ESI mass spectra (Figure 5.3A, B), indicating that *N*-acetylation promotes sodiation of Cys. This is presumably due to blocking of the

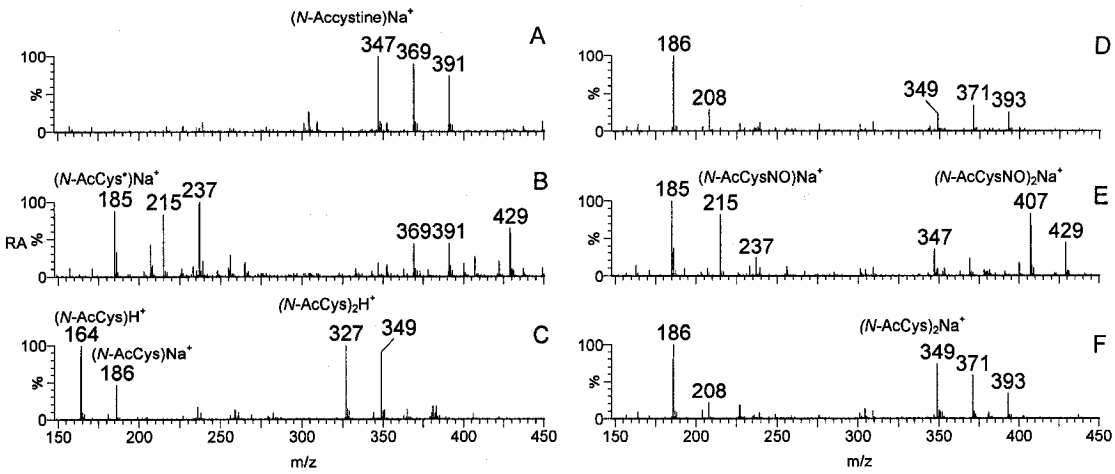

Figure 5.3. **ESI-MS analysis of 30-min AS/*N*-AcCys and $NaNO_2$/*N*-AcCys incubations *vs* pH.** 10 mM AS was incubated with 10 mM *N*-AcCys at pH (A) 6.59, (B) 3.80, and with $NaNO_2$ at pH (D) 7.05, (E) 3.10. Controls containing 10 mM *N*-AcCys only incubated in water (C) at pH 2.51 and (F) at pH 7.34 for 30 min. The experimental conditions are given in the legend of Figure 5.1.

α-amino group which is the most likely site of protonation in Cys. Control $NaNO_2$/*N*-AcCys incubations (Figure 5.3D, E) showed the same results as those for Cys but all ions were sodiated, and *N*-AcCys was found to be stable over the pH 3-9 range (pH 7.34 spectrum, Figure 5.3F).

The reactions of AS with HCys and *N*-AcHCys were also compared using ESI-MS. The major peaks at m/z 269, 291, 313, and 335 in the spectrum of 30-min AS/HCys incubations at pH 5-9 (Figure 5.4A, B) are assigned to the protonated and sodiated ions of the disulfide, Hcystine. When the incubations were carried out at pH 3.50, the protonated and sodiated ions of HCysNO (m/z 165, 187) and of $HCys^{\bullet}$ (m/z 135, 157), formed on HCysNO homolysis ($HCysNO \rightarrow HCys^{\bullet} + NO^{\bullet}$) in the ion source, gave rise to the major peaks in the spectrum, but weak Hcystine peaks are also present (Figure 5.4C). Peaks at m/z 251 and 253 are due to the loss of H_2O (-18 u) from the disulfide and the

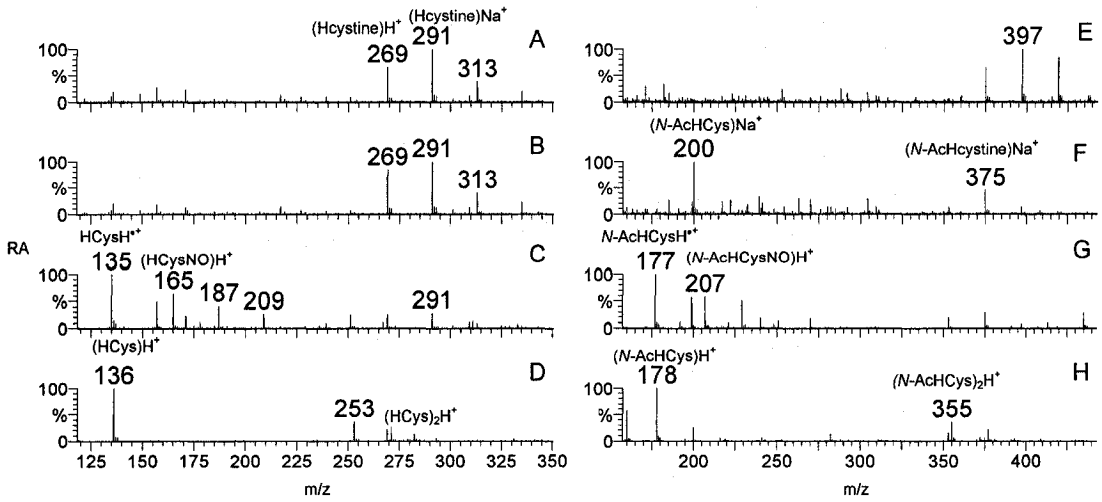

Figure 5.4. **ESI-MS analysis of 30-min AS/HCys and AS/*N*-AcHCys incubations *vs* pH.** 10 mM AS was incubated with 10 mM HCys at pH (A) 7.16, (B) 5.51, (C) 3.50, and with 10 mM *N*-AcHCys at pH (E) 7.22, (F) 5.53, (G) 2.18. Controls containing (D) 10 mM HCys only, and (H) 10 mM *N*-AcHCys only in water at pH 6.55 and 2.77, respectively. The experimental conditions are given in the legend of Figure 5.1.

HCys dimer, respectively, in the ion source (Figure 5.4C, D). Similar to the AS/Cys incubations, no sulfinamide was detected at m/z 167 in the spectra of the AS/HCys incubations at any pH. Control experiments show that nitrite reacts with HCys to form HCysNO at pH <4 but does not react with thiol at pH 5-9 as observed for Cys. HCys is also stable in the pH range of 3-9 (Figure 5.5). The most abundant peak at m/z 136 in the spectrum of HCys only (Figure 5.4D) arises from unreacted HCys and the minor peak corresponds to the HCys dimer (m/z 271). Thus, the formation of disulfides in the AS/HCys incubations is due to reaction with HNO but not nitrite.

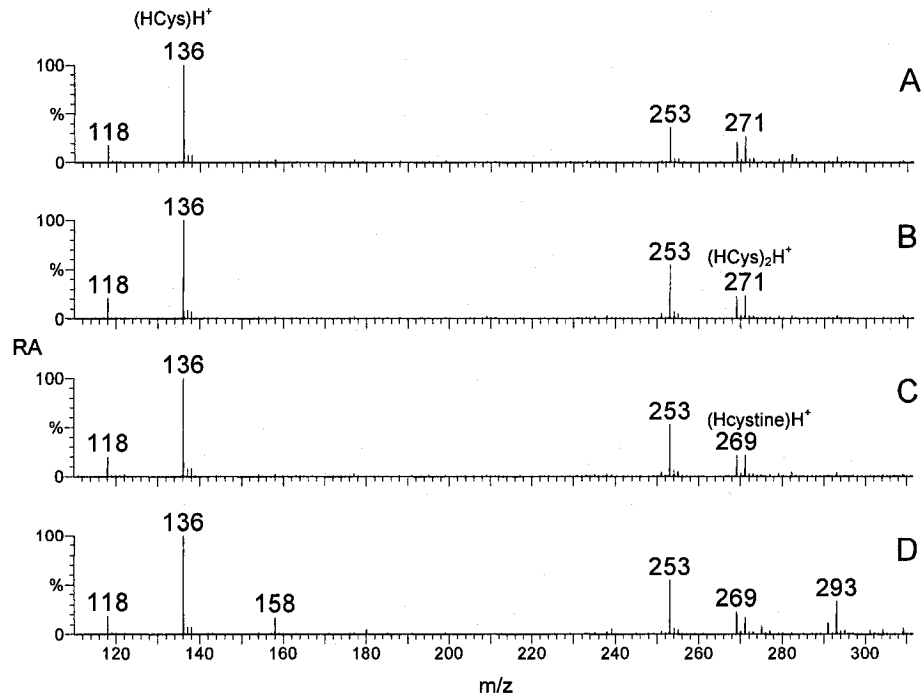

Figure 5.5. **ESI mass spectra of HCys stability *vs* pH.** 5 mM HCys in water at pH (A) 2.64, (B) 6.40, (C) 7.23, and (D) 8.79 after standing at room temperature for 30 min. The pH of the HCys solution was adjusted with HCl or NaOH. Other conditions are given in the legend of Figure 5.1.

When HCys was replaced by *N*-AcHCys, the disulfide (m/z 353) also formed during 30 min incubation with AS at pH 5-9 (Figure 5.4E, F), whereas *N*-AcHCysNO

(m/z 207) and *N*-AcHCys$^{\bullet}$ (m/z 177) formed at pH <4 as expected (Figure 5.4G). Most of the peaks arise from sodiated ions with mass of [M-(n-1)H+nNa, n=1-3] as in the AS/*N*-AcCys incubations. However, unlike HCys, unreacted *N*-AcHCys (m/z 200, 222) was detected (as sodiated ions) in the spectrum of the AS/*N*-AcHCys incubations at pH ~5.5 (Figure 5.4F) but not at pH ~7.2 (Figure 5.4B). (*N*-AcHCys)H^+ (m/z 178) and (*N*-AcHCys)$_2H^+$ (m/z 355) dominate the spectrum of *N*-AcHCys only, and the loss of H_2O from *N*-AcHCys in the ion source gives rise to the peak at m/z 160 (Figure 5.4H).

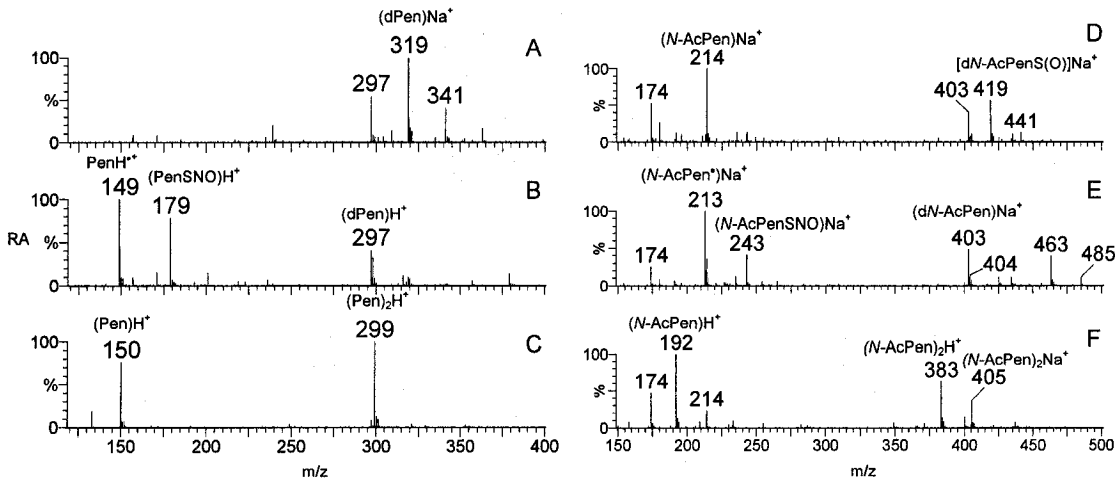

Figure 5.6. **ESI-MS analysis of 30-min AS/Pen and AS/*N*-AcPen incubations *vs* pH.** 10 mM AS was incubated with 10 mM Pen at pH (A) 7.50, (B) 2.21, and with 10 mM *N*-AcPen at pH (D) 7.58, (E) 3.60. Controls containing (C) Pen only in water at pH 4.47, and (F) *N*-AcPen only in water at pH 2.89. The experimental conditions are given in the legend of Figure 5.1.

The reactions of HNO with penicillamine, a thiol-containing drug, were also examined. The ESI-MS results parallel those obtained for the AS/Cys and AS/HCys incubations. The protonated and sodiated ions of the disulfide (dPen, m/z 297, 319, 341, 363) appear in the spectra of the AS/Pen incubations at pH 5-9 (Figure 5.6A), but the MH^+ ions of Pen$^{\bullet}$ (m/z 149) and PenSNO (m/z 179) with minor disulfide peaks dominate

the spectra of the pH 3.6 incubations (Figure 5.6B). Similar to *N*-AcHCys, *N*-AcPen exhibits lower reactivity with HNO than Pen as revealed by the presence in the spectrum of sodiated ions of the unreacted thiol (m/z 214) after incubation with AS at pH 7.58 (Figure 5.6D). The *S*-oxide disulfide [d*N*-AcPenS(O)Na^+, m/z 419] also appears in spectrum D, and similar spectra were obtained after incubation in the pH range 5-9 (data not shown). At pH <4, sodiated ions of *S*-nitrosated *N*-AcPen (m/z 243) and its dimer (m/z 463, 485) appear in the spectrum (Figure 5.6E).

5.3.2 Reaction of HNO with the CX dipeptides

Based on the products formed in the incubations of AS with the GSH derivatives (Chapter 4), it appears that charge and conformation of the thiol may control the sulfinamide/disulfide ratio. In particular, CG with Cys at the N-terminus formed more sulfinamide than γEC with Cys at the C-terminus (Figure 4.14, Table 4.5). Thus, four additional CX dipeptides (Figure 5.7) were incubated with AS to investigate the effects of

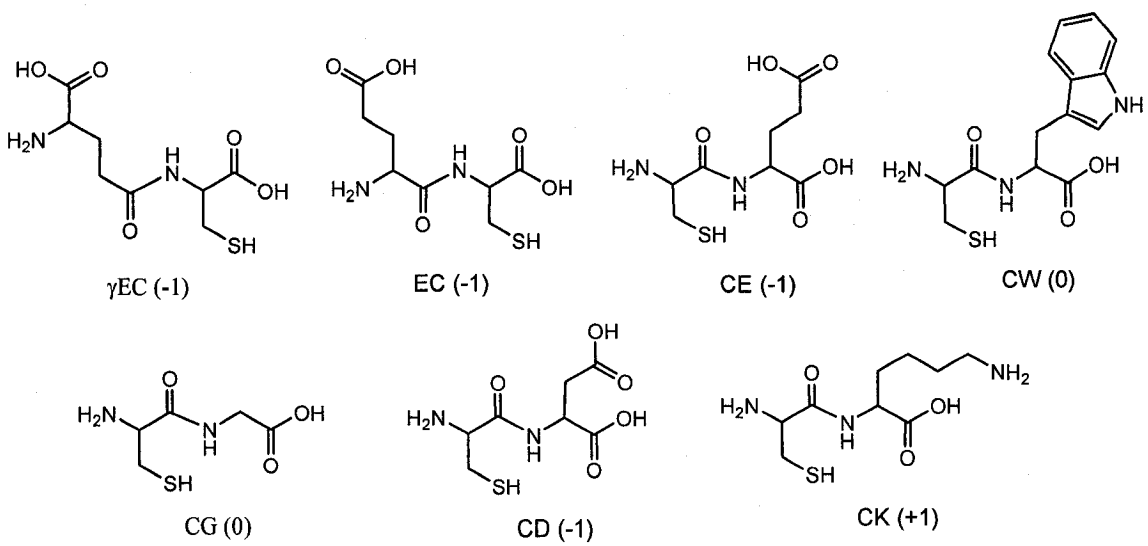

Figure 5.7. **Structures of the dipeptides, γEC, EC, CE, CG, CD, CW and CK** (overall charge at pH 7)

charge on the sulfinamide *vs* disulfide yield. The EC peptide was included to compare the the effects of α- *vs* γ-linkage on the products obtained since γEC was studied in Chapter 4.

Significant sulfinamide formed in the AS/CE incubations since protonated and sodiated sulfinamide ions (CE-$SONH_2$, m/z 282, 304, 326) and $(M+14)H^+$ ions (m/z 265), a sulfinamide marker (Section 4.3.1), dominate the spectrum at pH 5.40 (Figure 5.8B). The sulfinamide is also present in the spectrum at pH 7.45, although the disulfide (dCE) ions are more abundant (Figure 5.8A, B). In contrast, protonated and sodiated disulfide ions give rise to the major peaks in the spectra of the AS/EC incubations and negligible sulfinamide was detected (Figure 5.8D, E), similar to the AS/γEC

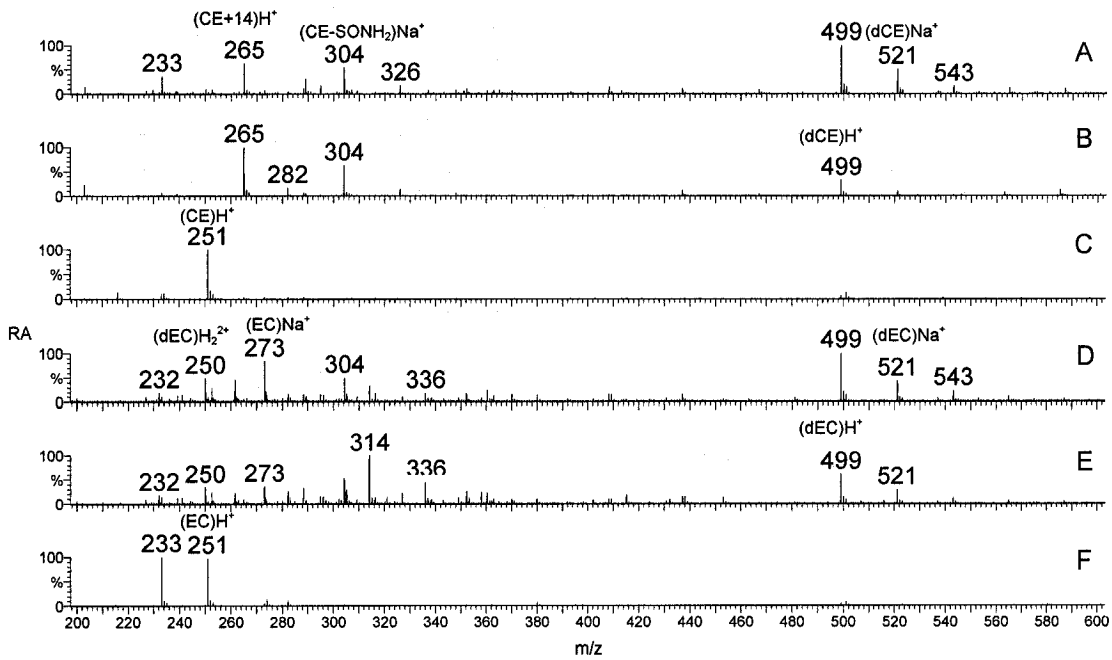

Figure 5.8. **ESI mass spectra of 30-min AS/CE and AS/EC incubations.** 5 mM AS was incubated with 5 mM CE at pH (A) 7.45, (B) 5.40, and with 5 mM EC at pH (D) 7.55, (E) 5.43. Controls contained (C) 5 mM CE only in water at pH 2.88, and (F) 5 mM EC only in water at pH 3.12. The experimental conditions are given in the legend of Figure 5.1.

incubations (Figure 4.14). Although a minor peak at m/z 304 could arise from the sodiated ion of the sulfinamide, the absence of the marker $(M+14)H^+$ ion (m/z 265) suggests that the m/z 304 peak may be an impurity (Figure 5.8D). Also, MH^+ and MNa^+ ions of unreacted EC (m/z 251, 273) appear in the spectra, indicating the low reactivity of this thiol with HNO (Figure 5.8D). The peaks at m/z 233, 232 are due to loss in the ion source of H_2O from EC and from the doubly charged disulfide (MH_2^{2+}). Thus, although EC and CE have the same charge (-1) at neutral pH (Figure 5.7), their HNO reactions vary considerably.

In the incubation of AS with CK, which has opposite overall charge to CE (Figure 5.7), mainly sulfinamide (m/z 281, 303, 325) was formed at lower pH (e.g., 5.19; Figure 5.9B) and disulfide (m/z 497, 519, 541, 563) at higher pH (e.g., pH 7.57; Figure 5.9A). Fragment ions due to the loss of NH_3 (m/z 264 = 281-17) and both NH_3 and H_2O (m/z 246 = 281-17-18) from the sulfinamide (m/z 281) are present in the spectrum (Figure 5.9B). However, unreacted CK (m/z 250) was detected in the 30-min AS/CK incubation at pH 7.57 (Figure 5.9A), indicating that CK has lower reactivity with HNO than CE.

CD, which possesses the same overall charge as CE but a $-CH_2COOH$ *vs* $-CH_2CH_2COOH$ side chain (Figure 5.7), forms largely the sulfinamide on incubation with AS. At pH 5.42, $(M+14)H^+$ (m/z 251) and the protonated and sodiated ions (m/z 268, 290, 312) of the sulfinamide are predominant (Figure 5.9E). However, the peaks of the protonated and sodiated disulfide ions (m/z 471, 493, 515, 537, 559) intensify upon increasing the pH to 7.45, although the sulfinamide ions are still visible (Figure 5.9D). These results are similar to those of AS/CE incubations (Figure 5.8A, B), indicating that the E→D substitution in CX does not affect the sulfinamide/disulfide ratio.

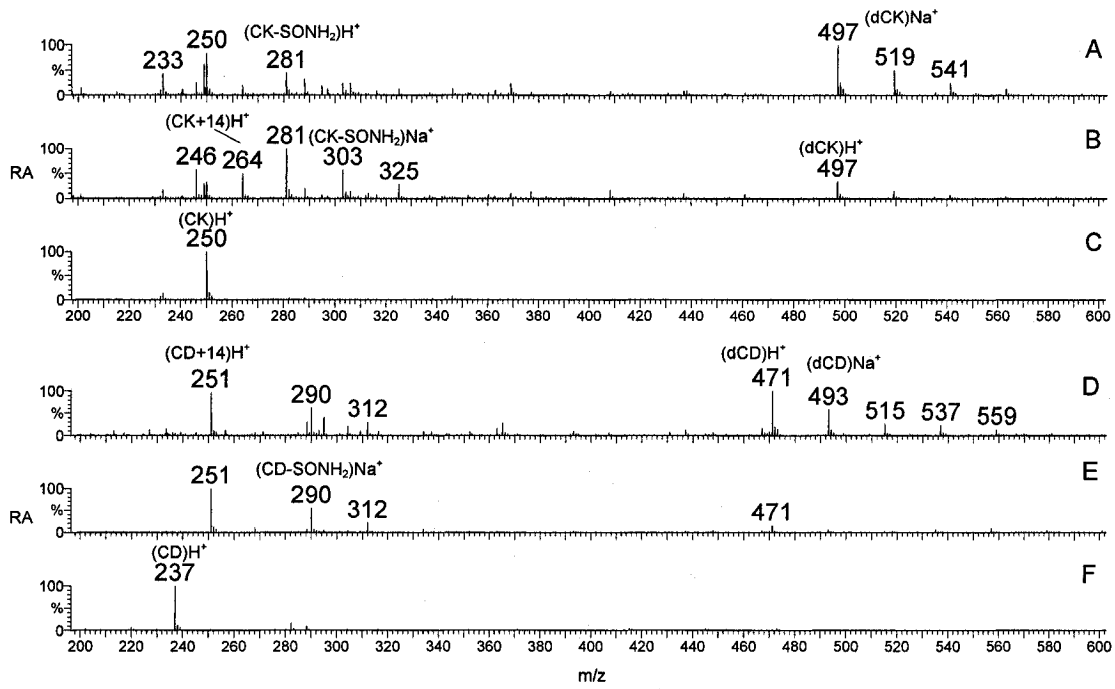

Figure 5.9. **ESI mass spectra of 30-min AS/CK and AS/CD incubations.** 5 mM AS was incubated with 5 mM CK at pH (A) 7.57, (B) 5.19, and with 5 mM CD at pH (D) 7.40, (E) 5.42. Controls contained (C) CK only in water at pH 2.98 and (F) CD only in water at pH 2.55. The experimental conditions are given in the legend of Figure 5.1.

The MH^+ and MH_2^{2+} ions of the disulfide (m/z 613, 307) dominate the spectrum of the AS/CW incubations at pH 7.17 (Figure 5.10A) with just a weak peak due to the sodiated disulfide ion appearing at m/z 635. The $(M+14)H^+$ peak (m/z 322), corresponding to the sulfinamide marker (Section 4.3.1), is the major peak at pH 5.52 with a minor disulfide peak (Figure 5.10B). Compared to the other dipeptides, the sodiated ions of the CW derivatives are of low abundance, suggesting that the C-terminal Trp residue possesses low Na^+ affinity. At a given pH, more disulfide is formed in the AS/CW incubations than in the AS/CE incubations (Figures 5.10 *vs* 5.8A, B) but less than in the AS/CG incubations (Figure 4.14F, G). Thus, both the polarity and size of residue modulate the reactivity of Cys with HNO in the CX dipeptides.

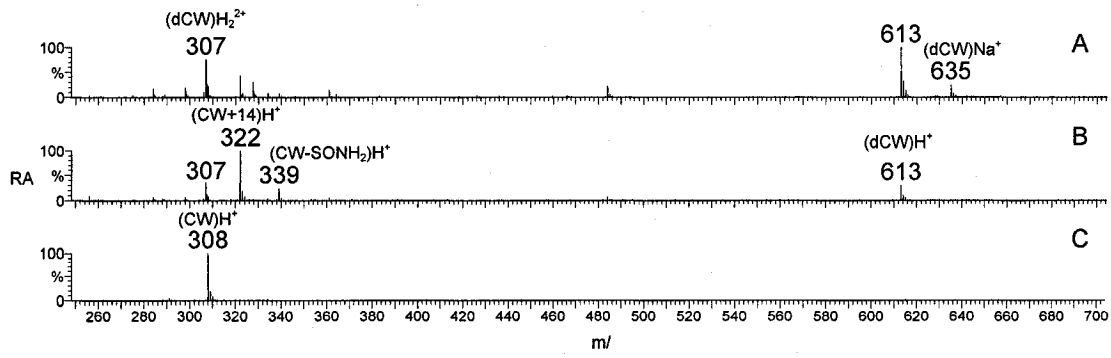

Figure 5.10. **ESI mass spectra of 30-min AS/CW incubations.** 5 mM AS was incubated with 5 mM CW at pH (A) 7.17, (B) 5.52. The control contained (C) CW in water at pH 2.85. The experimental conditions are given in the legend of Figure 5.1.

5.4 Discussion

5.4.1 Thiol-containing amino acids

The reaction of HNO with the thiol-containing amino acids, Cys, HCys, and Pen at pH 5-9 leads exclusively to the disulfides. No sulfinamide was detected indicating that their *N*-hydroxysulfenamide intermediate reacts with a second RSH faster than it decays to the RS^+=NH cation, which leads to the sulfinamide, $RSONH_2$ (Scheme 4.1). Thus, the thiol pK_a [Cys (8.33), HCys (8.76), and Pen (11.08)] does not control the products formed in the HNO reactions, indicating that the thiol and not the thiolate form is reactive with HNO in the pH range of 5-8.

No sulfinamide appeared in the spectra of the AS incubations with *N*-AcCys, *N*-AcHCys and *N*-AcPen. However, *N*-AcHCys is less reactive with HNO than HCys, since it was not fully consumed after 30-min incubation with AS at pH 5.53 (Figure 5.4). Conversion to the disulfide is more complete at higher pH (e.g., 7.22) perhaps due increased thiolysis of the *N*-hydroxysulfenamide intermediate (Scheme 4.1***a***) by the

thiolate anion. The thiol pK_a of HCys (8.76) increased by ~1 pH-unit upon *N*-acetylation (9.66), so that thiolysis by *N*-AcHCys may be less efficient, thereby slowing the rate of disulfide formation compared to that for HCys.

Extensive unreacted *N*-AcPen and little disulfide were present in all its AS incubations in the pH range 5-9 (Figure 5.6D). Thus, *N*-AcPen exhibits poor reactivity with HNO although its thiol pK_a (10.21) is lower than that of Pen (11.08) (Table 3.2). These results suggest that the *N*-AcPen reactivity with HNO may be attenuated by steric shielding by the two methyl groups adjacent to the thiol (*99*) (Figure 3.3) as well as electrostatic repulsion due to its -1 charge at neutral pH *vs* Pen which is uncharged.

5.4.2 Thiol-containing dipeptides

Based on the ESI-MS data, the CX (X = Gly, Glu, Asp, Lys, Trp) dipeptides undergo enhanced sulfinamide formation compared to free Cys and the γEC and EC dipeptides. Although their thiol pK_a values vary significantly [Cys (8.33), EC (10.32), γEC (11.23) (Table 3.2)], they all undergo efficient HNO-induced disulfide formation. However, in the CX dipeptides the carboxylate group can interact more with the *N*-hydroxysulfenamide group to promote sulfinamide formation via path ***b*** of Scheme 4.1. The CE and CD dipeptides have two carboxylate groups *vs* one in CG (Figure 5.7), which may explain the increased sulfinamide formation at a given pH. The large size and low polarity of Trp render the environment around the thiol more hydrophobic in CW, which may suppress ionization and disulfide formation, thereby increasing the sulfinamide yield compared to that of CG (Figure 4.14F, G). CK possesses a flexible, positively charged ε-amino group as well as the carboxylate group at the C-terminal. Interaction of the ε-

amino group with the thiol should enhance its ionization and hence disulfide formation, but the experimental data (Figure 5.9A, B) reveal that more sulfinamide is formed upon incubation of AS with CK than with CG. The ε-amino group may interact with the carboxylate group such that the effect on thiol ionization is less than expected.

5.4.3 HNO marker development

No direct method is available for HNO detection at present, especially under physiolgical conditions (*59*). Therefore, an efficient, specific method to monitor HNO is necessary for studies on HNO biochemistry, particularly for *in vivo* studies. Sulfinamide, a product of the reaction of a thiol with HNO, but not with other NO_xS, could be used as a marker of HNO. Our studies reveal that sulfinamide formation is preferred at low pH (5-6), and is controlled by the thiol's structure. Charged residues such as Glu at the C-terminus of Cys promote sulfinamide formation more than at the N-terminus. Also, the α-amino group of Cys-containing peptides affects the products since more sulfinamide was formed in the *N*-AcGSH/AS *vs* GSH/AS incubations under the same conditions.

Table 5.1 summarizes the relative sulfinamide yields based on MS analysis of the AS/RSH incubations. *N*-AcGSH, CE, and CD give the highest sulfinamide yields at pH ~7.4 (Table 5.1), but also form disulfide (Figures 4.6, 5.8, 5.9). However, *N*-acetylation of CE or CD may further increase the sulfinamide yield and these are good candidates for the further development of a HNO marker that yields sulfinamide exclusively on reaction with HNO at pH 7.4. Also, sulfinamide formation should be investigated in the presence of high GSH concentration since its concentration *in vivo* is 0.5-10 mM (*1*). In contrast,

the HNO concentration is expected to be very low *in vivo* although there are no data due to the absence of an effective method of HNO measurement (*59*).

Table 5.1. **Relative sulfinamide yields in the 30-min incubations of RSH with AS[a]**

RSH (Charge)		EtGSH (0)	GSH (-1)	*N*-AcGSH (-2)	CD (-1)	CE (-1)	CK (+1)	CW (0)	CG (0)	R'SH[b]
Sulfinamide yield[a]	pH ~6.0	0.81	3.35	9.42	5.96	3.12	3.43	1.75	0.76	0
	pH ~ 7.4	0.13	0.43	1.19	0.88	0.70	0.51	0.32	0.10	0

[a] Relative sulfinamide yields were estimated from the relative abundances of the sulfinamide *vs* disulfide peaks in the ESI mass spectra. Larger numbers indicate more sulfinamide relative to disulfide.

[b] R'SH includes Cys, HCys, Pen, *N*-AcCys, *N*-AcHCys, *N*-AcPen, γEC, and EC.

6 GENERAL CONCLUSIONS AND SUGGESTIONS FOR FUTURE WORK

6.1 Chapter 2

The procedure described here for the *N*-acetylation of GSH and HCys was performed at room temperature in aqueous medium. The only reagent used was NHSA, which is very effective in *N*-acetylation in a short time (10-30 min). Previous methods required activators such as dimethylaminopyridine in addition to an acylating reagent such as acyl chloride, or diethyl ether, and 6-24 h reaction time with pH adjustments (*58*). Only one step is required to form the *N*-acetylated disulfides using NHSA (Scheme 2.1) and the products are stable and easy to purify using solid-phase extraction (SPE) or dialysis. The *N*-acetylated RSHs, which are produced using gel-bound TCEP suspended in water, were collected by centrifugation and did not need any further purification, since TCEP and its oxidized form (Scheme 2.1) remain immobilized on the agarose gel. Compared to the previously reported methods (*58*), the disulfide group does not need to be blocked before *N*-acetylation, and thiol deblocking and purification are simple and efficient.

N-acetylation was carried out on a small scale here (31 mg of GSSG or 5 mg of Hcystine), but it could be readily scaled up to the gram scale. NHSA is relatively expensive ($139 Cdn per 100 mg NHSA which will *N*-acetylate 50 mg of GSSG or 21 mg of Hcystine) but it can be generated *in situ* (Section 2.4) with cheaper reagents to reduce the cost for large-scale production. Also, other acyl groups can be introduced into the thiol. The immobilized TCEP gel ($146 Cdn per 10 mL of a 50% water slurry which will reduce ~40 mg of *N*-AcGSSG or 20 mg of *N*-AcHcystine) can not be regenerated as stated by the supplier, so use of a different immobilized reductant such as DTT that can

be regenerated would reduce the cost. However, the method described here is an ideal method for *N*-acetylation of water-soluble, thiol-containing molecules required in milligram to gram quantities.

6.2 Chapter 3

The pK_a values of the low-mass thiols were measured by the pH-metric method at Merck Frosst (Montreal, Canada). The measured values agree with the reported values where available (Table 3.1 *vs* 3.2), but only 5 of the 13 thiols examined here have reported pK_a values. The thiol pK_a increased upon *N*-acetylation of HCys but decreased upon *N*-acetylation of Pen because of the relative values of the thiol and α-amino pK_as of HCys and Pen are reversed (Table 3.2, Section 3.4).

6.3 Chapters 4 and 5

Nitroxyl is known to form under physiological conditions (*28, 29, 31*) and it may play a significant role in protecting the cardiovascular system. Glutathione (GSH) is the most likely biological target of HNO, and ESI-MS analysis revealed that the sulfinamide ($GSONH_2$) and disulfide (GSSG) were formed in AS/GSH incubations at pH>5 but GSSG was the dominant product at pH >7 or at GSH at high concentrations. Thus, under normal physiological conditions, HNO could change the intracellular GSH/GSSG ratio and affect cell function. Under certain conditions (e.g., low local pH) HNO may also play a role in cell signaling by converting GSH to $GSONH_2$, which may not reform the free thiol under physiological conditions. Disulfides only were detected in the reaction of AS with Cys, *N*-AcCys, HCys and Pen at pH>5.

N-acetylation of Pen decreased its reactivity with HNO and led to *S*-oxide disulfide (RSOSR) formation. Control experiments with $NaNO_2$ confirmed that the products formed in the AS incubates are due to reaction with HNO at pH>5 but with HNO_2 at pH<4, which yields RSNOs.

The reactions of HNO with seven Cys-containing dipeptides were investigated. The ESI-MS data showed that dipeptides with Glu or Asp on the C-terminus of Cys gave high sulfinamide yields on incubation with AS. Since sulfinamide may be a specific marker for HNO, modification of the CD and CE dipeptides might be considered in the further design and development of a thiol-based HNO marker.

6.4 Suggestions for future work

(1) Optimize the method for large scale *N*-acetylation of RSH based on the procedure described in Chaper 2 for the 5-30 milligram scale.

(2) Since $GSONH_2$ is hydrolyzed to GSO_2H at low pH but is stable at neutral pH, the sulfinamide should be isolated under neutral or weakly basic conditions.

(3) Sulfinamides are converted to sulfinic acids which can be enzymatically reduced to the thiol. Thus, $GSONH_2$ should be exposed to yeast-cell and red-blood-cell lysates and plasma to establish if the sulfinamide is likely to be hydrolyzed enzymatically *in vivo*.

(4) Factors that control the reactivity of the putative *N*-hydroxysulfenamide should be investigated by computational chemistry.

(5) A thiol-containing HNO marker should react with HNO to form the sulfinamide exclusively under physiological conditions. Since the sulfinamide yield is higher for

N-AcGSH compared to GSH, the CD and CE dipeptides should be *N*-acetylated and the sulfinamide yields in their AS incubations determined.

(6) After development of a HNO marker, the analytical methodology should be optimized for routine laboratory use.

(7) All the RSH/AS incubations should be reanalyzed by HPLC-UV to obtain product yields since ESI-MS analysis does not provide quantitative data.

(8) The effects of the different RSHs on AS decomposition should be monitored optically to confirm that the thiols react with HNO and not AS.

REFERENCES

1. Wu, G., Fang, Y. Z., Yang, S., Lupton, J. R., and Turner, N. D. Glutathione metabolism and its implications for health, (2004), *J Nutr* 134, 489-92.
2. Sies, H. Glutathione and its role in cellular functions, (1999), *Free Radic Biol Med* 27, 916-21.
3. Fang, Y. Z., Yang, S., and Wu, G. Free radicals, antioxidants, and nutrition, (2002), *Nutrition* 18, 872-9.
4. Townsend, D. M., Tew, K. D., and Tapiero, H. The importance of glutathione in human disease, (2003), *Biomed Pharmacother* 57, 145-55.
5. Casagrande, S., Bonetto, V., Fratelli, M., Gianazza, E., Eberini, I., Massignan, T., Salmona, M., Chang, G., Holmgren, A., and Ghezzi, P. Glutathionylation of human thioredoxin: a possible crosstalk between the glutathione and thioredoxin systems, (2002), *Proc Natl Acad Sci U S A* 99, 9745-9.
6. Lo Bello, M., Nuccetelli, M., Caccuri, A. M., Stella, L., Parker, M. W., Rossjohn, J., McKinstry, W. J., Mozzi, A. F., Federici, G., Polizio, F., Pedersen, J. Z., and Ricci, G. Human glutathione transferase P1-1 and nitric oxide carriers; a new role for an old enzyme, (2001), *J Biol Chem* 276, 42138-45.
7. Di Simplicio, P., Franconi, F., Frosali, S., and Di Giuseppe, D. Thiolation and nitrosation of cysteines in biological fluids and cells, (2003), *Amino Acids* 25, 323-39.
8. Zhang, Y., and Hogg, N. The mechanism of transmembrane S-nitrosothiol transport, (2004), *Proc Natl Acad Sci U S A* 101, 7891-6.
9. Aruoma, O. I., Halliwell, B., Hoey, B. M., and Butler, J. The antioxidant action of N-acetylcysteine: its reaction with hydrogen peroxide, hydroxyl radical, superoxide, and hypochlorous acid, (1989), *Free Radic Biol Med* 6, 593-7.
10. Khan, M., Sekhon, B., Jatana, M., Giri, S., Gilg, A. G., Sekhon, C., Singh, I., and Singh, A. K. Administration of N-acetylcysteine after focal cerebral ischemia protects brain and reduces inflammation in a rat model of experimental stroke, (2004), *J Neurosci Res* 76, 519-27.
11. Martinez, M., Hernandez, A. I., and Martinez, N. N-Acetylcysteine delays age-associated memory impairment in mice: role in synaptic mitochondria, (2000), *Brain Res* 855, 100-6.

12. Park, S. W., Kim, S. H., Park, K. H., Kim, S. D., Kim, J. Y., Baek, S. Y., Chung, B. S., and Kang, C. D. Preventive effect of antioxidants in MPTP-induced mouse model of Parkinson's disease, (2004), *Neurosci Lett* 363, 243-6.
13. Miller, J. W., Nadeau, M. R., Smith, D., and Selhub, J. Vitamin B-6 deficiency vs folate deficiency: comparison of responses to methionine loading in rats, (1994), *Am J Clin Nutr* 59, 1033-9.
14. Vallance, P., Leone, A., Calver, A., Collier, J., and Moncada, S. Endogenous dimethylarginine as an inhibitor of nitric oxide synthesis, (1992), *J Cardiovasc Pharmacol* 20 Suppl 12, S60-2.
15. Stuhlinger, M. C., and Stanger, O. Asymmetric dimethyl-L-arginine (ADMA): a possible link between homocyst(e)ine and endothelial dysfunction, (2005), *Curr Drug Metab* 6, 3-14.
16. Bendini, M. G., Lanza, G. A., Mazza, A., Giordano, A., Leggio, M., Menichini, G., De Cristofaro, R., Moriconi, E., Cozzari, L., Farina, S. M., and Giordano, G. [Risk factors for cardiovascular diseases: what is the role for homocysteine?], (2007), *G Ital Cardiol (Rome)* 8, 148-60.
17. Selhub, J. Homocysteine metabolism, (1999), *Annu Rev Nutr* 19, 217-46.
18. Zoungas, S., McGrath, B. P., Branley, P., Kerr, P. G., Muske, C., Wolfe, R., Atkins, R. C., Nicholls, K., Fraenkel, M., Hutchison, B. G., Walker, R., and McNeil, J. J. Cardiovascular morbidity and mortality in the Atherosclerosis and Folic Acid Supplementation Trial (ASFAST) in chronic renal failure: a multicenter, randomized, controlled trial, (2006), *J Am Coll Cardiol* 47, 1108-16.
19. Bonaa, K. H., Njolstad, I., Ueland, P. M., Schirmer, H., Tverdal, A., Steigen, T., Wang, H., Nordrehaug, J. E., Arnesen, E., and Rasmussen, K. Homocysteine lowering and cardiovascular events after acute myocardial infarction, (2006), *N Engl J Med* 354, 1578-88.
20. van Meurs, J. B., Dhonukshe-Rutten, R. A., Pluijm, S. M., van der Klift, M., de Jonge, R., Lindemans, J., de Groot, L. C., Hofman, A., Witteman, J. C., van Leeuwen, J. P., Breteler, M. M., Lips, P., Pols, H. A., and Uitterlinden, A. G. Homocysteine levels and the risk of osteoporotic fracture, (2004), *N Engl J Med* 350, 2033-41.

21. Gomber, S., Dewan, P., and Dua, T. Homocystinuria: a rare cause of megaloblastic anemia, (2004), *Indian Pediatr* 41, 941-3.

22. Sun, J., Xu, Y., Zhu, Y., and Lu, H. Methylenetetrahydrofolate reductase gene polymorphism, homocysteine and risk of macroangiopathy in Type 2 diabetes mellitus, (2006), *J Endocrinol Invest* 29, 814-20.

23. Heydrick, S. J., Weiss, N., Thomas, S. R., Cap, A. P., Pimentel, D. R., Loscalzo, J., and Keaney, J. F., Jr. L-Homocysteine and L-homocystine stereospecifically induce endothelial nitric oxide synthase-dependent lipid peroxidation in endothelial cells, (2004), *Free Radic Biol Med* 36, 632-40.

24. Moncada, S., Palmer, R. M., and Higgs, E. A. Nitric oxide: physiology, pathophysiology, and pharmacology, (1991), *Pharmacol Rev* 43, 109-42.

25. Shiva, S., Crawford, J. H., Ramachandran, A., Ceaser, E. K., Hillson, T., Brookes, P. S., Patel, R. P., and Darley-Usmar, V. M. Mechanisms of the interaction of nitroxyl with mitochondria, (2004), *Biochem J* 379, 359-66.

26. Shafirovich, V., and Lymar, S. V. Nitroxyl and its anion in aqueous solutions: spin states, protic equilibria, and reactivities toward oxygen and nitric oxide, (2002), *Proc Natl Acad Sci U S A* 99, 7340-5.

27. Bartberger, M. D., Fukuto, J. M., and Houk, K. N. On the acidity and reactivity of HNO in aqueous solution and biological systems, (2001), *Proc Natl Acad Sci U S A* 98, 2194-8.

28. Miranda, K. M., Paolocci, N., Katori, T., Thomas, D. D., Ford, E., Bartberger, M. D., Espey, M. G., Kass, D. A., Feelisch, M., Fukuto, J. M., and Wink, D. A. A biochemical rationale for the discrete behavior of nitroxyl and nitric oxide in the cardiovascular system, (2003), *Proc Natl Acad Sci U S A* 100, 9196-201.

29. Fukuto, J. M., Stuehr, D. J., Feldman, P. L., Bova, M. P., and Wong, P. Peracid oxidation of an N-hydroxyguanidine compound: a chemical model for the oxidation of N omega-hydroxyl-L-arginine by nitric oxide synthase, (1993), *J Med Chem* 36, 2666-70.

30. Wink, D. A., Feelisch, M., Fukuto, J., Chistodoulou, D., Jourd'heuil, D., Grisham, M. B., Vodovotz, Y., Cook, J. A., Krishna, M., DeGraff, W. G., Kim, S., Gamson, J., and

Mitchell, J. B. The cytotoxicity of nitroxyl: possible implications for the pathophysiological role of NO, (1998), *Arch Biochem Biophys* 351, 66-74.

31. Wong, P. S., Hyun, J., Fukuto, J. M., Shirota, F. N., DeMaster, E. G., Shoeman, D. W., and Nagasawa, H. T. Reaction between S-nitrosothiols and thiols: generation of nitroxyl (HNO) and subsequent chemistry, (1998), *Biochemistry* 37, 5362-71.
32. Spencer, N. Y., Patel, N. K., Keszler, A., and Hogg, N. Oxidation and nitrosylation of oxyhemoglobin by S-nitrosoglutathione via nitroxyl anion, (2003), *Free Radic Biol Med* 35, 1515-26.
33. Sharpe, M. A., and Cooper, C. E. Reactions of nitric oxide with mitochondrial cytochrome c: a novel mechanism for the formation of nitroxyl anion and peroxynitrite, (1998), *Biochem J* 332 (Pt 1), 9-19.
34. Saleem, M., and Ohshima, H. Xanthine oxidase converts nitric oxide to nitroxyl that inactivates the enzyme, (2004), *Biochem Biophys Res Commun* 315, 455-62.
35. Niketic, V., Stojanovic, S., Nikolic, A., Spasic, M., and Michelson, A. M. Exposure of Mn and FeSODs, but not Cu/ZnSOD, to NO leads to nitrosonium and nitroxyl ions generation which cause enzyme modification and inactivation: an in vitro study, (1999), *Free Radic Biol Med* 27, 992-6.
36. Poderoso, J. J., Carreras, M. C., Schopfer, F., Lisdero, C. L., Riobo, N. A., Giulivi, C., Boveris, A. D., Boveris, A., and Cadenas, E. The reaction of nitric oxide with ubiquinol: kinetic properties and biological significance, (1999), *Free Radic Biol Med* 26, 925-35.
37. Pino, R. Z., and Feelisch, M. Bioassay discrimination between nitric oxide (NO.) and nitroxyl (NO-) using L-cysteine, (1994), *Biochem Biophys Res Commun* 201, 54-62.
38. Shoeman, D. W., Shirota, F. N., DeMaster, E. G., and Nagasawa, H. T. Reaction of nitroxyl, an aldehyde dehydrogenase inhibitor, with N-acetyl-L-cysteine, (2000), *Alcohol* 20, 55-9.
39. DeMaster, E. G., Redfern, B., and Nagasawa, H. T. Mechanisms of inhibition of aldehyde dehydrogenase by nitroxyl, the active metabolite of the alcohol deterrent agent cyanamide, (1998), *Biochem Pharmacol* 55, 2007-15.

40. Kim, W. K., Choi, Y. B., Rayudu, P. V., Das, P., Asaad, W., Arnelle, D. R., Stamler, J. S., and Lipton, S. A. Attenuation of NMDA receptor activity and neurotoxicity by nitroxyl anion, NO, (1999), *Neuron* 24, 461-9.

41. Cook, N. M., Shinyashiki, M., Jackson, M. I., Leal, F. A., and Fukuto, J. M. Nitroxyl-mediated disruption of thiol proteins: inhibition of the yeast transcription factor Ace1, (2003), *Arch Biochem Biophys* 410, 89-95.

42. Tao, L., Murphy, M. E., and English, A. M. S-nitrosation of Ca(2+)-loaded and Ca(2+)-free recombinant calbindin D(28K) from human brain, (2002), *Biochemistry* 41, 6185-92.

43. Wink, D. A., Miranda, K. M., Katori, T., Mancardi, D., Thomas, D. D., Ridnour, L., Espey, M. G., Feelisch, M., Colton, C. A., Fukuto, J. M., Pagliaro, P., Kass, D. A., and Paolocci, N. Orthogonal properties of the redox siblings nitroxyl and nitric oxide in the cardiovascular system: a novel redox paradigm, (2003), *Am J Physiol Heart Circ Physiol* 285, H2264-76.

44. Fukuto, J. M., Chiang, K., Hszieh, R., Wong, P., and Chaudhuri, G. The pharmacological activity of nitroxyl: a potent vasodilator with activity similar to nitric oxide and/or endothelium-derived relaxing factor, (1992), *J Pharmacol Exp Ther* 263, 546-51.

45. Pagliaro, P., Mancardi, D., Rastaldo, R., Penna, C., Gattullo, D., Miranda, K. M., Feelisch, M., Wink, D. A., Kass, D. A., and Paolocci, N. Nitroxyl affords thiol-sensitive myocardial protective effects akin to early preconditioning, (2003), *Free Radic Biol Med* 34, 33-43.

46. Bai, P., Bakondi, E., Szabo, E., Gergely, P., Szabo, C., and Virag, L. Partial protection by poly(ADP-ribose) polymerase inhibitors from nitroxyl-induced cytotoxity in thymocytes, (2001), *Free Radic Biol Med* 31, 1616-23.

47. Hughes, M. N., and Cammack, R. Synthesis, chemistry, and applications of nitroxyl ion releasers sodium trioxodinitrate or Angeli's salt and Piloty's acid, (1999), *Methods Enzymol* 301, 279-87.

48. Ma, X. L., Gao, F., Liu, G. L., Lopez, B. L., Christopher, T. A., Fukuto, J. M., Wink, D. A., and Feelisch, M. Opposite effects of nitric oxide and nitroxyl on postischemic myocardial injury, (1999), *Proc Natl Acad Sci U S A* 96, 14617-22.

49. Takahira, R., Yonemura, K., Fujise, Y., and Hishida, A. Dexamethasone attenuates neutrophil infiltration in the rat kidney in ischemia/reperfusion injury: the possible role of nitroxyl, (2001), *Free Radic Biol Med* 31, 809-15.

50. Smith, P. A. S. a. H., G. E. The alleged role of nitroxyl in certain reactions of aldehydes and alkyl halides, (1960), *J Am Chem Soc* 82, 5371-40.

51. Miranda, K. M., Dutton, A. S., Ridnour, L. A., Foreman, C. A., Ford, E., Paolocci, N., Katori, T., Tocchetti, C. G., Mancardi, D., Thomas, D. D., Espey, M. G., Houk, K. N., Fukuto, J. M., and Wink, D. A. Mechanism of aerobic decomposition of Angeli's salt (sodium trioxodinitrate) at physiological pH, (2005), *J Am Chem Soc* 127, 722-31.

52. Feelisch, M., Stamler J. S. (1996) in *Methods in Nitric Oxide Research* (Feelisch, M., Stamler J. S., Ed.) pp 71-115, Wiley, New York.

53. Fukuto, J. M., Hobbs, A. J., and Ignarro, L. J. Conversion of nitroxyl (HNO) to nitric oxide (NO) in biological systems: the role of physiological oxidants and relevance to the biological activity of HNO, (1993), *Biochem Biophys Res Commun* 196, 707-13.

54. Zamora, R., Grzesiok, A., Weber, H., and Feelisch, M. Oxidative release of nitric oxide accounts for guanylyl cyclase stimulating, vasodilator and anti-platelet activity of Piloty's acid: a comparison with Angeli's salt, (1995), *Biochem J* 312 (Pt 2), 333-9.

55. Dutton, A. S., Fukuto, J. M., and Houk, K. N. Mechanisms of HNO and NO production from Angeli's salt: density functional and CBS-QB3 theory predictions, (2004), *J Am Chem Soc* 126, 3795-800.

56. Bonner, F. T., Stedman, G. (1996) in *Methods in Nitric Oxide Research* (Feelisch, M., Stamler, J. S., Ed.) pp 3-18, Wiley, New York.

57. Shen, B., and English, A. M. Mass spectrometric analysis of nitroxyl-mediated protein modification: comparison of products formed with free and protein-based cysteines, (2005), *Biochemistry* 44, 14030-44.

58. D'Silva, C., Al-Timari, A., and Douglas, K. T. Synthesis of N-acylglutathione derivatives by dimethylaminopyridine catalysis, (1982), *Biochem J* 207, 329-32.

59. Miranda, K. M. The chemistry of nitroxyl (HNO) and implications in biology, (2005), *Coordination Chemistry Reviews* 249, 433-455.

60. Tao, L., and English, A. M. Protein S-glutathiolation triggered by decomposed S-nitrosoglutathione, (2004), *Biochemistry* 43, 4028-38.

61. Badia, A., Carlini, R., Fernandez, A., Battaglini, F., Mikkelsen, S. R., English, A. M. Intramolecular electron-transfer rates in ferrocene-derivatized glucose oxidase, (1993), *J. Am. Chem. Soc.* 115, 7053-7060.

62. Salvucci, M. E. Covalent modification of a highly reactive and essential lysine residue of ribulose-1,5-bisphosphate carboxylase/oxygenase activase, (1993), *Plant Physiol* 103, 501-8.

63. Lewis, P. N., Guillemette, J. G., and Chan, S. Histone accessibility determined by lysine-specific acetylation in chicken erythrocyte nuclei, (1988), *Eur J Biochem* 172, 135-45.

64. Sondej, M., Seok, Y. J., Badawi, P., Koo, B. M., Nam, T. W., and Peterkofsky, A. Topography of the surface of the Escherichia coli phosphotransferase system protein enzyme IIAglc that interacts with lactose permease, (2000), *Biochemistry* 39, 2931-9.

65. Ragone, R. Homocystine solubility and vascular disease, (2002), *Faseb J* 16, 401-4.

66. Grabarek, Z., and Gergely, J. Zero-length crosslinking procedure with the use of active esters, (1990), *Anal Biochem* 185, 131-5.

67. http://www.piercenet.com/Products/Browse.cfm?fldID=02040114.

68. Soll, R., and Beck-Sickinger, A. G. On the synthesis of orexin A: a novel one-step procedure to obtain peptides with two intramolecular disulphide bonds, (2000), *J Pept Sci* 6, 387-97.

69. Jones, J. (1992) *Amino acid and peptide synthesis*, Oxford Univerisity Press, Oxford, UK.

70. Gilbert, H. F. Molecular and cellular aspects of thiol-disulfide exchange, (1990), *Adv Enzymol Relat Areas Mol Biol* 63, 69-172.

71. Harris, T. K., and Turner, G. J. Structural basis of perturbed pKa values of catalytic groups in enzyme active sites, (2002), *IUBMB Life* 53, 85-98.

72. Krezel, A., and Bal, W. Structure-function relationships in glutathione and its analogues, (2003), *Org Biomol Chem* 1, 3885-90.

73. Tajc, S. G., Tolbert, B. S., Basavappa, R., and Miller, B. L. Direct determination of thiol pKa by isothermal titration microcalorimetry, (2004), *J Am Chem Soc* 126, 10508-9.

74. Oram, P. D., Fang, X., Fernando, Q., Letkeman, P., and Letkeman, D. The formation of constants of mercury(II)--glutathione complexes, (1996), *Chem Res Toxicol* 9, 709-12.

75. Li, N. C., Manning, R. A. Some metal complexes of sulfur-containing amino acids, (1955), *J Am Chem Soc* 77, 5225-5228.

76. Friedman, M., Cavins, J. F., and Wall, J. S. Relative nucleophilic reactivities of amino groups and mercaptide ions in addition reactions with α,β-unsaturated compounds, (1965), *J Am Chem Soc* 87, 3672-82.

77. Backs, S. J., Rabenstein, D. L. Nuclear magnetic resonance studies of the solution chemistry of metal complexes. 16. Complexation of trimethyllead by sulfhydryl-containing amino acids and related molecules, (1981), *Inorg. Chem.* 20, 410-415.

78. Edsall, J. T., Martin, R. B., and Hollingworth, B. R. Ionization of Individual Groups in Dibasic Acids, with Application to the Amino and Hydroxyl Groups of Tyrosine, (1958), *Proc Natl Acad Sci U S A* 44, 505-18.

79. Avdeef, A., Comer, J. E. A., Thomson, S. J. pH-metric log P. 3. Glass electrode calibration in methanol-water, Applied to pKa determination of water-insolubel substances, (1993), *Anal Chem* 65, 42-49.

80. Avdeef, A., Box, K. J., Comer, J. E., Gilges, M., Hadley, M., Hibbert, C., Patterson, W., and Tam, K. Y. PH-metric log P 11. pKa determination of water-insoluble drugs in organic solvent-water mixtures, (1999), *J Pharm Biomed Anal* 20, 631-41.

81. Avdeef, A., Bucher, J. J. Accurate measurement of the concentration of hydrogen ions with a glass electrode: Calibrations using the prideaus and other universal buffer solutions and a computer-controlled automatic titrator, (1978), *Anal Chem* 50, 2137-2142.

82. Soovali, L., Kaljurand, I., Kutt, A., and Leito, I. Uncertainty estimation in measurement of pKa values in nonaqueous media: A case study on basicity scale in acetonitrile medium, (2006), *Analytica Chimica Acta* 566, 290-303.

83. Bulaj, G., Kortemme, T., and Goldenberg, D. P. Ionization-reactivity relationships for cysteine thiols in polypeptides, (1998), *Biochemistry* 37, 8965-72.

84. Smalley, J. F., Chalfant, K., and Feldberg, S. W. An indirect laser-induced temperature jump determination of the surface pKa of 11-mercaptoundecanoic acid monolayers self-assembled on gold, (B 1999), *J Phys Chem* 103, 1676-85.

85. Britto, P. J., Knipling, L., and Wolff, J. The local electrostatic environment determines cysteine reactivity of tubulin, (2002), *J Biol Chem* 277, 29018-27.

86. Donzelli, S., Espey, M. G., Thomas, D. D., Mancardi, D., Tocchetti, C. G., Ridnour, L. A., Paolocci, N., King, S. B., Miranda, K. M., Lazzarino, G., Fukuto, J. M., and Wink, D. A. Discriminating formation of HNO from other reactive nitrogen oxide species, (2006), *Free Radic Biol Med* 40, 1056-66.

87. Grossi, L., and Montevecchi, P. C. S-nitrosocysteine and cystine from reaction of cysteine with nitrous acid. A kinetic investigation, (2002), *J Org Chem* 67, 8625-30.

88. Rubino, F. M., Verduci, C., Giampiccolo, R., Pulvirenti, S., Brambilla, G., and Colombi, A. Characterization of the disulfides of bio-thiols by electrospray ionization and triple-quadrupole tandem mass spectrometry, (2004), *J Mass Spectrom* 39, 1408-16.

89. Hoffman, W. E., Charbel, F. T., Edelman, G., and Ausman, J. I. Brain tissue acid-base changes during ischemia, (1997), *Neurosurg Focus* 2, E2; discussion 1 p following E2.

90. Eisinger, J., Flores, J., and Salhany, J. M. Association of cytosol hemoglobin with the membrane in intact erythrocytes, (1982), *Proc Natl Acad Sci U S A* 79, 408-12.

91. Fiddian-Green, R. G. Gastric intramucosal pH, tissue oxygenation and acid-base balance, (1995), *Br J Anaesth* 74, 591-606.

92. Fu, X., Mueller, D. M., and Heinecke, J. W. Generation of intramolecular and intermolecular sulfenamides, sulfinamides, and sulfonamides by hypochlorous acid: a potential pathway for oxidative cross-linking of low-density lipoprotein by myeloperoxidase, (2002), *Biochemistry* 41, 1293-301.

93. Biteau, B., Labarre, J., and Toledano, M. B. ATP-dependent reduction of cysteine-sulphinic acid by S. cerevisiae sulphiredoxin, (2003), *Nature* 425, 980-4.

94. Vivancos, A. P., Castillo, E. A., Biteau, B., Nicot, C., Ayte, J., Toledano, M. B., and Hidalgo, E. A cysteine-sulfinic acid in peroxiredoxin regulates H2O2-sensing by the antioxidant Pap1 pathway, (2005), *Proc Natl Acad Sci U S A* 102, 8875-80.

95. Jacob, C., Holme, A. L., and Fry, F. H. The sulfinic acid switch in proteins, (2004), *Org Biomol Chem* 2, 1953-6.

96. Walshe, J. M. The story of penicillamine: a difficult birth, (2003), *Mov Disord* 18, 853-9.

97. Xia, Y., Cardounel, A. J., Vanin, A. F., and Zweier, J. L. Electron paramagnetic resonance spectroscopy with N-methyl-D-glucamine dithiocarbamate iron complexes distinguishes nitric oxide and nitroxyl anion in a redox-dependent manner: applications in identifying nitrogen monoxide products from nitric oxide synthase, (2000), *Free Radic Biol Med* 29, 793-7.

98. Lopez, B. E., Shinyashiki, M., Han, T. H., and Fukuto, J. M. Antioxidant actions of nitroxyl (HNO), (2007), *Free Radic Biol Med* 42, 482-91.

99. Rabenstein, D. L. Thiol/disulfide exchange reactions of captopril and penicillamine with arginine vasopressin and oxytocin, (1995), *Bioorganic Chem* 23, 109-118.